FORSCHUNGSZENTRUM ROSSENDORF

WISSENSCHAFTLICH-TECHNISCHE BERICHTE
FZR-283
Dezember 1999
ISSN 1437-322X

Institute of Bioinorganic and Radiopharmaceutical Chemistry

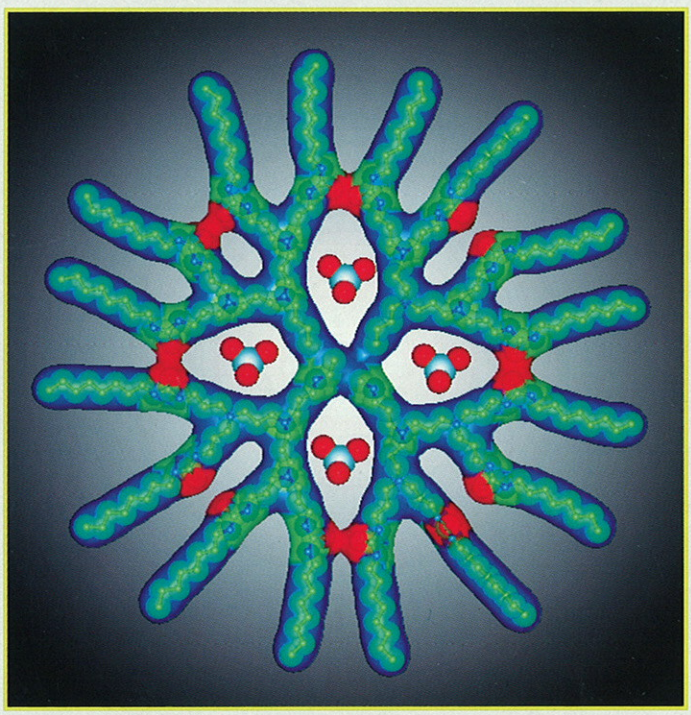

Report
July - December 1999

Cover Picture:
Urea-functionalized dendrimer which shows very efficient phase transfer of pertechnetate ions.

Forschungszentrum Rossendorf e. V.

Postfach 51 01 19; D-01314 Dresden
Bundesrepublik Deutschland
Telefon (03 51) 260 31 70
Telefax (03 51) 260 32 32
E-Mail johannsen@fz-rossendorf.de

FORSCHUNGSZENTRUM ROSSENDORF

WISSENSCHAFTLICH-TECHNISCHE BERICHTE

FZR-283

Dezember 1999

Institute of Bioinorganic and Radiopharmaceutical Chemistry

Report

July – December 1999

Editor:
Prof. Dr. B. Johannsen
Editorial staff: Dr. S. Seifert

CONTENTS

I. RESEARCH REPORTS

TUMOUR AGENTS AND TUMOUR DIAGNOSIS

1. Distribution Behaviour of 3-*O*-Methyl-6-[^{18}F]Fluoro-L-3,4-Dihydroxyphenylalanine in Wistar Rats, Normal Mice and Tumour-Bearing Nude Mice

R. Syhre, P. Brust, D. Zips[1], F. Füchtner, J. Steinbach, B. Johannsen
[1]TU Dresden, Klinik und Poliklinik für Strahlentherapie

Introduction

3-*O*-Methyl-6-[^{18}F]fluoro-L-3,4-dihydroxyphenylalanine (OMFD) is known as a non-toxic metabolite of 6-[^{18}F]fluoro-L-3,4-dihydroxyphenylalanine (FDOPA). OMFD itself has proved to be a promising PET tracer for tumour imaging, especially for tumour visualization and localization [1].
The synthesis of OMFD is easy and produces the tracer in a high yield after a relatively short preparation time [2]. This synthetic amino acid was found to be largely metabolically stable and not involved in the biosynthesis of proteins [3].
The aim of this study was to investigate the uptake and retention behaviour of OMFD in Wistar rats, normal BALB/C mice and tumour-bearing nude mice. The suitability of OMFD as a tumour-detecting agent is supported by a competition study using L-phenylalanine as a substrate for the amino acid transport system L.

Materials and Methods

The animal studies were carried out in accordance with the relevant national regulations.
The experiments were performed in Wistar rats (male; 5 - 6 weeks old), Balb/C mice as well as nude mice bearing human squamous cell carcinoma (male and female; 5 to 6 weeks old). The tumours were transplanted 15 to 20 days prior to the animal studies. At the time of the study the tumour weight was 0.7 ± 0.4 g.
The animals were injected into the tail vein under a light ether anaesthesia. OMFD solution (~ 5 MBq OMFD/ml; saline ; pH 4.5 - 5.0; radiochemical purity ≥ 90 %). The injection volume was 0.5 ml for rats and 0.2 ml for mice, respectively. 5 to 120 min p.i. the animals were sacrificed by heart puncture (ether anaesthesia). Selected organs, including tumour, were isolated for weighing and counting. The accumulated radioactivity in the tissue was calculated as a percentage of the injected dose per organ and per gram tissue.
To evaluate the uptake of OMFD by a specific amino acid transport system present in the brain and in various tumours, the distribution pattern was studied 5 minutes after intravenous co-injection of 0.5 ml OMFD and L-phenylalanine (100 mg/kg body weight).
The effect of L-phenylalanine as a competitive agent on the tumour uptake was investigated in L-phenylalanine-loaded nude mice. For this test 0.2 ml of L-phenylalanine/saline (25 mg/100 g BW) was intraperitoneally injected into the animals 30 minutes prior to the OMFD injection. The biodistribution was determined 60 minutes after radiotracer injection as described before.

Results and Discussion

Table 1 shows the tracer distribution pattern of the animal species studied as a percentage of the injected dose per organ.
It is shown that OMFD is able to cross the blood-brain-barrier of rats and mice. The initial radioactivity uptake in the brain, heart and lungs was similar low (< 1 % ID/organ) and even decreased slowly with the time in all of animal species studied (Table 1).
The renal path shows the main elimination part (approx. 50 % ID up to 120 min p.i.) of OMFD among the animals investigated. However, the retention behaviour of OMFD in the kidneys suggests that the rate of renal clearance may differ between the animal species. In addition to the high kidney activity of OMFD, a significant uptake in Balb/C and in nude mice was measured in the pancreas (6 % ID corresponding to ~30 % ID/gram tissue) followed by the liver, whereas in rats the uptake in the liver was significantly higher than in the pancreas (Table 1). This prominent accumulation in the pancreas of mice was also observed after the injection of various [^{18}F]fluoro-L-amino acid derivatives, such as FDOPA, fluoro-L-prolines and fluoro-L-tyrosines, respectively [4 - 6]. The results of distribution studies in rats (Table 1) as well as of clinical studies indicate that the high pancreas uptake is specific for mice and negligible for the clinical use of these compounds [1, 5, 7].

Table 1. Biodistribution of OMFD in Wistar rats, Balb/C mice and nude mice as a percentage of the injected dose per organ (mean ± SD; n = 6).

		Wistar rats		
min p.i.	5	30	60	120
Brain	0.64 ± *0.06*	0.51 ± *0.10*	0.42 ± *0.05*	0.39 ± *0.03*
Pancreas	1.26 ± *0.18*	0.69 ± *0.13*	0.47 ± *0.06*	0.44 ± *0.02*
Spleen	0.31 ± *0.04*	0.20 ± *0.02*	0.15 ± *0.02*	0.14 ± *0.03*
Kidneys	7.40 ± *0.41*	5.21 ± *0.66*	4.21 ± *0.38*	4.74 ± *0.68*
Lungs	0.38 ± *0.05*	0.21 ± *0.02*	0.19 ± *0.01*	0.15 ± *0.02*
Heart	0.74 ± *0.17*	0.39 ± *0.08*	0.29 ± *0.02*	0.27 ± *0.04*
Femur	0.70 ± *0.10*	0.77 ± *0.08*	0.76 ± *0.03*	0.74 ± *0.06*
Liver	5.41 ± *1.03*	3.64 ± *0.26*	3.03 ± *0.24*	2.87 ± *0.44*
		Balb/C mice		
Brain	0.84 ± *0.08*	0.84 ± *0.18*	0.57 ± *0.14*	0.32 ± *0.06*
Pancreas	6.00 ± *0.37*	3.21 ± *0.67*	2.29 ± *0.74*	1.06 ± *0.60*
Spleen	0.67 ± *0.10*	0.29 ± *0.05*	0.21 ± *0.04*	0.09 ± *0.06*
Kidneys	13.05 ± *0.94*	6.52 ± *0.38*	7.39 ± *0.25*	6.56 ± *0.60*
Lungs	0.58 ± *0.03*	0.28 ± *0.05*	0.18 ± *0.04*	0.10 ± *0.01*
Heart	0.91 ± *0.07*	0.35 ± *0.05*	0.28 ± *0.05*	0.15 ± *0.01*
Femur	0.52 ± *0.16*	0.78 ± *0.22*	0.58 ± *0.14*	0.56 ± *0.07*
Liver	5.37 ± *0.48*	3.17 ± *0.62*	1.72 ± *.13*	1.04 ± *0.21*
		Nude mice		
Brain	0.74 ± *0.10*	0.79 ± *0.14*	0.66 ± *0.26*	0.53 ± *0.13*
Pancreas	6.30 ± *1.18*	3.22 ± *0.67*	1.54 ± *0.34*	2.19 ± *0.32*
Spleen	0.55 ± *0.22*	0.34 ± *0.12*	0.42 ± *0.11*	0.24 ± *0.07*
Kidneys	10.63 ± *1.27*	3.26 ± *1.27*	1.93 ± *0.35*	1.06 ± *0.09*
Lungs	0.49 ± *0.11*	0.24 ± *0.06*	0.25 ± *0.14*	0.19 ± *0.03*
Heart	0.80 ± *0.16*	0.39 ± *0.22*	0.47 ± *0.12*	0.32 ± *0.06*
Femur	0.82 ± *0.53*	0.69 ± *0.20*	0.64 ± *0.18*	0.52 ± *0.27*
Liver	4.41 ± *1.05*	3.63 ± *1.27*	2.67 ± *0.59*	1.79 ± *0.39*

Nude mice*:15; 45; 60; 120 min p.i.

During the interval of investigation (5 min to 120 min) up to 16 % of the injected dose was retained in the skeleton (% ID femur*20) of the animals. The *in vivo* stability of this ^{18}F-labelled compound without significant defluorination within the organism was indicated by the fact that no increase against time was observed.

The blood clearance of OMFD was faster for rats than for mice (Fig. 1).

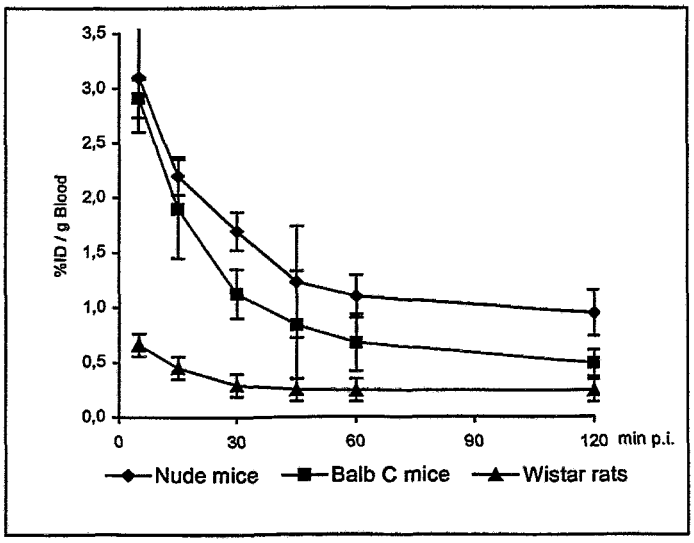

Fig.1. Blood clearance of OMFD after injection in Wistar rats. Balb/C mice and nude mice (% ID/g ± SD; n = 6)

Fig. 2 shows the time course of tumour accumulation after injection of OMFD in tumour-bearing nude mice. It is apparent that a peak of the tumour uptake occurred at 60 min p.i. At this time 12.4 ± 1.6 % of the injected dose per gram tumour was accumulated. The tumour activity slowly decreased with the time to reach 9.8 ± 1.7 % ID/g at 120 min p.i.

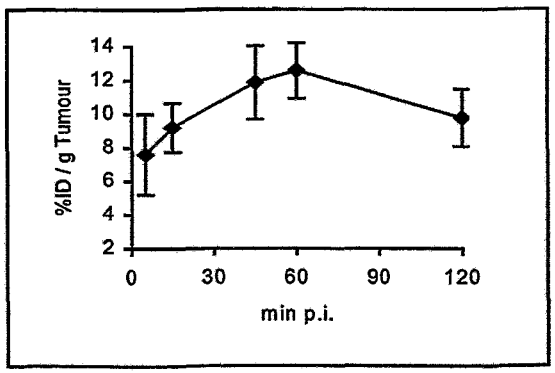

Fig. 2. Time-dependent tumour uptake of OMFD in nude mice (% ID/g ± SD; n = 6; tumour weight 0.45 ± 0.37 g).

These good tumour uptake values result in representative tumour-to-blood and tumour-to-tissue ratios as shown in Fig. 3.
Interestingly, no significant changes in uptake were observed after co-injection of OMFD and L-phenylalanine compared with the OMFD distribution data in most organs of rats (Table 2). However, the presence of L-phenylalanine significantly reduced the initial uptake of OMFD in the brain and in the heart. It was especially the significantly diminished brain uptake (~70 %) after L-phenylalanine co-injection which confirmed that the compound crosses the blood-brain barrier through the amino acid transport system L [8, 9].

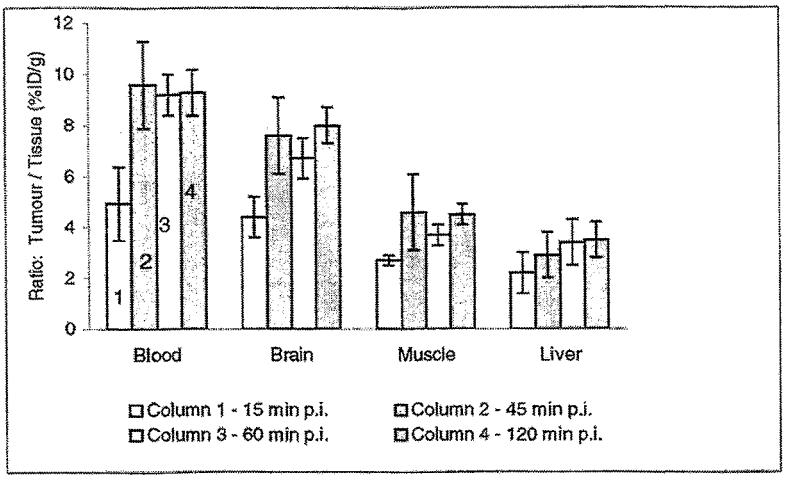

Fig. 3. Time course of tumour/non-tumour ratios after injection of OMFD in nude mice (ratio: % ID/g / % ID/g ± SD; n = 6; tumour weight 0.45 ± 0.37 g)

Furthermore, the competition according to the tumour uptake of OMFD was demonstrated by investigating L-phenylalanine-loaded nude mice. The comparison of the tumour uptake as well as of the tumour/non-tumour ratios (Fig. 4) indicates that L-phenylalanine influences the distribution of OMFD *in vivo*. These results suggest that tumour uptake of OMFD was clearly reduced (approx. 20 %) by inhibition of the system L transporter.

Table 2. Comparison of the distribution patterns of OMFD in rats with and without L-phenylalanine as a competitive agent of the amino-acid transport system L (Wistar rats; 5 min p.i.; mean ± SD; n = 8).

	OMFD		OMFD + L-phenylalanine	
	% ID/Organ	% ID/g	%ID/Organ	% ID/g
Blood		0.69 *0.05*		0.79 ± *0.15*
Brain	0.63 ± *0.06*	0.44 ± *0.04*	0.21 ± *0.02*	0.15 ± *0.01*
Pancreas	1.11 ± *0.22*	3.91 ± *0.37*	1.11 ± *0.13*	3.61 ± *0.64*
Spleen	0.39 ± *0.05*	1.00 ± *0.08*	0.35 ± *0.02*	0.93 ± *0.17*
Kidney	6.49 ± *0.38*	4.64 ± *0.42*	7.78 ± *0.88*	5.04 ± *0.66*
Muscle	0.37 ± *0.10*	0.70 ± *0.09*	0.38 ± *0.09*	0.61 ± *0.09*
Heart	0.49 ± *0.05*	0.84 ± *0.06*	0.37 ± *0.04*	0.58 ± *0.11*
Lung	0.81 ± *0.12*	0.74 ± *0.07*	0.88 ± *0.15*	0.76 ± *0.15*
Femur	0.48 ± *0.05*	0.68 ± *0.05*	0.43 ± *0.05*	0.60 ± *0.09*
Liver	6.77 ± *0.73*	0.91 ± *0.06*	7.40 ± *0.42*	0.92 ± *0.16*

In summary, the biodistribution pattern of 3-*O*-methyl-6-[^{18}F]fluoro-L-3,4-dihydroxyphenylalanine (OMFD) obtained in normal and tumour-bearing animals suggests that this compound is a useful tracer for tumour imaging, with a high tumour uptake as well as a good tumour/non-tumour contrast.

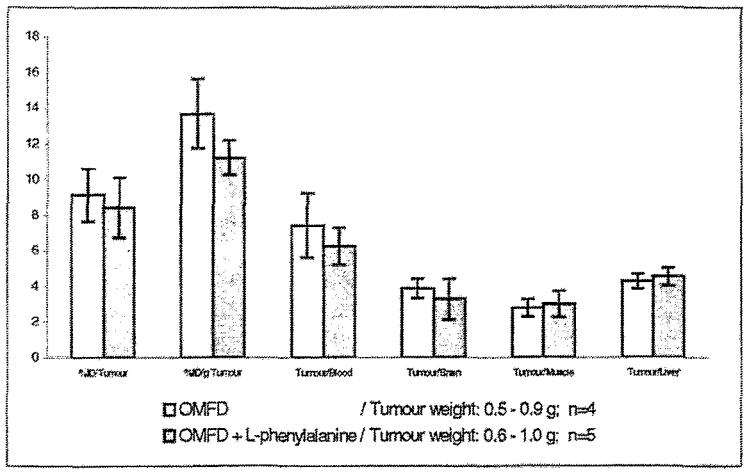

Fig. 4. Tumour uptake and tumour/non-tumour ratios of OMFD in nude mice compared with the values obtained after injection of OMFD in L-phenylalanine-loading animals (ratio: % ID/g / % ID/g ± SD; 60 min p.i.; L-phenylalanine injection 30 min prior to OMFD)

References

[1] Füchtner F., Steinbach J., Vorwieger G., Bergmann R., Syhre R., Brust P., Beuthien-Baumann B., Burchert W., Zips D., Baumann M. and Johannsen B. (1999) 3-O-Methyl-6-[^{18}F]fluoro-L-DOPA – a promising substance for tumour imaging. *J. Labelled Compd. Radiopharm.* **42**, S267-S268.

[2] Füchtner F., Steinbach J., Lücke R., Smuda C. and Johannsen B. (1999) Preparation of 3-O-methyl-6-[^{18}F]fluor-L-DOPA . *Report January 1998 – June 1999,* Institute of Bioinorganic and Radiopharmaceutical Chemistry, FZR-270, pp. 13-16.

[3] Vorwieger G., Bergmann R., Syhre R., Füchtner F., Steinbach J., Brust P and Johannsen B. (1999) Metabolism of 6-[^{18}F]fluoro- 3-*O*-methyl -L-3.4-dihydroxyphenylalanine in the rat. *Report January 1998 – June 1999,* Institute of Bioinorganic and Radiopharmaceutical Chemistry, FZR-270, pp. 17-20.

[4] Wester H. J., Herz M., Senekowitch-Schmidtke R., Schwaiger M., Stöcklin G and Hamacher K. (1999) Preclinical evaluation of [^{18}F]fluoroprolines: diastereomeric effect on metabolism and uptake in mice. *Nucl. Med. Biol.* **26**, 259-265.

[5] Wester H. J., Herz M., Weber W. Heiss P., Senekowitch-Schmidtke R., Schwaiger M. and Stöcklin G. (1999) Synthesis and radiopharmacology of *O*-(2-[]fluoroethyl)-L-tyrosine for tumor imaging. *J. Nucl. Med.* **40**, 205-212.

[6] Inoue T., Tomoiyoshi K., Higuichi T., Ahmed K., Sarwar M., Aoyagi K., Amano S., Alyafei S., Zhang H. and Endo K. (1998) Biodistribution studies on *L*- 3-[fluorine-18]fluoro-alpha-methyl tyrosine: a potential tumor d-detecting agent. *J. Nucl. Med.* **39**, 205-212.

[7] Inoue T.,Shibasaki T., Oruchi N., Aoyagi K., Tomoiyoshi K., Amano S., Mikuni M., Ida I., Aoki J. and Endo K. (1999) ^{18}F alpha-methyl tyrosine: PET studies in patients with brain tumors. *J. Nucl. Med.* **40**, 399-405.

[8] Brust P. (1986) Changes in regional blood-brain transfer of L-leucine elicited by arginine-vasopressin. *J. Neurochem.* **46**, 534-541.

[9] Brust P. and Diemer N. H. (1990) Blood-brain transfer of L-phenylalanine declines after peripheral but not central nervous administration of vasopressin. *J. Neurochem.* **55**, 2098-2104.

2. ^{18}F-Labelled Neurotensin Receptor Ligands: Functional Studies

R. Bergmann, M. Scheunemann, P. Mäding, H. Rodig, P. Brust

Introduction

The development of novel and sophisticated molecular probes for peptide receptors has provided new tools for the early diagnosis and potential therapy of malignant disease. Neurotensin (NT) receptors have been frequently detected in tumour cells of Ewing's sarcoma, meningioma, astrocytoma, medulloblastoma, medullary thyroid cancers and small-cell lung cancers. However, these receptors are rarely expressed in non-small-cell lung cancer and breast carcinoma; and are absent in prostate, ovarian, renal-cell and hepatocellular carcinoma, neuroendocrine tumours of intestinal origin, pituitary adenoma, schwannoma, neuroblastoma and lymphoma [1]. The cell-line selective high expression of neurotensin receptors in ductal pancreatic adenocarcinoma might constitute the molecular basis for future clinical investigations, such as *in vivo* neurotensin receptor scintigraphy for early tumour diagnosis, radiotherapy with radiolabelled neurotensin analogues, and chemotherapy with neurotensin receptor antagonists [2].
The present work deals with the development and initial evaluation of radiolabelled [^{18}F]NT derivatives as probes for the scintigraphic localization of NT receptor-positive tumours and their metastases *in vivo*. To this end, NT analogues of improved biological stability to enzymatic degradation were labelled with ^{18}F [3]. We are currently employing *in vitro* tests to verify the suitability and effectiveness of these modifications. *In vivo* experiments in healthy and in tumour-bearing animals will be used to screen the labelled peptides for later clinical oncology trials.

In vitro binding studies

The neurotensin-derived peptides were labelled with no-carrier-added N-succinimidyl-4-[^{18}F]fluorobenzoate ([^{18}F]SFB) at high specific activity (5 - 15 TBq/mmol, 100 - 400 Ci/mmol) [3]. To verify that the additional fluorobenzoyl group on the N-terminus of the peptide does not alter the binding kinetics to the neurotensin receptor 1 (NTR1), we tested the *in vitro* accumulation of the labelled peptides in a colon adenocarcinoma cell line HT-29 (ATCC No. HTB38) which expresses the NTR1. This bioaccumulation results from a sequence of events beginning with the binding of the ligands to the receptor, followed by internalization of the receptor ligand complex and nonspecific binding and distribution of the ligand within the cells.

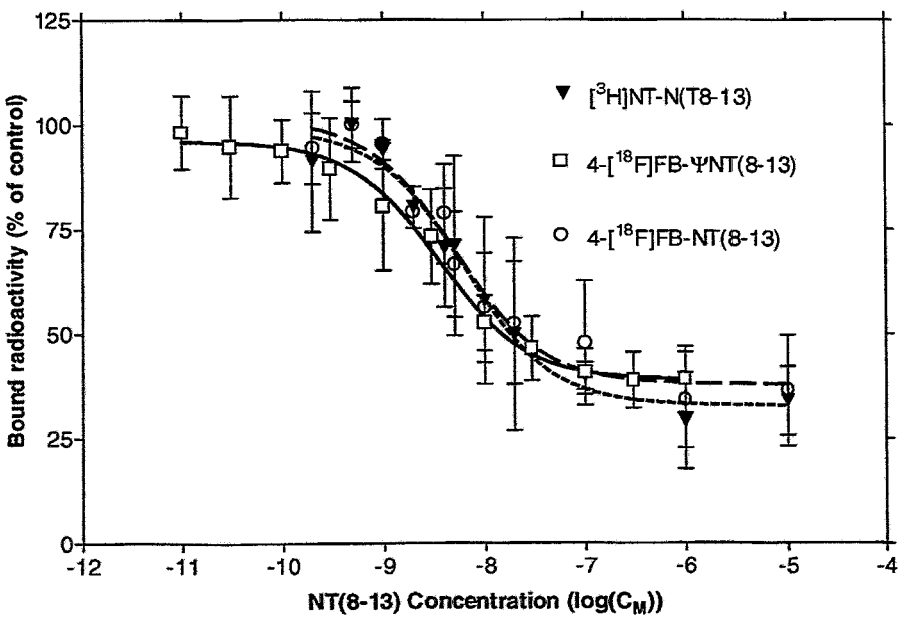

Fig. 1. Displacement curves for ^{18}F and ^{3}H-labelled analogue of NT in the presence of unlabelled peptide.

We carried out competition studies with [^{18}F]FB-NT(8-13), [^{18}F]FB-□NT(8-13) and [^{3}H]NT as radioligands and with NT(8-13) as a competitor. The apparent IC_{50}s (Fig 1) were 8 ± 3 nM, 3 ± 2 nM and 6 ± 2 nM, which comes close to NT(8-13) (1 nM). The nonspecific binding of the tracers was 38 % of the total binding at an NT(8-13) concentration of 1µM.

The accumulation of [^{18}F]FB-NT(8-13) and [^{18}F]FB-□NT(8-13) in the cells was measured at 37 °C and 4 °C in order to distinguish between saturable and reversible receptor binding which is not energy dependent and the subsequent internalization mediated by receptor endocytosis. More than 70 % of the [^{18}F]FB-NT(8-13) and [^{18}F]FB-□NT(8-13) receptor complexes were internalized after 30 min at 37 °C. At 4 °C about 26 % of the cell bound radioactivity remained within the cells after acid washing.
To evaluate the binding of [^{18}F]FB-NT(8-13) and [^{18}F]FB-□NT(8-13) to brain tissues expressing significant amounts of the high affinity NT receptor (NTR1) distribution we studied the *in vitro* binding of these tracers using autoradiography. The [^{18}F]FB-NT(8-13) and [^{18}F]FB-□NT(8-13) binding in rat brain slices (10 - 20 µm) was comparable to earlier reports [4]. The specific binding of [^{18}F]FB-NT(8-13) and [^{18}F]FB-□NT(8-13) was highest in the mesencephalon and in descending order, in the frontal, parietal, temporal, and occipital cortices and in the cerebellum.

Table 1. Tissue distribution (% ID/organ ± SD) of radioactivity derived from [^{18}F]FB-NT(8-13) and [^{18}F]FB-ψNT(8-13) in nude mice bearing human colon adenocarcinoma HT-29 30 minutes after simultaneous administration of saline or 2 µg NT(8-13) and 4-[^{18}F]FB-NT(8-13) (n = 4) or [^{18}F]FB-ψNT(8-13) (n = 4)

Tissue	4-[^{18}F]FB-NT(8-13)			4-[^{18}F]FB-ψNT(8-13)		
	Control	NT(8-13)	P values*	Control	NT(8-13)	P values*
Brain	0.01 ± <0.01	0.02 ± <0.01	0.77	0.06 ± 0.02	0.06 ± 0.02	0.77
Pancreas	0.12 ± 0.03	0.14 ± 0.03	0.16	0.09 ± 0.04	0.11 ± 0.07	0.77
Spleen	0.04 ± 0.02	0.04 ± 0.01	1.00	0.11 ± 0.05	0.10 ± 0.05	1.00
Kidney	1.89 ± 0.91	2.30 ± 0.68	0.29	4.11 ± 1.24	6.92 ± 3.94	0.39
Stomach	0.28 ± 0.19	0.49 ± 0.36	0.29	0.43 ± 0.15	0.66 ± 0.32	0.25
Heart	0.03 ± <0.01	0.04 ± 0.02	0.29	0.16 ± 0.07	0.16 ± 0.09	0.77
Lung	0.24 ± 0.08	0.34 ± 0.18	0.72	0.76 ± 0.19	0.82 ± 0.67	0.56
Liver	9.31 ± 3.78	20.81 ± 7.06	0.03	32.54 ± 9.24	38.14 ± 10.05	0.14
Tumor	0.06 ± 0.05	0.14 ± 0.07	0.16	0.12 ± 0.15	0.29 ± 0.21	0.08
Intestine	1.92 ± 0.52	2.08 ± 0.99	1.00	5.94 ± 2.72	3.27 ± 1.44	0.08

*P values (2-tailed P corrected for ties, Mann-Whitney-Test) for 30 min [^{18}F]FB-NT(8-13) or [^{18}F]FB-ψNT(8-13) in mice with and without NT(8-13) (2 µg) pretreatment.
% ID/organ = percentage injected dose per organ

In vivo evaluation

The biodistribution and biokinetics of the [^{18}F]FB-labelled compounds were evaluated in separate experiments with and without simultaneous injection of NT(8-13) in Wistar rats and in nude mice bearing the solid human colon adenocarcinoma HT-29 on the right leg. Radioactivity concentrations were measured by gamma-counting of tissue samples and by Positron Emission Tomography (PET).
We calculated the distribution and kinetics of the [^{18}F]FB-NT(8-13) and of [^{18}F]FB-□NT(8-13) relative to the tissue radioactivity concentration, assuming that the tracer was untransformed *in vivo*. The verification of ^{18}F-labelled metabolite formation will be the subject of a later study.
The biodistribution and biokinetics of [^{18}F]FB-NT(8-13) and of [^{18}F]FB-□NT(8-13) in rats and nude mice bearing a solid HT-29 cell tumour were qualitatively similar. The apparent blood clearance of the ^{18}F radioactivity after injection of [^{18}F]FB-NT(8-13) and [^{18}F]FB-□NT(8-13) was rapid in the control group. The co-injection of NT(8-13) resulted in a slower clearance of the radioactivity from the blood.

The biodistribution data from the experiments in mice are shown in the Table 1. The kidneys were the main excretory organs of [^{18}F]FB-NT(8-13) and of [^{18}F]FB-□NT(8-13), with a maximum of accumulated radioactivity occurring after 8 to 10 min post injection. The urine (collected 30 min post injection) of the animals contained 61 %ID ^{18}F radioactivity of [^{18}F]FB-NT(8-13) and 43 % ID of [^{18}F]FB-□NT(8-13). A high net uptake of both compounds was also measured in the liver and the intestine.

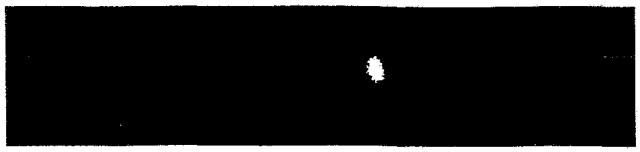

Fig. 2. Static PET 30 *min. p.i. of the* [^{18}F]FB-□NT(8-13) *accumulation in two animals* bearing HT-29 tumours of 0.5 cm diameter in the right leg

The *ex-vivo* autoradiography (Fig. 3) of the tumours demonstrated a non-homogeneous distribution of radioactivity in the tumours, with the highest radioactivity found in the growing zones. No necrotic regions were detected in these tumours by histology.

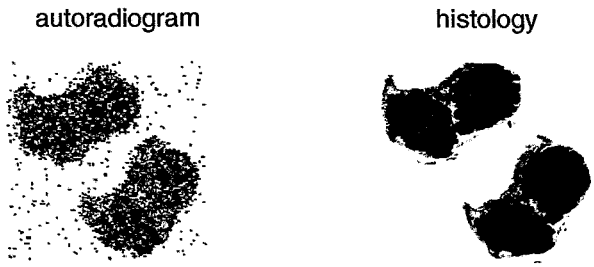

Fig. 3. *Ex vivo* autoradiography: Distribution of [^{18}F]FB-□NT(8-13) in an HT-29 tumour from tumour bearing mice

Conclusion

In conclusion it was demonstrated with PET that tumour tissue can be visually detected with the stabilized ^{18}F-labelled neurotensin derivative [^{18}F]FB-□NT(8-13). This compound may be used as a lead substance for the development of an ^{18}F-fluorobenzoylated stabilized neurotensin derivative for *in vivo* studies.

This work is supported by the European Union (BMH4-CT98-3198).

References

[1] Reubi J.C., Waser B., Schaer J.C. and Laissue J.A. (1999) Neurotensin receptors in human neoplasms: high incidence in Ewing's sarcomas. *Int. J. Cancer* **82**, 213-8.

[2] Reubi J.C., Waser B., Friess H., Buchler M. and Laissue J. (1998) Neurotensin receptors: a new marker for human ductal pancreatic adenocarcinoma. *Gut.* **42**, 546-50.

[3] Scheunemann M., Mäding P., Bergmann R., Steinbach J., Johannsen B. and Tourwe D. (1999) Reaction of neurotensin (8-13) and ist partially reduced congener with unlabelled and ^{18}F-labelled N-succinimidyl 4-fluorobenzoate (SFB). *Report January 1998 – June 1999,* Institute of Bioinorganic and Radiopharmaceutical Chemistry, FZR-270, pp. 26-28.

[4] Mendez M., Souaze F., Nagano M., Kelly P.A., Rostene W., Forgez P. (1997) High affinity neurotensin receptor mRNA distribution in rat brain and peripheral tissues. Analysis by quantitative RT-PCR. *J. Mol. Neurosci.* **9**, 93-102.

3. PET for Evaluation of the Tumour Metabolism in Malignant Lymphomas – Cost – Benefit Optimization

R. Naumann[1], B. Beuthien-Baumann[2], L. Schirmer[2], C. Tiepolt[2], J. Kropp[2], W.-G. Franke[2], G. Ehninger[1]
[1]Medizinische Klinik und Poliklinik I, [2]Klinik und Poliklinik für Nuklearmedizin, TU Dresden

Introduction

Positron Emission Tomography (PET) has the special advantage compared with conventional imaging techniques (ultrasonography, X-ray, CT, MRT) that it uses tumour metabolism to demonstrate the tumour location and to differentiate necrosis, vital tumour tissue and tumour recurrence [1].
Fluorine-18 fluorodeoxyglucose positron emission tomography (FDG-PET) has been shown to improve the diagnostic accuracy in the staging and follow-up of malignant lymphomas [2 - 4], based on the metabolic signal of the vital lesions.
At present PET is only available in a few places. It is an expensive method due to the elaborate technology. Recently it has become possible to extend the conventional double head gamma camera widely used in nuclear medicine to the coincidence mode (MCD system) and thus use this investigation more widely and more cost-effectively. For technical reasons, the resolution of the double head gamma camera is less than with the modern dedicated PET scanner.
In a prospective investigation this method was to be compared with the dedicated PET method with regard to its diagnostic accuracy.

Materials and Methods

Patients:
13 patients with Hodgkin's disease (7 female, 6 male, age 17 - 47 years) and 2 patients with high-grade NHL (1 female, 1 male, age 21 and 54 years) were investigated.
Blood glucose levels at the time of investigation were within physiological limits, none of the patients was diabetic.
Imaging procedures:
45 - 60 minutes after injection of 300 - 370 MBq ^{18}F-FDG, the patients were first investigated with dynamic positron emission tomography using a dedicated full-ring PET scanner (ECAT EXACT-HR+, Siemens) and afterwards with the double head gamma camera modified for coincidence detection (Solus EPIC, ADAC) for primary, recurrence and residual staging.

Results and Discussion

Whereas in the investigation of residual staging after chemotherapy and/or radiotherapy the results were consistent (7/5 cases), 3/10 patients were staged too low with the double head gamma camera according to the Ann Arbor classification (Table 1).

Table 1. Primary staging and restaging based on FDG imaging with the dual head coincidence system or the dedicated PET scanner

Stage	Dedicated PET	MCD system
I	0	0
II	3	6
III	4	3
IV	3	1

With the dedicated PET, 60 affected regions (lymph node regions or organ manifestations) were detected as compared to 46 with the double head gamma camera (Table 2, Fig. 1).

Table 2. Comparison of lesion detection with the dual head coincidence system and the dedicated PET scanner in various body regions.

Region	Dedicated PET	MCD system
cervical, supra-, infraclavicular	27	19
mediastinal, hilar	13	12
axilla	2	1
splenic hilum, porta of the liver	3	3
paraortal, iliacal	7	6
inguinal	2	1
spleen	2	2
bone marrow	1	1
skeleton	3	1
Σ	60	46 (77 %)

Fig. 1. A 20-year-old woman with recurrence of Hodgkin's disease. Several lymphomas were visualized with FDG. Pathological accumulation in the mediastinum and right parahilar region was only visualized with dedicated PET.

To summarize, the conventional double head gamma camera extended by the coincidence mode without attenuation correction cannot yet be recommended at least for primary staging.

Recently Zimny and colleagues investigated patients with suspected or known malignant diseases in a comparable setting. He summarized that MCD cannot yet replace dedicated PET in all oncological FDG studies [5]. Further technical refinement of the MCD method such as the introduction of attenuation correction is required to improve the image quality.

References

[1] Weber W. A., Avril N. and Schwaiger M. (1999) Relevance of positron emission tomography (PET) in oncology. *Strahlenther. Onkol.* **175**, 356-373.

[2] Bangerter M., Moog F., Buchmann I., Kotzerke J., Griesshammer M., Hafner M., Elsner K., Frickhofen N., Reske S. N. and Bergmann L. (1998) Whole-body 2-[^{18}F]-fluoro-2-deoxy-D-glucose positron emission tomography (FDG-PET) for accurate staging of Hodgkin's disease. *Ann. Oncol.* **9**, 1117-1122.

[3] Cremerius U., Fabry U., Neuerburg J., Zimny M., Osieka R. and Buell U. (1998) Positron emission tomography with 18F-FDG to detect residual disease after therapy for malignant lymphoma. *Nucl. Med. Commun.* **19**, 1055-1063.

[4] Jerusalem G., Beguin Y., Fassotte M. F., Najjar F., Paulus P., Rigo P. and Fillet G. (1999) Whole-body positron emission tomography using ^{18}F-fluorodeoxyglucose for posttreatment evaluation in Hodgkin's disease and non-Hodgkin's lymphoma has higher diagnostic and prognostic value than classical computed tomography scan imaging. *Blood.* **94**, 429-433.

[5] Zimny M., Kaiser H. J., Cremerius U., Sabri O., Schreckenberger M., Reinartz P. and Bull U. (1999) F-18-FDG positron imaging in oncological patients: gamma camera coincidence detection versus dedicated PET. *Nuklearmedizin* **38**, 108-114.

BRAIN BIOCHEMISTRY

4. Is the Lumped Constant a Real Constant?

H. Kuwabara[1], P. Brust
[1]Department of Neurosurgery, West Virginia University Morgantown, USA

Introduction

[^{18}F]Fluoro-deoxyglucose (FDG) is widely used for the measurement of glucose utilization in the brain with positron emission tomography (PET). The FDG-PET method requires a factor in order to correct for using FDG in place of native glucose in the measurement. The factor is often referred to as the "lumped constant" (LC) because the factor is a lumped effect of two constants of two independent systems, namely the transport ratio (τ or K_1^*/K_1) and the phosphorylation ratio (φ or k_3^*/k_3) [1]. (See Theory for the definitions of symbols.) In the brain, the value of τ is considered to be greater than one while the value of φ is considered to be significantly less than one (~0.3) [2, 3, 4]. This difference gives rise to a valid theoretical reason to expect that LC is a function of glucose concentration in plasma as described below. Thus, we examined the effects of glucose concentration in plasma on the value of LC in this project.

Theory

In the FDG-PET method, the regional glucose utilization, $rCMR_{glc}$ is given by:

$$rCMR_{glc} = K^* \cdot C_a / LC \qquad (1)$$

where K^* is the net clearance rate constant of FDG measured with PET, and C_a the concentration of glucose in plasma. Using τ and φ, LC is given by Kuwabara et al. [4]:

$$LC = \varphi + (\tau - \varphi)\frac{K^*}{K_1^*} \qquad (2)$$

where τ is the transport constant which is given by the unidirectional blood-brain clearance rate constant of FDG, K_1^*, over that of glucose, K_1 , and φ is given by the phosphorylation rate constant of FDG, k_3^*, over that of glucose, k_3. The equation indicates that LC is a real constant only when τ is equal to φ. It is reasonable to expect that K_1^* is more influenced by the plasma glucose concentration than K^* because K_1^* is related directly to the blood-brain transport of glucose while K^* is related both to transport and phosphorylation. Thus, it is likely that LC is influenced by the plasma glucose concentration [4].
In order to achieve our goal, it is necessary to obtain $rCMR_{glc}$ with an independent method. Unfortunately, $rCMR_{glc}$ is only accessible by the tracer method. However, the whole brain glucose utilization, $wCMR_{glc}$, is directly accessible. According to the Fick principle, $wCMR_{glc}$ of a steady state is given by:

$$wCMR_{glc} = \overline{F} \cdot (\overline{C}_a - \overline{C}_v) \qquad (3)$$

where $\overline{F}$ is the mean global blood flow, $\overline{C}_a$ and $\overline{C}_v$ are the mean glucose concentrations in the arterial and venous plasma. $\overline{C}_a$ can be replaced by C_a measured in plasma obtained from the femoral artery, and $\overline{C}_v$ by C_v measured in plasma obtained from the superior sagittal sinus, assuming blood from various brain regions is mixed well by the time it reaches the sampling site. $\overline{F}$ can be estimated in individuals in the same study as the glucose utilization measurement. When the Fick principle is applied to FDG, the rate of change in the whole brain radioactivity is given by:

$$dC_i^*(t)/dt = \overline{F} \cdot (\overline{C}_a^*(t) - \overline{C}_v^*(t)) \qquad (4)$$

where $C_i^*(t)$ is the whole brain radioactivity. When the equation is integrated from time 0 (FDG injection time) to T, the left hand side of the equation is given by $A^*(T) - v_0 \cdot C_a^*(T)$ where $\overline{A}^*(T)$ is the mean whole brain radioactivity measured with PET, v_0 the mean vascular volume in the tissue, and $C_a^*(t)$ the radioactivity in arterial plasma. $\overline{C}_a^*(t)$ can be replaced by $C_a^*(t)$ because there is little regional variation in $C_a^*(t)$. $\overline{C}_v^*(t)$ is not accessible because it is the mean radioactivity at the venous ends of capillaries. Assuming tiny tissue units, $\overline{C}_v^*(t)$ is related to the radioactivity at the venous ends of capillaries, $C_{v_i}^*(t)$, as follows:

$$\overline{C}_v^*(t) = \sum_{i=1}^{n} C_{v_i}^*(t)/n \tag{5}$$

We chose to sample venous blood at the distal end of the superior sagittal sinus. Let $\tilde{C}_{v_i}^*(t)$ denote the portion of the radioactivity due to $C_{v_i}^*(t)$ in plasma sampled at the site. $\tilde{C}_{v_i}^*(t)$ not only delays by Δt_i in timing relative to $C_{v_i}^*(t)$ due to the travel from the tissue to the sampling site but also is smeared (i.e., dispersion). According to the equation proposed by Iida et al. [5], $\tilde{C}_{v_i}^*(t)$ is related to $C_{v_i}^*(t)$ as follows:

$$C_{v_i}^*(t) = \tilde{C}_{v_i}^*(u) + \omega_i \cdot \frac{d\tilde{C}_{v_i}^*(u)}{du} \tag{6}$$

where u is equal to t+ Δt_i, and ω_i is the dispersion constant for the smearing of the radioactivity due to the travel. By integrating Equation 6 from time 0 to T, we obtain:

$$\int_0^T C_{v_i}^*(t)dt = \int_0^T \tilde{C}_{v_i}^*(u)du + \tilde{C}_{v_i}^*(T + \Delta t_i) \tag{7}$$

It is likely that both Δt_i and ω_i have normal distributions because the distances from the individual units to the sampling sites are likely to be distributed normally. Under these assumptions, $C_v^*(t)$ is related to $C_v^*(t)$ as follows:

$$\int \overline{C}_v^*(t)dt = \sum_{i=1}^{n} \left(\int_0^{T+\Delta t_i} \tilde{C}_{v_i}^*(u)du + \tilde{C}_{v_i}^*(T + \Delta t_i) \right) = \int_0^{T+\Delta t} \tilde{C}_v^*(u)du + \tilde{C}_v^*(T + \Delta t) \tag{8}$$

By substituting $\overline{C}_a^*(t)$ by $C_a^*(t)$, and $\overline{C}_v^*(t)$ by Equation 8 in the integration of Equation 4, we obtain:

$$A^*(T) - v_0 \cdot C_a^*(T) = \overline{F}\left(C_a^*(T) - \int_0^{T+\Delta t} \tilde{C}_v^*(u)du - \tilde{C}_v^*(T + \Delta t)\right) \tag{9}$$

There are three variables to estimate by the least squares method, namely $\overline{F}$, Δt, and ω in Equation 9, while $A^*(T)$ and $C_a^*(t)$ are measured in experiments, and v_0 is set to 0.035 ml/g.

Method

Data obtained in 22 pigs in a preceding paper were used [6]. Briefly, three rate constants of FDG, K_1^*, k_2^*, and k_3^*, and v_0 were estimated in 12 ROIs on each pig. The $rCMR_{glc}$ were calculated by Equation 1 where K^* of FDG was calculated as $K_1^* \cdot k_3^*/(k_2^* + k_3^*)$. The value of LC was set to 0.46 which was reported for the rat brain [1].

We estimated the whole brain blood flow using Equation 9 in 13 of the 22 pigs from which venous blood was taken successfully at the same schedule as arterial blood.

Results and Discussion

The $rCMR_{glc}$ averaged 19.7 ± 3.1 μmol/100g/min (mean ± SD) among 12 ROIs of 22 pigs. Individual $rCMR_{glc}$ were plotted against the mean concentrations of glucose in arterial plasma (0 - 45 minutes), C_a, in Fig. 1. These $rCMR_{glc}$ were not stable across C_a. They ($rCMR_{glc}$) were greater than the mean of all the ROIs in the pigs whose C_a was less than 2 μmol/ml. This sudden increase in calculated $rCMR_{glc}$ at low plasma glucose levels may or may not accompany an increase in the true $rCMR_{glc}$. For example, if the true $rCMR_{glc}$ remain unchanged, our observation should be an artifact due to using a fixed value for the lumped constant while adjustment in the value is appropriate. In fact, Crane et al. reported a sudden increase in K_1^* of [^{3}H]deoxy-glucose relative to K of [^{14}C]glucose when the brain glucose concentration was reduced below 0.5 μmol/g (which corresponded to 2 μmol/ml in plasma glucose concentration) [6]. The authors explained that, at a very low brain (and plasma) glucose level, the K_1^*-K ratio was close to τ because $rCMR_{glc}$ and the net uptake of [^{3}H]deoxyglucose were limited by blood-brain transport (i.e., transported glucose and tracer were immediately phosphorylated). When brain glucose content was above 0.5 μmol/g, the authors found the K_1^*-K ratio invariant. Our finding was in contrast to this. Calculated $rCMR_{glc}$ increased as a function of C_a between 3.5 and 11 μmol/ml ($rCMR_{glc} = 1.14 \cdot C_a + 11.7$, r^2=0.600. The regression line is shown in Fig. 1). Although the slope is close to unity, the equation indicated that calculated $rCMR_{glc}$ at 10 μmol/ml (23.1 μmol/100g/min) was about 42 % greater than calculated $rCMR_{glc}$ at 4 μmol/ml (16.3 μmol/100g/min) if a fixed value of LC was used. This finding indicated that it is necessary to adjust LC according to plasma glucose levels even within commonly encountered plasma glucose levels.

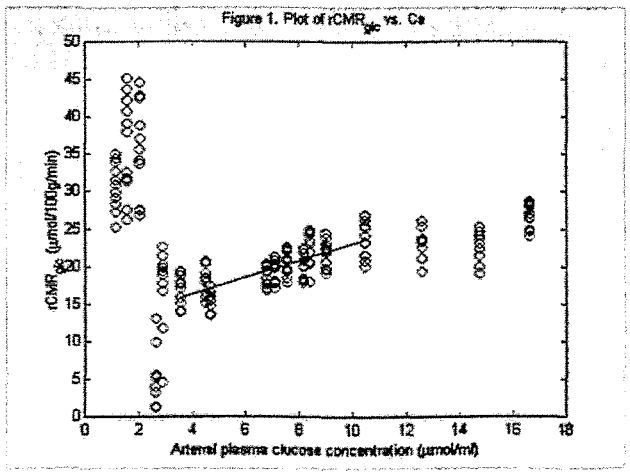

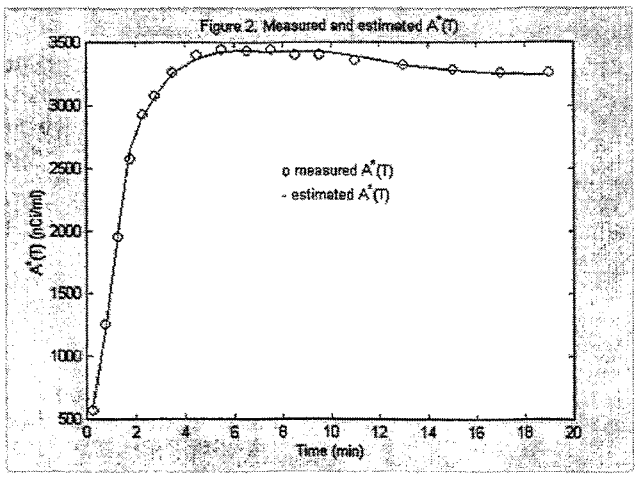

In the process of estimating the whole brain blood flow, calculated radioactivity in the brain using Equation 9 (Fig. 2, shown with the solid curve) was close to measured radioactivity (circles) in all 13 pigs. The whole brain blood flow averaged 35.5 ± 10.6 ml/100g/min. We found a relatively large coefficient of variation in the values (30 %). There are several explanations for the large variance. First, arterial blood was sampled not from the arterial end of brain capillaries but from the femoral artery. Measured C_a^* was modified to account for this fact using two constants similar to Δt and ϖ defined for the venous blood. The two constants were estimated for the whole brain. The error on the estimation may have propagated to the estimation of the whole brain blood flow. Second, sampled blood from the superior sagittal sinus may not reflect the average of the whole brain. Venous blood samples may have been contaminated by blood from outside the brain. The arterio-venous difference in glucose concentration was 0.64 ± 0.21 μmol/ml. It was our surprise to find a relatively large coefficient of variation also in this variable (34%). The measurements were made in duplication and values were in close agreement among duplications. Again it was not certain whether venous blood obtained through the catheter reflects samples from the same brain regions among pigs, although we tried to place the tip of the catheter in a fixed place (5 cm posterior to the bregma). The product of the whole brain blood flow and the arterio-venous glucose concentration difference, $wCMR_{glc}$ by the Fick principle (Equation 3), was 23.2 ± 11.9 μmol/100g/min (coefficient of variation: 51.5%). The large variation precluded detailed examination of the relationship between $wCMR_{glc}$ and the plasma glucose level. In the 13 pigs, the product of $K^*$and C_a averaged 9.1 ± 2.2 μmol/100g/min. We found the value of LC to be 0.39 (ratio) in this experiment to equate $wCMR_{glc}$ by the Fick principle and $wCMR_{glc}$ by Equation 1.

Summary

1. Calculated $rCMR_{glc}$ increased as a function of C_a between 3.5 and 11 μmol/ml ($rCMR_{glc}$ = 1.14 · C_a +11.7, r^2=0.600) when a fixed LC was used. Thus, there is a need for adjusting LC according to plasma glucose levels.
2. When plasma glucose was below 2 μmol/ml, there was a sudden increase in calculated $rCMR_{glc}$. This phenomenon suggested that $rCMR_{glc}$ and the net uptake of FDG were limited by the transport at very low glucose levels.
3. We demonstrated that the whole brain blood flow could be estimated with the FDG-PET method. However, a large variance in calculated $wCMR_{glc}$ by the Fick principle precluded detailed comparisons of $wCMR_{glc}$ with plasma glucose levels.

References

[1] Sokoloff L., Reivich M., Kennedy C., Des Rosiers M. H., Patlak C. S., Pettigrew K. D., Sakurada O. and Shinohara M. (1977) The [^{14}C]deoxyglucose method for the measurement of local cerebral glucose utilization: theory, procedure, and normal values in the conscious and anesthetized albino rat. *J. Neurochem.* **28**, 897-916.

[2] Cunningham V. J. and Cremer J. E. (1981) A method for the simultaneous estimation of regional rates of glucose influx and phosphorylation in rat brain using radiolabeled 2-deoxyglucose. *Brain Res.* **221**, 319-330.

[3] Crane P. D., Pardridge W. M., Braun L. D. and Oldendorf W. H. (1983) Kinetics of transport and phosphorylation of 2-fluoro-2-deoxy-D-glucose in rat brain. *J. Neurochem.* **40**, 160-167.

[4] Kuwabara H., Evans A. C. and Gjedde A. (1990) Michaelis-Menten constraints improved cerebral glucose metabolism and regional lumped constant measurements with [^{18}F]fluorodeoxyglucose. *J. Cereb. Blood Flow Metab.* **10**, 180-189.

[5] Iida H., Kanno I., Miura S., Murakami M., Takahashi K. and Uemura K. (1986) Evaluation of regional differences of tracer appearance time in cerebral tissue using [15O]water and dynamic positron emission tomography. *J. Cereb. Blood Flow Metab.* **6**, 536-545.

[6] Crane P. D., Pardridge W. M., Braun L. D., Nyerges A. M. and Oldendorf W. H. (1981) The interaction of transport and metabolism on brain glucose utilization: a reevaluation of the lumped constant. *J. Neurochem.* **36**, 1601-1604.

5. Blood-Brain Transport of Glucose Studied with [^{11}C]3-*O*-Methylglucose and [^{18}F]Fluorodeoxyglucose

H. Kuwabara[1], P. Brust, R. Bergmann, P. Mäding, J. Steinbach
[1]Department of Neurosurgery, West Virginia University Morgantown, USA

Introduction

The blood-brain transport of glucose may be involved in the pathophysiology of some neurological diseases including Alzheimer's disease [1]. The transport makes it possible for glucose, the brain's sole energy source, to enter the brain. In this project, we examined which tracer was more suitable for investigating blood-brain glucose transport, [^{18}F]fluoro-deoxyglucose (FDG) or [^{11}C]3-*O*-methylglucose (OMG). FDG is widely used for measurements of glucose metabolism in the brain. FDG has two fates in the brain, namely being phosphorylated and trapped in the brain or being transported back to the circulation. This dual-fate feature made the estimates of the unidirectional blood-brain clearance of FDG, a measure of glucose transport, uncertain [2]. In contrast, OMG has only one fate in the brain because it is not metabolized [3,4]. Thus, OMG is expected to yield accurate estimates of glucose transport.

Theory

The unidirectional blood-brain clearance rate constant of FDG and OMG (K_1^*) is relevant to the blood-brain transport of glucose because glucose and tracer compete for the saturable transport. It was demonstrated repeatedly by several authors that the Michaelis-Menten equation describes the facilitated transport of glucose in animal experiments [5,6]. Accordingly, (K_1^*) is related to the maximal transport of OMG or FDG (T^*_{max}), the half saturation constants of glucose and OMG or FDG (K_t and K_t^*), and the concentration of glucose in plasma (C_a) by the following equation [7] (Symbols with stars are of radiotracer and those without stars are of glucose throughout the text):

$$K_1^* = \frac{T^*_{max}}{K_t^*(1 + C_a/K_t)} \qquad \ldots(1)$$

In the derivation of the equation, the concentration of OMG or FDG in plasma was considered negligible compared to C_a. The equation can be rearranged as follows:

$$K_1^* = \frac{T'_{max}}{K_t + C_a} \qquad \ldots(2)$$

where T'_{max} is equal to $T^*_{max} \cdot K_t/K_t^*$. The two constants T'_{max} and K_t can be estimated using a plot of K_1^* versus C_a. It is not practical to repeat measurements of K_1^* in one individual an adequate number of times to estimate the constants (at least at six concentrations). Therefore, we measured K_1^* in a group of pigs at varying concentrations of plasma glucose and estimated the constants, assuming that the constants are common among individuals.

The ratio of K_1^* to the brain-blood clearance rate constant (k_2^*) is another variable which is relevant to the blood-brain transport of glucose. According to the Michaelis-Menten equation, the ratio, denoted by V_e, is common between glucose and the radiotracer and given by [8]:

$$V_e = \frac{K_1}{k_2} = \frac{K_1^*}{k_2^*} = \frac{K_t + M_e}{K_t + C_a} \qquad \ldots(3)$$

where M_e is the content of free glucose in a brain region. (Strictly speaking, we need to differentiate the content as M_e and the concentration as C_a. We will treat them equally for the sake of simplicity in this paper). Separately, the glucose utilization of the region is given by:

$$c = K_1 \cdot C_a - k_2 \cdot M_e \qquad \ldots(4)$$

Eliminating $k_2 \cdot M_e$ using Equations (3) and (4), we obtain the following equation:

$$V_e = \frac{1}{1 + c/[K_1 \cdot K_t]} \qquad \ldots(5)$$

Complete derivation of the equation can be found in a paper under preparation. Substituting K_1 with $T_{max}/(K_t + C_a)$, we obtain the following equation:

$$V_e = \frac{[T_{max} \cdot K_t / c]}{[T_{max} \cdot K_t / c] + K_t + C_a} \qquad \ldots(6)$$

Thus, we can estimate $[T_{max} \cdot K_t/c]$ and $[T_{max} \cdot K_t/c] + K_t$ from a plot of V_e versus C_a, assuming common values among individual pigs for the two constants.

Methods

We studied 22 pigs (~6 weeks old, body weight ~20 kg) in this project. Under isoflurane anesthesia, each pig underwent one OMG-PET scan and, 4 hours later, one FDG-PET scan. All pigs were on a fast at least one day prior to the study. Concentrations of glucose in plasma were reduced in 6 pigs by subcutaneous injection of insulin (~5 I.U.) and increased in 9 pigs by means of intravenous bolus injections of 20 % glucose, which were followed by a continuous infusion of 5 – 20 % glucose. In the remaining 7 pigs, no attempts were made to modify the plasma glucose concentration. In all pigs, plasma glucose levels were monitored at intervals ranging between 5 and 10 minutes. In experiments in which plasma glucose levels were modified, glucose levels were maintained starting 30 minutes before tracer injection throughout the PET experiments by means of additional subcutaneous insulin or adjustments of glucose infusion rates.

PET studies started with a slow-bolus injection of OMG (465 ± 146 MBq, in 5 ml saline) or FDG (998 ± 167 MBq in 5-10 ml saline) over 30 seconds or one minute into the vein. PET data acquisition was also started at the start of the injection (time 0). A total of 26 frames were recorded with the Siemens EXACT HR+ PET across 60 minutes. There were 6 thirty-second frames, followed by 7 one-minute frames, 5 two-minute frames, and 8 five-minute frames. Arterial blood was sampled from the femoral artery and venous blood was sampled from the superior sagittal vein. Both arterial and venous blood was withdrawn with pumps at a constant speed for the first 20 minutes. Blood samples were collected into test tubes every 20 seconds for the first 6 minutes and every minute thereafter. Blood samples were taken manually every 5 minutes after 20 minutes. Samples were immediately placed on ice. Concentrations of glucose in arterial and venous plasma were determined every 5 minutes by the ECA PD 10 automated glucose analyzer. The radioactivity in plasma was determined with the Wallac 1480 Wizard 3" automated gamma counter which was cross-calibrated with the PET.

We obtained the radioactivity in brain regions as functions of time, $A^*(T)$, as follows: First, templates of regions of interest (ROIs) were defined for left and right frontal, temporal, parietal, and occipital lobes, basal ganglia, and cerebellum on magnetic resonance images of a pig (12 ROIs). Then, the templates were modified in space for the orientation and sizes of the individual pig's brain. The individualized templates were repeatedly applied on individual PET frames to obtain $A^*(T)$. $A^*(T)$ was expressed in nCi/ml after being corrected for physical decay of the isotope to time 0. The radioactivity in arterial plasma, $C^*_a(t)$, was expressed in nCi/ml with decay correction. Also prepared were glucose concentrations in arterial blood, which were the means of the five samples taken during the first 20 minutes. It is known that the estimates of K_1^* were determined largely by the data obtained during the first 20 minutes [2].

The regional rate constants of OMG were estimated by the mean of the least squares method using the following equation:

$$A^*(T) = K_1^* \cdot \int_0^T C_a^*(t) \cdot e^{-k_2^*(t-T)} dt + V_0 \cdot C_a^*(T) \quad ...(7)$$

where V_0 is the effective vascular volume of the region. The regional rate constants of FDG were estimated using the following equation:

$$A^*(T) = K^* \int_0^T C_a^*(t) dt + (K_1^* - K^*) \cdot \int_0^T C_a^*(t) \cdot e^{-(k_2^*+k_3^*)\cdot(t-T)} dt + V_0 \cdot C_a^*(T) \quad ...(8)$$

where k_3^* is the phosphorylation rate constant of FDG and K^* is the net clearance rate constant of FDG, which is equal to $K_1^* \cdot k_3^* / (k_2^* + k_3^*)$.

Results and Discussion

Estimates of K_1^* of OMG (left panel) and FDG (right panel) were plotted against plasma glucose level in Fig. 1, for the right parietal lobe. The curves indicate the best fit to the data by Equation (2). Among 12 ROIs, estimates of T'_{max} of OMG averaged 0.79 ± 0.04 μmol/g/min (mean ± SD, range: 0.74-0.86 μmol/g/min), and T'_{max} of FDG averaged 2.2 ± 0.22 μmol/g/min (range: 1.9-2.6 μmol/g/min). Recently, Van Zijl et al., reported a value of 0.83 ± 0.19 μmol/g/min for T'_{max} of [1-13C]glucose in the cat brain with a fixed K_t (5 μmol/ml) using magnetic resonance spectroscopy [9]. According to Crane et al, T'_{max} of FDG was calculated as1.06 μmol/g/min in the rat brain [10]. These values were in agreement with our value for OMG. Estimates of K_t of glucose averaged 7.1 ± 0.8 μmol/ml (range: 6.2 - 9.0 μmol/ml) in OMG experiments, and 15.6 ± 2.1 μmol/ml (range: 13.0-18.7 μmol/ml) in FDG experiments. Crane et al. reported a value of 11.0 μmol/ml for the rat brain which is in agreement with our values by OMG [10]. The corrected residual square sums (residual square sum over mean K_1^*) were significantly greater for FDG experiments than for OMG experiments (t=-11.7, paired t test). This finding confirmed that estimates of K_1^* by FDG suffered uncertainty. It was speculated that the uncertainty, especially in lower glucose levels, explained the differences between T'_{max} as well as between K_t obtained by the two tracers, as discussed later. Assuming the values obtained by OMG were correct, K_t of glucose obtained in OMG experiments was greater than those reported for human and animal experiments (~4.8 mM). There are several reasons to explain the differences. In previously published experiments, solutions of varying glucose concentrations were injected into the carotid artery as boluses together with reference markers to obtain plots of K_1^* versus glucose concentration [4, 5]. In this project, we chose to maintain plasma glucose level constant throughout the measurements of K_1^* of OMG or FDG with PET in order to make the experimental conditions close to the physiology.

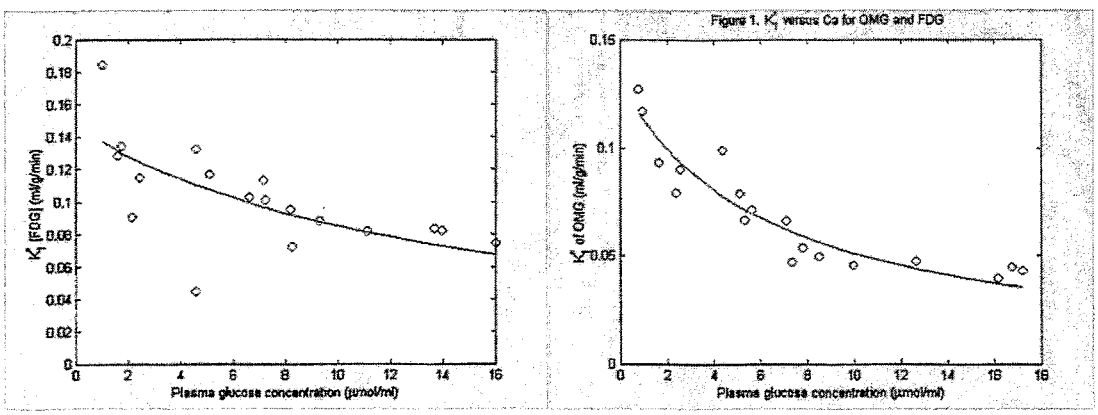

In Fig. 2, estimates of V_e of OMG (left panel) and FDG (right panel) were plotted against plasma glucose levels. The lines indicate the best fit to the data by Equation (6). Regional estimates of $[T_{max} K_t/c]$ averaged 7.1 ± 0.29 μmol/ml (range: 6.6 - 7.5 μmol/ml) in OMG experiments, and –0.48 ± 0.81 μmol/ml (range: -1.5-0.30 μmol/ml) in FDG experiments. Regional estimates of $[T_{max} \cdot K_t/c] + K_t$ averaged 14.5 ± 0.58 μmol/ml (range: 13.6 - 15.3 μmol/ml) in OMG experiments, and 4.9 ± 3.5 μmol/ml (range: 1.6 - 10.9 μmol/ml) in FDG experiments. The estimate of K_t which was given by the difference of the two estimates was 7.4 ± 0.3 μmol/ml (range: 6.9 - 7.8) by OMG, and –4.2±1.8 μmol/ml (range: -7.0 - -2.4) by FDG. The regional values of K_t yielded by the V_e - C_a plots were very close to K_t given by the K_1^* - C_a plots with OMG. In contrast, K_t given by the two plots of FDG were incomparable. Values of V_e were greater by several folds obtained by FDG than when obtained by OMG at lower C_a (<4 μmol/ml). The finding confirmed the uncertainty of rate constants obtained with FDG. Our results indicated that V_e of OMG may be used to characterize blood-brain transport of glucose. For example, changes in K_t due to a pathophysiology may be detected by this method. However, it is questionable whether changes in T_{max} can be detected because the other constant, $[T_{max} \cdot K_t/c]$, also includes other two variable which are subject to changes in neurological conditions. The advantage of this method is that V_e may be estimated as the ratio of the radioactivity in brain regions to the radioactivity in plasma when OMG is in a near steady state (some times after OMG injection) without arterial blood sampling. This feature makes the method especially useful to studying elderly, diseased subjects.

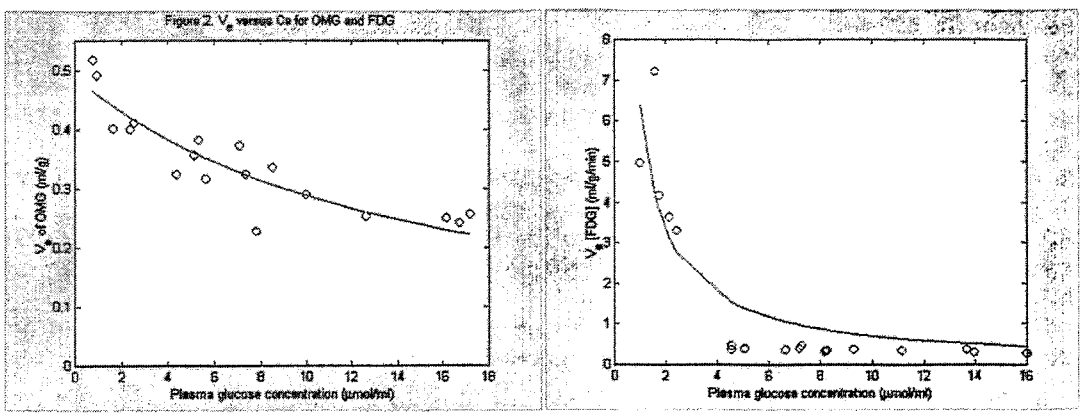

Summary

1. Blood-brain transport of glucose was described by the Michaelis-Menten equation when it was studied with [^{11}C]3-*O*-methylglucose and PET.
2. Estimates of K_1^* and V_e of FDG suffered uncertainty when tested by the Michaelis-Menten equation. Thus, [^{11}C]3-*O*-methylglucose should be used to investigate blood-brain glucose transport.
3. K_1^* itself does not give information on the blood-brain transport of glucose because K_1^* is a function of plasma glucose level. It requires two Michaelis-Menten constants to characterize the blood-brain transport of glucose.

References

[1] Piert M., Koeppe R. A., Giordani B., Berent S. and Kuhl D. E. (1996) Diminished glucose transport and phosphorylation in Alzheimer's disease determined by dynamic FDG-PET. *J. Nucl. Med.* **37,** 201-208.

[2] Kuwabara H., Evans A. C. and Gjedde A. (1990) Michaelis-Menten constraints improved cerebral glucose metabolism and regional lumped constant measurements with [^{18}F]fluorodeoxyglucose. *J. Cereb. Blood Flow Metab.* **10,** 180-189.

[3] Vyska K., Magloire J. R., Freundlieb C., Hock A., Becker V., Schmid A., Feinendegen L. E., Kloster G., Stöcklin G. and Schuier F. J. (1985) In vivo determination of the kinetic parameters of glucose transport in the human brain using ^{11}C-methyl-D-glucose (CMG) and dynamic positron emission tomography (dPET). *Eur. J. Nucl. Med.* **11,** 97-106.

[4] Brooks D. J., Beaney R. P., Lammertsma A. A., Herold S., Turton D. R., Luthra S. K., Frackowiak R. S., Thomas D. G., Marshall J. and Jones T. (1986) Glucose transport across the blood-brain barrier in normal human subjects and patients with cerebral tumours studied using [^{11}C]3-*O*-methyl-D-glucose and positron emission tomography. *J. Cereb. Blood Flow Metab.* **6,** 230-239.

[5] Pardridge W. M. and Oldendorf W. H. (1975) Kinetics of blood-brain transport of hexoses. *Biochim. Biophys. Acta* **382,** 377-392.

[6] Cremer J. E., Cunningham V. J., Pardridge W. M., Braun L. D. and Oldendorf W. H. (1979) Kinetics of blood-brain barrier transport of pyruvate, lactate and glucose in suckling, weanling and adult rats. *J. Neurochem.* **33,** 439-445.

[7] Sokoloff L., Reivich M., Kennedy C., Des Rosiers M. H., Patlak C. S., Pettigrew K. D., Sakurada O. and Shinohara M. (1977) The [^{14}C]deoxyglucose method for the measurement of local cerebral glucose utilization: theory, procedure, and normal values in the conscious and anesthetized albino rat. *J. Neurochem.* **28,** 897-916.

[8] Gjedde A. and Diemer N. H. (1983) Autoradiographic determination of regional brain glucose content. *J. Cereb. Blood Flow Metab.* **3,** 303-310.

[9] Van Zijl P. C., Davis D., Eleff S. M., Moonen C. T., Parker R. J. and Strong J. M. (1997) Determination of cerebral glucose transport and metabolic kinetics by dynamic MR spectroscopy. *Am. J. Physiol.* **273,** E1216-E1227.

[10] Crane P. D., Pardridge W., Braun L. D. and Oldendorf W. H. (1983) Kinetics of transport and phosphorylation of 2-fluoro-2-deoxy-D-glucose in rat brain. *J. Neurochem.* **40,** 160-167.

6. Regional Estimation of Michaelis-Menten Constants of Blood-Brain Glucose Transport in Single Subjects with [^{11}C]3-*O*-Methylglucose

H. Kuwabara[1], P. Brust, P. Mäding, R. Bergmann, J. Steinbach
[1]Department of Neurosurgery, West Virginia University Morgantown, USA

Introduction

It is generally believed that the unidirectional blood-brain clearance rate constant of [^{18}F]fluoro-deoxyglucose (FDG) (K_1^*) is a usable index of blood-brain glucose transport [1]. In a preceding study [2], we demonstrated that [^{11}C]3-*O*-methylglucose (OMG) yielded more accurate estimates of K_1^* than did FDG, and that K_1^* is a function of plasma glucose level with two constants, namely relative maximal transport of OMG (T'_{max}) and the half-saturation constant of glucose (K_t) of the Michaelis-Menten equation. In that study, the two constants were estimated in a group of pigs with different plasma glucose concentrations, assuming common values for the constants among individuals.

In this study, we examined whether the two constants could be estimated regionally in a single subject with acceptable accuracy when subjects are scanned with OMG twice at different glucose levels. It is expected that such a method is useful to detect changes in blood-brain glucose transport in pathological conditions.

Theory

According to the Michaelis-Menten equation for blood-brain glucose transport, K_1^* of OMG is given by [2,3]:

$$K_1^* = \frac{T'_{max}}{K_t + C_a} \tag{1}$$

where C_a is the glucose concentration in plasma. By rearranging this equation, we obtain:

$$T'_{max} = K_1^* \cdot (K_t + C_a) \tag{2}$$

When K_1^* is measured at two plasma glucose concentrations, T'_{max} and K_t are given as solutions of the following equations:

$$\begin{aligned} T'_{max} &= K_1^*[1^{st}] \cdot (K_t + C_a[1^{st}]) \\ T'_{max} &= K_1^*[2^{nd}] \cdot (K_t + C_a[2^{nd}]) \end{aligned} \tag{3}$$

where [1st] and [2nd] are to denote that variables are obtained in the 1st and 2nd OMG-PET studies, respectively.

Methods

We studied 6 young pigs (~6 weeks old; body weight ~20 kg) under isoflurane anesthesia in this study. Each pig was studied with OMG and PET twice, at low and high plasma glucose levels. Prior to the first OMG experiment, blood glucose level was lowered by subcutaneous injection of insulin (~5 I.U.) and maintained throughout the experiment. Then, blood glucose level was increased by means of an intravenous bolus injection of 20 % glucose, and maintained by a continuous infusion of 5 – 20 % glucose throughout the second OMG experiment. PET procedures which were identical for the two studies, can be found elsewhere[2]. Briefly, at time 0, a slow bolus injection of OMG, over one minute, was administered and PET scanning was started. A total of 26 PET frames were taken across 60 minutes. Arterial blood was sampled frequently at the beginning and at prolonged intervals toward the end of the study.

Standard ROI templates were adjusted in locations and sizes to individual pigs. The radioactivity was obtained as a function of time in 12 brain regions by applying modified standard ROI templates on successive PET frames. The ROIs included left and right frontal, temporal, parietal, and occipital lobes, basal ganglia, and cerebellum.

The unidirectional blood-brain and brain-blood clearance rate constants (K_1^* and k_2^*, respectively) of OMG were estimated by least squares optimization using the following equation:

$$A^*(T) = K_1^* \int_0^T C_a^*(t) \cdot e^{-k_2(T-t)} dt + v_o \cdot C_a^*(T) \qquad (4)$$

where $A^*(T)$ is the radioactivity in a brain region measured with PET, $C_a^*(t)$ the radioactivity in arterial plasma, and v_0 the effective vascular volume in the region. The product of $v_0 \cdot C_a^*(t)$ is used to subtract the radioactivity in the vascular space.
In one analysis, we estimated regional values of T'_{max} and K_t by Equation 1, assuming common values across individual pigs. In the other analysis, we estimated the constants by Equation 3 for individual regions in each pig.

Results and Discussion

Regional estimates of T'_{max} by Equation 3 averaged 0.83 ± 2.6 μmol/g/min and K_t averaged 7.7 ± 36 μmol/ml. We found that one pig was responsible for the large variance. In this pig, plasma glucose concentrations were 4.7 μmol/ml in one experiment and 3.8 μmol/ml in the other experiment while the differences ranged from 7.7 to 8.9 μmol/ml in the remaining experiments. Thus, this pig was excluded from the calculation of T'_{max} and K_t when Equation 3 was used. Regional estimates of the two constants are shown in the Table below together with the values obtained by Equation 1 [2].

Table 1. Regional estimates of T'_{max} and K_t obtained by one OMG-PET study

	T'_{max} (μmol/g/min)		K_t (μmol/ml)	
Regions	Equation 1	Equation 3	Equation 1	Equation 3
Frontal lobe	1.01	1.09 ± 0.21	9.3	10.2 ± 2.4
Temporal lobe	1.05	1.16 ± 0.34	12.5	13.8 ± 4.4
Parietal lobe	1.06	1.12 ± 0.19	10.5	11.2 ± 2.2
Occipital lobe	1.00	1.07 ± 0.20	10.4	11.3 ± 2.3
Basal ganglia	1.06	1.18 ± 0.45	13.1	14.8 ± 6.8
Cerebellum	1.01	1.12 ± 0.36	9.9	11.3 ± 4.7
Mean	1.03 ± 0.03	1.12 ± 0.04*	10.9 ± 1.5	12.1 ± 1.8*

* Values by Equation 3 are greater than values by Equation 1 (paired t-test, $p < 0.001$).

Regional estimates of T'_{max} by Equation 3 (=y) correlated with the estimates by Equation 1 (=x) ($y = 1.16 \cdot x - 0.08$, $r^2 = 0.721$), although the estimates by Equation 3 were significantly greater than the estimates by Equation 1 ($t = 9.63$, $p < 0.001$, paired t-test). We found a range of coefficients of variations (COVs) among individual pigs between 17 and 37 %. With a 17 % COV, 9 subjects are needed to detect a 30 % change in T'_{max} at a power of 0.8, a commonly accepted level [4]. With a 37% COV, such a change cannot be detected with that 0.8 confidence level, and 16 pigs are needed to detect a 50% change in T'_{max}. Regional estimates of K_t by Equation 3 (=y) correlated with the estimates by Equation 1 (=x) ($y = 1.15 \cdot x - 0.45$, $r^2 = 0.975$). The estimates by Equation 3 were significantly greater than the estimates by Equation 1 ($t = 7.94$, $p < 0.001$, paired t-test). Regional COVs among individual pigs ranged from 20 % to 46 %. With a 20 % COV, 12 pigs are needed to detect a 30 % change in K_t at the 0.8 confidence level. With a 46 % COV, even 50 % change cannot be detected. Thus, the proposed method may not be used to compare K_t between two groups unless the difference between the groups is expected to be greater than 50 %.

We found that both T'_{max} and K_t of this study were significantly greater than those estimates obtained using Equation 1 in the preceding study. In order to understand the reason for the differences, regional estimates of K_1^* of OMG were plotted against plasma glucose concentration in Fig. 1. The curve in the figure demonstrates K_1^* calculated by Equation 1 using the mean estimates of T'_{max} (0.79 μmol/g/min) and K_t (7.1 μmol/ml) of the preceding study. Estimates of K_1^* of this study distributed across plasma glucose levels in a similar manner to K_1^* of the preceding study. However, K_1^* values of this study were below the curve in a majority of regions at lower plasma glucose levels (<3 μmol/ml) and above the curve in a majority of regions at higher glucose levels (>8 μmol/ml). In short, K_1^* values of this study changed less with plasma glucose concentration than K_1^* values of the preceding study, which made both estimates greater. Fig. 2 illustrates this phenomenon for the right parietal lobe. In the figure, individual K_1^* values of this study were plotted against the plasma glucose concentration with open circles together with a solid curve indicating predicted K_1^* by Equation 1 (T'_{max} and K_t in Table), and K_1^* values of the preceding study with crosses with a dotted curve for predicted K_1^* (T'_{max} = 0.78 μmol/g/min and K_t = 6.7 μmol/ml). There are two possible explanations for the differences in the estimates between the two studies. First, the range of plasma glucose concentrations in the preceding study was about 50 % larger than the range of this study. Second, the variations in K_1^* values were relatively large in each study at lower glucose levels (<3 μmol/ml). K_1^* values ranged between 0.065 and 0.113 ml/g/min for this study and between 0.061 and 0.128 ml/g/min for the preceding study. In order to cope with potential errors caused by the large K_1^* variance at low plasma glucose levels,

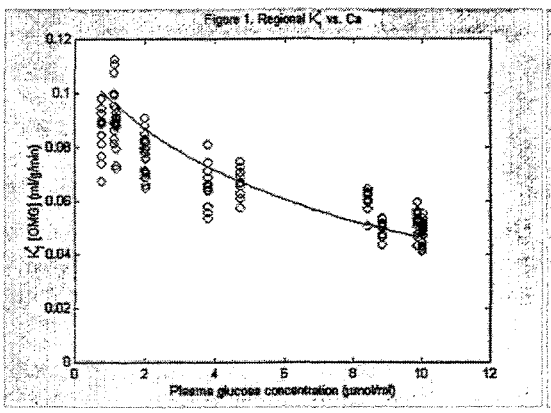

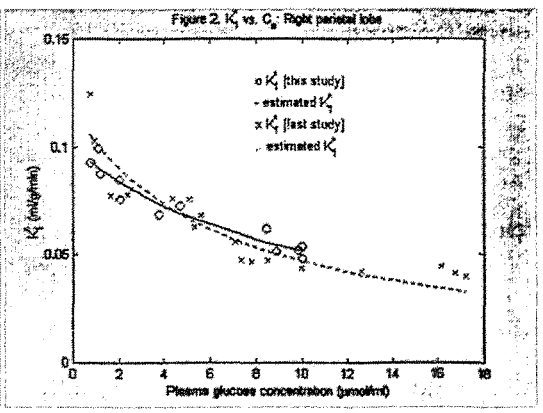

Equation 1 was modified as follows:

$$\frac{1}{K_1^*} = \frac{1}{T'_{max}} \cdot C_a - \frac{K_t}{T'_{max}} \qquad (5)$$

This equation may be less sensitive to the variations in K_1^* values at lower glucose levels because the contributions by high K_1^* values on the residual square sum decrease when inverted. Using Equation 5, we obtained 1.05 ± 0.06 μmol/g/min for T'_{max} and 11.3 ± 1.8 μmol/ml for K_t in this study, and 1.09 ± 0.10 μmol/g/min for T'_{max} and 12.1 ± 1.8 μmol/ml for K_t in the preceding study. There were no significant differences between the two studies for both constants. It is premature to conclude which equation is more accurate at this point.

Summary

1. Two Michaelis-Menten constants of blood-brain glucose transport T'_{max} and K_t can be estimated in individual subjects with two [^{11}C]3-O-methylglucose-PET studies at high and low plasma glucose levels.
2. Due to relatively large variances among individual regional estimates of T'_{max} and K_t, it is important to consider sample sizes when planning experiments.
3. An alternative linear equation (Equation 5) may be robust against a large variance in K_1^* at lower glucose levels.

References

[1] Schmidt K. C., Lucignani G. and Sokoloff L. (1996) Fluorine-18-fluorodeoxyglucose PET to determine regional cerebral glucose utilization: a re-examination. *J. Nucl. Med.* **37**, 394-399.

[2] Kuwabara H., Brust P., Bergmann R., Mäding P. and Steinbach J. (1999) Blood-brain transport of glucose studied with [^{11}C]3-O-methylglucose and [^{18}F]fluoro-deoxyglucose. *This report*, pp. 18-22.

[3] Sokoloff L., Reivich M., Kennedy C., Des Rosiers M. H., Patlak C. S., Pettigrew K. D., Sakurada O. and Shinohara M. (1977) The [^{14}C]deoxyglucose method for the measurement of local cerebral glucose utilization: theory, procedure, and normal values in the conscious and anesthetized albino rat. *J. Neurochem.* **28,** 897-916.

[4] Keppel G. (1973) Design and analysis: A researcher's handbook. *Printice-Hall*, Inc Englewood Cliffs, NJ, pp. 70-76.

7. Relationship between Brain Tissue pO_2 and Dopamine Synthesis of the Basal Ganglia

R. Bauer[1], P. Brust, B. Walter[1], G. Vorwieger, R. Bergmann, F. Füchtner, J. Steinbach, E. El-Hallag[1], A. Fritz[1], U. Zwiener[1], B. Johannsen
[1]Institute of Pathophysiology, Friedrich Schiller University Jena

Introduction

It is now firmly established that both excitotoxicity and oxygen radical-mediated processes contribute prominently to the pathophysiology of perinatal hypoxic-ischemic brain injury [1, 2]. The striatum, innervated with interacting corticostriatal glutaminergic and nigrostriatal dopaminergic projections, is a structure particularly susceptible to ischemic/hypoxic neuronal damage during perinatal period [3]. This may be caused by early hyperactivity of both transmitter systems due to O_2 lack. The dopaminergic system in immature brains is obviously sensitive to changes in brain tissue oxygen tension ($t_{brain}pO_2$) because even small decrease of $t_{brain}pO_2$ will cause significant increase in striatal extracellular dopamine concentration [4]. The reason behind this phenomena remains quite unclear. From findings in studies on newborn rats it was postulated that hypoxia may increase the releasable dopamine pool [5]. However, other data suggested that mild hypoxia-induced extracellular dopamine increase resulted from inhibition of re-uptake [6].
Until now no in vivo measurements were made of dopamine metabolism in the newborn brain. Therefore, we estimated the activity of the aromatic amino acid decarboxylase (AADC), the ultimate enzyme in dopamine synthesis, in relation to $t_{brain}pO_2$, regional cerebral blood flow (CBF) and cerebral metabolic rate of oxygen ($CMRO_2$) during normal conditions and asphyxia in newborn piglets. We postulate that the changes in brain oxidative metabolism may induce profound effects on striatal dopamine synthesis in newborn brain.

Material and Methods

The animal experiments were performed according to the German Law on the Protection of Animals. The study was approved by the committee of the Saxon state government for animal research (75-9185.81-4.6/95). Methods were described in detail elsewhere [7-10].

Results

Table 1. Hemodynamic values, arterial blood gases, acid-base balance, metabolic and regional cerebral blood flow values for newborn piglets during normoxia and asphyxia.

	Normoxia	Control 2	Asphyxia
MAP (mm Hg)	72 ± 6	66 ± 24	78 ± 14
Heart rate (min^{-1})	241 ± 45	240 ± 43	293 ± 75 *
Arterial pCO_2 (mm Hg)	37 ± 2	38 ± 3	73 ± 2 **
Arterial pH	7.48 ± 0.03	7.47 ± 0.01	6.98 ± 0.09 **
Arterial pO_2 (mm Hg)	121 ± 32	120 ± 29	39 ± 6 **
Arterial base excess (mmol • l^{-1})	4 ± 2	4 ± 1	-13 ± 4 **
Arterial glucose (mmol • l^{-1})	7.5 ± 1.0	7.6 ± 1.2	9.0 ± 4.4
Arterial lactate (mmol • l^{-1})	2.4 ± 1.5	2.4 ± 1.2	13.5 ± 3.9 **
Cortical CBF (ml • 100 g^{-1} • min^{-1})	73 ± 24	61 ± 15	191 ± 88 **
Striatal CBF (ml • 100 g^{-1} • min^{-1})	48 ± 10	56 ± 20	211 ± 81 **

(Values are means ± SD for 8 piglets. MAP: mean arterial blood pressure; CBF: cerebral blood flow; * $p < 0.05$, ** $p < 0.01$ * indicate significant differences to stage "Normoxia").

Table 1 summarizes the values for mean arterial blood pressure (MAP), heart rate, arterial blood gases, acid-base balance and energy fuels during normoxia and asphyxia, when blood flow measurements were made. The values obtained during the first PET-study and asphyxia (control 2) are within the physiological range in both groups studied and consistent with other data obtained from mildly anesthetized and artificially ventilated newborn piglets [11, 12]. Similarly, there was no changed in the values for regional cerebral hemodynamics and parameters of cerebral oxidative metabolism during the first PET scan measurement and control 2 period (Tables 1 and 2).

Table 2. Forebrain hemodynamic and variables of forebrain oxidative metabolism during normoxia and hypoxia/hypercapnia.

	Normoxia		Control 2		Asphyxia	
Forebrain CBF ($ml \bullet 100\ g^{-1} \bullet min^{-1}$)	70	± 21	61	± 15	203	± 94 **
Forebrain CVR ($mmHg \bullet 100\ g \bullet min \bullet ml^{-1}$)	1.1	± 0.3	1.1	± 0.5	0.5	± 0.3 **
Forebrain O_2-delivery ($\mu mol \bullet 100\ g^{-1} \bullet min^{-1}$)	321	± 90	284	± 48	335	± 190
$CMRO_2$ ($\mu mol \bullet 100\ g^{-1} \bullet min^{-1}$)	167	± 49	139	± 39	143	± 38

(Values are means ± SD for 8 piglets. (CBF: cerebral blood flow, CVR: cerebrovascular resistance, $CMRO_2$: cerebral metabolic rate of oxygen; ** $p < 0.01$ * indicate significant differences to stage "Normoxia").

Asphyxia resulted in a reduction of arterial pO_2 by about one-third and doubling of arterial pCO_2, an increase in heart rate but no change in arterial pressure. There was combined respiratory and metabolic acidosis with increased arterial lactate concentrations. Although cerebral blood flow increased due to reduced cerebrovascular resistance (CVR, $p < 0.01$), brain oxygen delivery as well as $CMRO_2$ remained unchanged. Despite this, brain tissue pO_2 was markedly reduced (Fig. 1, $p < 0.01$). Furthermore, the rate of FDOPA decarboxylation which reflects dopamine synthesis was markedly increased during asphyxia (Fig. 1; $p < 0.01$).

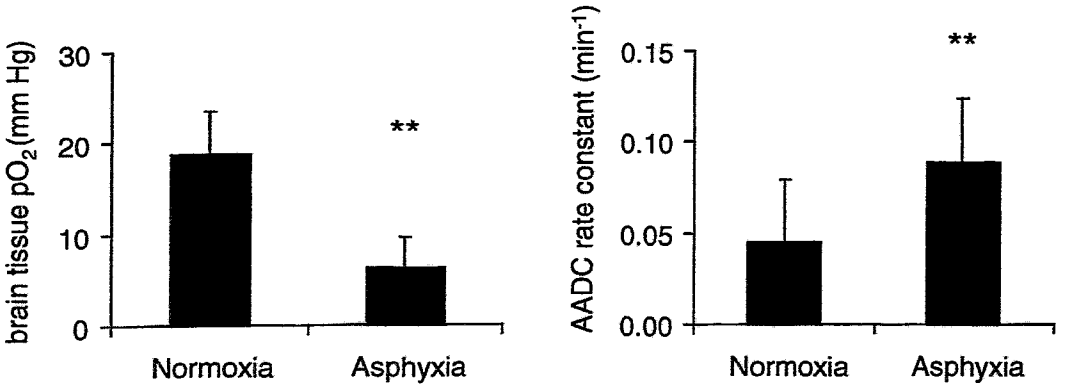

Fig. 1. Effect of moderate asphyxia on brain tissue pO_2 and striatal ^{18}F-DOPA decarboxylation (indicated DOPA decarboxylase (DDC) activity rate constant k_3) in newborn piglets (n = 8; mean + SD, ** $p < 0.01$, * indicate comparison between normoxia and asphyxia).

Discussion

Our results show that brain tissue pO_2 is reduced due to hypoxemia while cerebral O_2 delivery and also $CMRO_2$ remains maintained. Indeed, systemic hypoxia/hypercapnia induces a circulatory redistribution even in immature mammals which favors the blood flow towards the heart, brain and adrenals at the expense of the other organs and tissues. This is mainly effected by an increase in sympathoadrenal activity. However, in contrast to older animals, cardiovascular response in newborns is mainly caused by circulating catecholamines because of delayed central sympathetic maturity [13]. Direct stimulation of adrenal medulla and extramedullar chromaffin cells by reduced arterial pO_2 is mainly responsible for increased catecholamine release in newborn rats early after birth [14]. Neurogenic activation via increased efferent sympathetic tone appears to be rather unlikely since peripheral chemoreceptors remain insensitive for a certain time after birth. Resetting takes several days even in precocial animals like newborn lambs [15].

Under such conditions of reduced brain tissue pO_2 a marked increase of extracellular dopamine content occurs in newborn piglets [16]. The hypothesis that increases in extracellular dopamine during hypoxic insult play an important role in the pathogenesis of neuronal injury in newborn brain is supported by numerous findings from different injury models. Direct neurotoxic effects of dopamine on cultures were shown [17, 18]. Furthermore, dopamine can play an important role in ischemia-reperfusion injury through over-stimulation of the glutamatergic receptors during ischemia, resulting in an increase in neuronal damage in the striatum [19 - 21]. Another proposed mechanism for the neurotoxic effect of dopamine is through an increase the production of free radicals. There are several pathways for free radical generation in the brain, where dopamine may contributes. Oxidation of the excess dopamine released during ischemia by molecular oxygen may occur during reperfusion could result in the formation of superoxide anion radicals, which further may oxidize dopamine and may form covalent bonds with sulfhydyl-containing cellular components [22]. Dopamine can react with hydroxyl radicals to form the dopaminergic neurotoxin, 6-hydroxydopamine, which generates free radicals during ist spontaneous rapid autooxidation [23]. Furthermore, the enzymatic oxydation of dopamine by monoamine oxidase results also in the formation of hydrogen peroxide, a hydroxyl radical precursor [24]. A further contributing factor to neurotoxicity of dopamine may be due to an increase in cerebral metabolism of glucose by an uncoupling of flow and metabolism of the striatum after forebrain ischemia [25]. This increase of extracellular dopamine content is determined by the balance of its active uptake, release and washout from the brain. Previous in vitro studies have suggested that hypoxia per se increased the release of dopamine [26], whereas synaptosomes obtained from rat cerebral cortex after a hypoxic period exhibited a unaffected rate of dopamine efflux although re-uptake appeared to be impaired [27]. Our results indicate for the first time that the striatal dopamine synthesis rate is markedly increased by about 1.8 fold during moderate asphyxia. Reasons for short-term AADC upregulation, however, remained unclear.
In summary, our findings indicate that a marked increase in dopamine synthesis is associated with moderately reduced brain tissue pO_2. However, an asphyxia-induced CBF increase impedes an alteration of brain oxidative metabolism.

References

[1] Tuor U. I., Del Bigio M. R.and Chumas P. D. (1996) Brain damage due to cerebral hypoxia/ischemia in the neonate: pathology and pharmacological modification. *Cerebrovasc. Brain Metab. Rev.* **8**, 159-193.

[2] Vannucci R. C.and Perlman J. M. (1997) Interventions for perinatal hypoxic-ischemic encephalopathy. *Pediatrics* **100**, 1004-1014.

[3] Martin L. J., Brambrink A. M., Lehmann C., Portera Cailliau C., Koehler R., Rothstein J. and Traystman R. J. (1997) Hypoxia-ischemia causes abnormalities in glutamate transporters and death of astroglia and neurons in newborn striatum. *Ann. Neurol.* **42**, 335-348.

[4] Huang C. C., Lajevardi N. S., Tammela O., Pastuszko A., Delivoria Papadopoulos M. and Wilson D. F. (1994) Relationship of extracellular dopamine in striatum of newborn piglets to cortical oxygen pressure. *Neurochem. Res.* **19**, 649-655.

[5] Gordon K., Statman D., Johnston M. V., Robinson T. E., Becker J. B. and Silverstein F. S. (1990) Transient hypoxia alters striatal catecholamine metabolism in immature brain: an in vivo microdialysis study. *J. Neurochem.* **54**, 605-611.

[6] Akiyama Y., Ito A., Koshimura K., Ohue T., Yamagata S., Miwa S. and Kikuchi H. (1991) Effects of transient forebrain ischemia and reperfusion on function of dopaminergic neurons and dopamine reuptake in vivo in rat striatum. *Brain Res.* **561**, 120-127.

[7] Brust P., Bauer R., Walter B., Bergmann R., Füchtner F., Vorwieger G., Steinbach J., Johannsen B. and Zwiener U. (1998) Simultaneous measurement of [^{18}F]FDOPA metabolism and cerebral blood flow in newborn piglets. *Int. J. Dev. Neurosci.* **16**, 353-364.

[8] Brust P., Bauer R., Vorwieger G., Walter B., Bergmann R., Füchtner F., Steinbach J., Zwiener U. and Johannnsen B. (1999) Upregulation of the aromatic amino acid decarboxylase under neonatal asphyxia. *Neurobiol. Dis.* **6**, 131-139.

[9] Bauer R., Bergmann R., Walter B., Brust P., Zwiener U. and Johannsen B. (1999) Regional distribution of cerebral blood volume and cerebral blood flow in newborn piglets – effect of hypoxia/hypercapnia. *Brain Res. Dev. Brain Res.* **12**, 89-98.

[10] Bauer R., Brust P., Walter B., Vorwieger G., Bergmann R., Füchtner F., Steinbach J., El-Hallag, E., Fritz, A., Johannnsen B. and Zwiener U. (2000) Relation between brain tissue pO_2 and dopamine synthesis of basal ganglia – A ^{18}FDOPA-PET study in newborn piglets. *J. Perinat. Med.*, in press.

[11] Buckley N. M., Gootman P. M., Yellin E. L. and Brazeau P. (1979) Age-related cardiovascular effects of catecholamines in anesthetized piglets. *Circulation Research* **45**, 282-292.

[12] Lerman J., Oyston J. P., Gallagher T. M., Miyasaka K. A. G, Volgyesi G. A. and Burrows F. A. (1990) The minimum alveolar concentration (MAC) and hemodynamic effects of Halothane, Isoflurane, and Sevoflurane in newborn swine. *Anesthesiology* **73**, 717-721.

[13] Lee J. C., Werner J. C. and Downing E. (1980) Adrenal contribution to cardiac responses elicited by acute hypoxia in piglets. *Am. J. Physiol.* **239**, H751-H755.

[14] Mojet M. H., Mills E., Duchen M. R. (1997) Hypoxia-induced catecholamine secretion in iso-lated newborn rat adrenal chromaffin cells is mimicked by inhibition of mitochondrial respiration. *J Physiol. Lond.* **504**, 175-189.

[15] Hanson M. A. (1988) The importance of baro- and chemoreflexes in the control of the fetal cardiovascular system. *J. Dev. Physiol.* **10**, 491-511.

[16] Pastuszko A., Saadat Lajevardi N., Chen J., Tammela O., Wilson D. F., Delivoria-Papadopoulos M. (1993) Effects of graded levels of tissue oxygen pressure on dopamine metabolism in the striatum of newborn piglets. *J. Neurochem.* **60**, 161-166.

[17] Parenti M., Rusconi L., Cappabianca V., Parati E. A. and Groppetti A. (1988) Role of dopamine in manganese neurotoxicity. *Brain Res.* **473**, 236-240.

[18] Rosenberg P. A. (1988) Catecholamine toxicity in cerebral cortex in dissociated cell culture. *J. Neurosci.* **8**, 2887-2894.

[19] Knapp A. G., and Dowling J. E. (1987) Dopamine enhances excitatory amino acid-gated conductances in cultured retinal horizontal cells. *Nature* **325**, 437-439

[20] Globus M. Y., Busto R., Dietrich W. D., Martinez E., Valdes I. and Ginsberg M. D. (1988) Effect of ischemia on the in vivo release of striatal dopamine, glutamate, and gamma-aminobutyric acid studied by intracerebral microdialysis. *J. Neurochem.* **51**, 1455-1464.

[21] Buisson A., Callebert J., Mathieu E., Plotkine M. and Boulu R. G. (1992) Striatal protection induced by lesioning the substantia nigra of rats subjected to focal ischemia. *J. Neurochem.* **59**, 1153-1157.

[22] Graham D. G., Tiffany S. M., Bell W. R. Jr. and Gutknecht W. F. (1978) Autoxidation versus covalent binding of quinones as the mechanism of toxicity of dopamine, 6-hydroxydopamine, and related compounds toward C1300 neuroblastoma cells in vitro. *Mol. Pharmacol.* **14**, 644-653.

[23] Slivka A. andCohen G. (1985) Hydroxyl radical attack on dopamine. *J. Biol. Chem.* **260**, 15466-15472.

[24] Maker H. S., Weiss C., Silides D. J. and Cohen G. (1981) Coupling of dopamine oxidation (monoamine oxidase activity) to glutathione oxidation via the generation of hydrogen peroxide in rat brain homogenates. *J. Neurochem.* **36**, 589-593.

[25] Ginsberg M. D., Graham D. I. and Busto R. (1985) Regional glucose utilization and blood flow following graded forebrain ischemia in the rat: correlation with neuropathology. *Ann. Neurol.* **18**, 470-481.

[26] Freeman G. B. and Gibson G. E. (1986) Effect of decreased oxygen on in vitro release of endogenous 3,4-dihydroxyphenylethylamine from mouse striatum. *J. Neurochem.* **47**, 1924-1931.

[27] Pastuszko A., Wilson D. F. and Erecinska M. (1982) Neurotransmitter metabolism in rat brain synaptosomes: effect of anoxia and pH. *J. Neurochem.* **38**, 1657-1667

8. Mapping the Serotonin Uptake Site in Swine Brain with [^{3}H]Citalopram Radioluminography

P. Cumming[1], M. Kretzschmar, R. Bergmann, D. Smith[1], P. Brust
[1]PET Center, Aarhus Kommunehospital, Aarhus, Denmark.

Introduction

Plasma membrane transporters for serotonin are markers for the pre-synaptic terminals of serotonin fibres throughout the mammalian brain. Changes in the serotonin uptake site density have been implicated in the pathophysiology of Parkinson's disease [1] and the neurotoxicity of psychostimulants [2]. We have employed living swine for investigations of serotonin uptake sites by positron emission tomography [3]. However, the distribution of serotonin uptake sites in pig brain *in vitro* has not been reported. In order to facilitate the interpretation of positron emission tomograms obtained *in vivo* [4], we have used radioluminography to map the binding in vitro of [^{3}H]citalopram to serotonin uptake sites in cryostat sections from swine brain.

Experimental

Three female pigs (40 kg, Danish Landrace) were killed by overdose with ketamine/lorazepam. After rapid removal, the brains (100 g) were frozen at –20^0 C, and stored for one week at – 80^0 C. Sagittal sections 30 micron thick were cut from the whole brains, and thaw-mounted to polylysine-coated glass slides. Series of adjacent sections were collected at four positions in the sagittal plane: 18, 12, 6, and 0 mm lateral to the midline. After a brief pre-incubation for 15 min in 50 mM Tris-HCl buffer (pH 7.4) , containing 120 mM NaCl and 5mM KCl the sections were covered with a solution (2 ml each) containing the same buffer and [^{3}H]citalopram (specific activity 82 Ci/mmol, New England Nuclear) at one of six concentrations ranging from 0.1 nM to 10 nM. For determination of the non-specific binding, some sections were incubated in the incubation medium modified by the addition of fluoxetine hydrochloride (Research Biochemicals) at a final concentration of 20 µM. After incubations for 120 minutes at room temperature, the slides were placed in ice-cold Tris buffer for 20 minutes (2x), dipped in cold de-ionized water, and quickly dried under air at room temperature.

Slides were placed on tritium-sensitive radioluminography plates (Raytest), along with calibrated standards (Amersham) for a period of ten days, and then quantified using commercial image analysis software AIDA 2.11 (Raytest).

Results

The non-specific binding in all regions of the brain in the presence of excess fluoxetine at the highest radioligand concentration was less than the specific binding present in cerebellar cortex, the gray matter brain region with the lowest density of serotonin uptake sites. An example of the pattern of total and non-specific binding for 5 nM [^{3}H]citalopram in a sagittal brain section is illustrated in Figure 1. The linear Scatchard analysis was used to estimate the saturation binding parameters *in vitro*. The apparent affinity of [^{3}H]citalopram binding was close to 5 nM in all brain regions. Typical values for the binding site density in some regions of particular interest, in descending order of concentration, were as follows: Basolateral amygdala (250 fmol/mg tissue), substantia nigra pars reticulata (200 fmol/mg tissue), superficial layer of the superior colliculus (150 fmol/mg tissue), corpus striatum (50-100 fmol/mg tissue), dorsolateral thalamus (60 fmol/mg tissue), entorhinal cortex (60 fmol/mg tissue), anterior cingulate cortex (40 fmol/mg tissue) hippocampus (20 fmol/mg tissue) occipital cortex (15 fmol/mg tissue), and cerebellar cortex (10 fmol/mg tissue).

Discussion

The specific binding of citalopram in swine brain was highly heterogenous, consistant with the pattern of distribution reported in man and rodent [5]. The binding site density was 25-fold higher in the region of high concentration (basolateral amygdala) than in the region of lowest density (cerebellum), validating the

use of cerebellum as a non-binding reference region in positron emission tomographic studies of serotonin uptake sites. The absolute binding site densities were comparable with those obtained in pig brain membranes [6]. In general, the highest concentrations of binding sites were found in limbic brain regions and in small structures of the mesencephalon. Within the thalamus, the specific binding was observed in boundries of the specific thalamic nuclei.

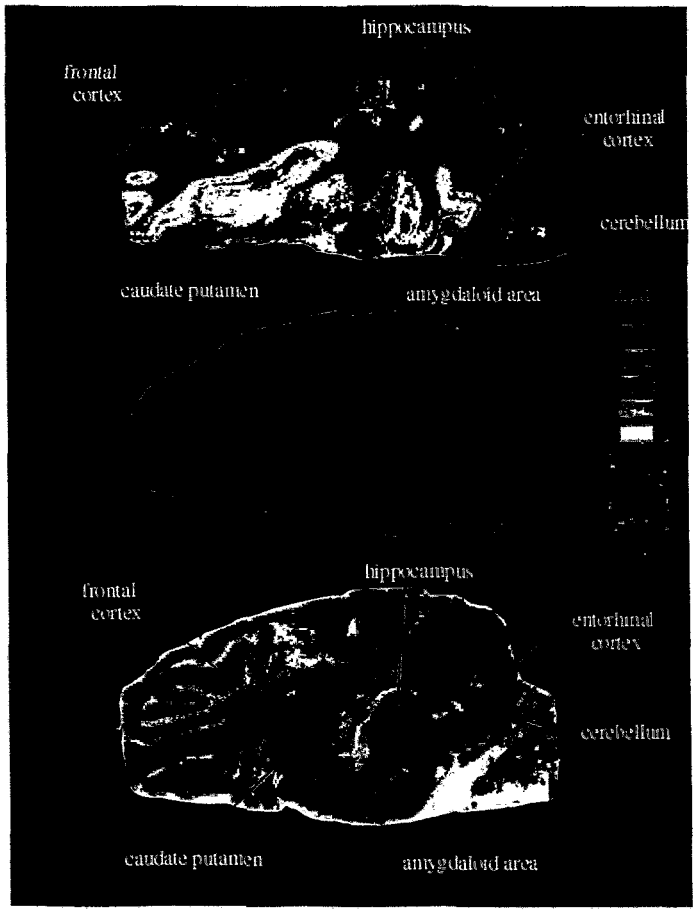

Fig. 1. In vitro autoradiograms (above and middle), radioactivity scale and histological image (below) of sagittal brain sections of the swine showing the total binding (above) and unspecific binding (middle) of [^{3}H]citalopram in several brain regions .

The fine structure of the distribution of serotonin uptake sites in pig brain is scaled smaller than the resolution of most available positron emission tomographs. Therefore, the binding in specific regions on anatomical interest must necessarily be blurred extensively due to effects of partial volume. We contend that statistical parametric mapping of binding in a population of swine may provide a route for quantitative assay of serotonin binding sites in vivo. This approach may be facilitated by the recent appearance of a sterotaxic atlas of the swine brain [7].

References

[1] Chinaglia G., Landwehrmeyer B., Probst A. and Palacios J. M. (1993) Serotoninergic terminal transporters are differentially affected in Parkinson's disease and progressive supranuclear palsey: an autoradiographic study with [^{3}H]citalopram. *Neuroscience* **54,** 691-699.

[2] McCann D. U., Szabo Z., Scheffel U., Dannals R. F. and Ricaurte G. A. (1998) Positron emission tomographic evidence of toxic effect of MDMA ("Ecstasy") on brain serotonin neurons in humans beings. *Lancet* **352,** 1433-1437.

[3] Smith D. F., Gee A. D., Hansen S. B., Moldt P., Nielsen E. O., Scheel-Kruger J. and Gjedde A. (1999) Uptake and distribution of a new SSRI, NS2381, studied by PET in living porcine brain. *Eur. Neuropsychopharmacol.* **9,** 351-359.

[4] Brust P., Scheffel U. and Szabo Z. (1999) Radioligands for the study of the 5-HT transporter in vivo. *IDrugs* **2,** 129-145.

[5] Duncan G. E., Little K. Y., Kirkman J. A., Kaldas R. S., Stumpf W. E. and Breese G. R. (1992) Autoradiographic characterization of [^{3}H]imipramine and [^{3}H]citalopram binding in rat and human brain: species differences and relationships to serotonin innervation patterns. *Brain Res.* **591,** 181-197.

[6] Erreboe I., Plenge P. and Mellerup E. T. (1995) Differences in brain 5-HT transporter dissociation rates among animal species. *Pharmacol. Toxicol.* **76,** 376-379.

[7] Felix B., Leger M. E, Albe-Fessard D., Marcilloux J. C., Rampin O. and Laplace J. P. (1999) Sterotaxic atlas of the pig brain. *Brain Res. Bull.* **49,** 1-137.

9. Correlation of the Capacity for Continuous Selective Attention and Eye Movement Disturbances with $rCMR_{glu}$ in Patients with Spasmodic Torticollis

J. Pinkert, I. Gerdsen, B. Ripke, R. Fötzsch, L. Oehme, J. Missimer, N.Galley and W.-G. Franke

Introduction

Idiopathic spasmodic torticollis is a subtype of adult-onset focal dystonia causing abnormal head posture. Apart from clinical signs recent studies on torticollis patients have shown a reduced performance of tasks related to temporal processing as an indicator of a probable affection of higher cognitive functions such as strategy use and working memory [1] and disturbances in voluntary eye movements with the intrusion of macro saccades during the smooth tracking paradigm [2, 3]. Elevated saccadic intrusions were observed by electronystagmographic recordings from the majority of torticollis patients of our neurological outpatient clinic.

Basal ganglia dysfunction with abnormal basal ganglia output has been suggested to underlie this clinical syndrome. Previous activation studies with PET and $H_2{}^{15}O$ on idiopathic torsion dystonia have shown overactive striatal and frontal accessory areas and an underactivity of the primary motor cortex and caudal supplementary motor area, while ^{18}F-FDG studies confirmed the bilateral hypermetabolism of nucleus lentiformis in spasmodic torticollis. Recent neuropsychological studies on torticollis patients revealed an impaired visuospatial function, suggesting the involvement of complex cortical functions [4]. It is not yet understood, however, how characteristic patterns of the disease are related to the underlying neural networks on cortical and subcortical levels.

^{18}F-FDG-PET can be used to analyse metabolic activity as an indicator of affected network representations in torticollis.

The aim of the present study was to investigate the relationship between regional cerebral metabolic rates of glucose (CMRglu), the number of saccadic intrusions during the smooth eye tracking paradigm and the level of continuous selective attention based on rather complex visuo-motor functions, including working memory, to analyse the metabolic activity as an indicator of affected network representations in torticollis.

Material and Methods

16 patients with spasmodic torticollis (7 female and 9 male, age 24 - 71 years, median age 56.4 years) underwent ^{18}F-FDG PET imaging using a 32-ring ECAT EXACT HR+ scanner (FWHM = 4 mm, axial field of view (FOV) = 15.5 cm, Siemens / CTI Inc., Knoxville, TN). All patients had normal MRI scans. For comparison data sets from 11 age matched normal volunteers were obtained from the PSI.

Before the examination the patients gave their written informed consent after thorough explanation of the procedures. The clinical symptoms of the torticollis patients were assessed on the TWSTR and TSUI scales by two independent raters. All subjects were strictly right handed. The torticollis patients had their last botulinum injection 4 - 10 weeks before the scanning.

Patients were prepared by fasting for at least 12 h before the PET examination. PET images were acquired with the patients in a resting state, with their eyes open in a darkened PET scanner room, ears unplugged and with a minimum ambient noise. The head was placed in a special head holder to minimize movement during scanning. The scanning plane was parallel to the cantho-meatal line.

After a 15-min transmission scan (three ^{68}Ga/^{68}Ge rod sources), dynamic PET emission scans were performed in 2D mode. About 300 MBq ^{18}F-FDG was intravenously injected within 1 min. A time frame schedule of 10 x 120 and 7 x 240 s was used. Once during each time frame an arterialized blood sample was manually drawn from an indwelling catheter placed in the cubital vein for the measurement of plasma activity. The radioactivity concentration was measured with an automated gamma counter (1480 Wizard 3", Wallac Inc., Turku, Finland), cross-calibrated to the PET scanner.

PET images were reconstructed in a 128x128 matrix using a Hanning filter (cut-off frequency 0.5) and corrected for measured photon attenuation and decay.

Images of the cerebral metabolic rates for glucose (CMR_{glu}) were calculated by a voxel-based graphical analysis using measured input function and tissue radioactivity concentration (Patlak plot) in IDL on a SUN workstation and smoothed with a boxcar filter.

The absolute glucose consumption rate was calculated for each pixel using maps of CMR_{glu}, blood glucose concentration and a lumped constant of 0.42.

These images were spatially transformed to a standard atlas (Talairach and Tournoux) and globally normalized, using proportional scaling. Differences between the scans of the patients group and those of 11 healthy controls were statistically analysed using SPM95, setting the threshold to $p < 0.01$.
A multi-subject design with covariates was chosen to scan for a correlation between regional CMR_{glu} changes with covariates.
Attentional functioning connected with the ability to differentiate visual stimuli and translate them into adequate motor responses was measured by means of the d2 test [5, 6]. In this exercise subjects are given a sheet of paper with lines consisting of the letters "p" and "d" in a random sequence and points of a various number (minimum one, maximum four) above and below them belonging to each letter.
The subjects are asked to cross out all "d`s" with two points as quickly and accurately as possible. They are asked to start at the beginning of the first line and to continue from the beginning of the next line after 20 seconds or when the experimenter tells them to.
The error rate as a measure of accuracy and the difference between the total number of checked letters and the error rate as a measure of selective attention in the D2 test as well as the number of saccadic intrusions counted during the smooth pursuit were used as covariates in the SPM analysis.
Electronystagmographic examinations were carried out using a Nicolet Nystar nystagmograph. The number of saccadic intrusions during the smooth eye tracking paradigm were counted automatically by the Nicolet software.

Results and Discussion

SPM analyses for torticollis patients in comparison with age matched controls demonstrated a significantly elevated bilateral glucose metabolism in the basal ganglia ($p < 0.01$). The stereotactic coordinates were in strict accordance with the nucleus lentiformis. This finding was supported by similar results obtained by Magyar-Lehmann *et al.* [7]. They also found a higher glucose metabolism in the nucleus lentiformis in patients with dystonia.
No relations were found to exist between the glucose metabolism and the clinical symptoms of torticollis patients measured on the TWSTR and TSUI scales or the duration of the disease.
The SPM covariate analyses with the number of saccadic intrusions during the smooth eye tracking paradigm confirmed a significant correlation with the glucose metabolism in the visual cortical areas and extrastriatal association areas with an increased number of saccadic intrusions ($p < 0.01$, see Fig. 1). In contrast to our previous results obtained in torticollis patients with SPECT and an increased perfusion during smooth tracking in the posterior parietal cortex, the frontal eye field and cerebellum, the elevated glucose metabolism under resting conditions in the visual cortex may indicate a higher basal neuronal activity in the visual cortex in torticollis patients.
A subgroup of the subjects show a d2 performance which scores below the age-related average while there is a significant correlation between the extent of diminution of the selective attention score in the d2 test and the glucose metabolism in the prefrontal cortical areas (see Fig. 2) in the torticollis patients.

An affected accuracy score in the d2 test was found to be associated with a reduced glucose metabolism in the anterior cingulate (see Fig. 3).

This study confirms previous data on bilateral nucleus lentiformis hypermetabolism in spasmodic torticollis. In some cases it also suggests the involvement of impaired associative functions, visuo-motor capacity and working memory which are necessary to achieve a sufficient performance in the continuous selective attention exercise. The extent of affection is assumed to be connected with the degree to which there is a diminution of glucose metabolism in the prefrontal cortex and the anterior cingulate. These areas are parts of the system which controls processes of continuous selective visual attention connected with corresponding motor responses as a rather complex cognitive function.
Thus we conclude that the pathology of spasmodic torticollis may not only be based on basal ganglia dysfunction.

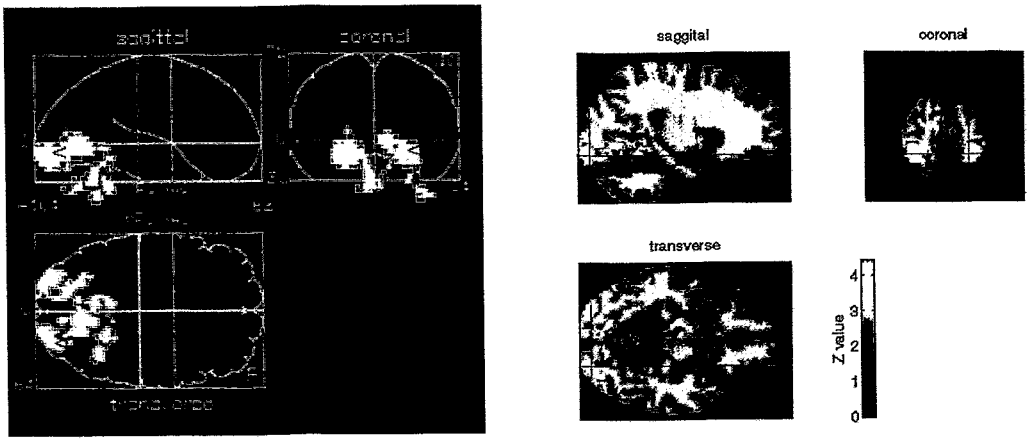

Fig. 1. Positive correlation of $rCMR_{glu}$ with the total number of saccades in patients with spasmodic torticollis, SPM projections (left) and areas with significant correlation (search threshold $p < 0.01$) matched with the MRI T1 template (right)

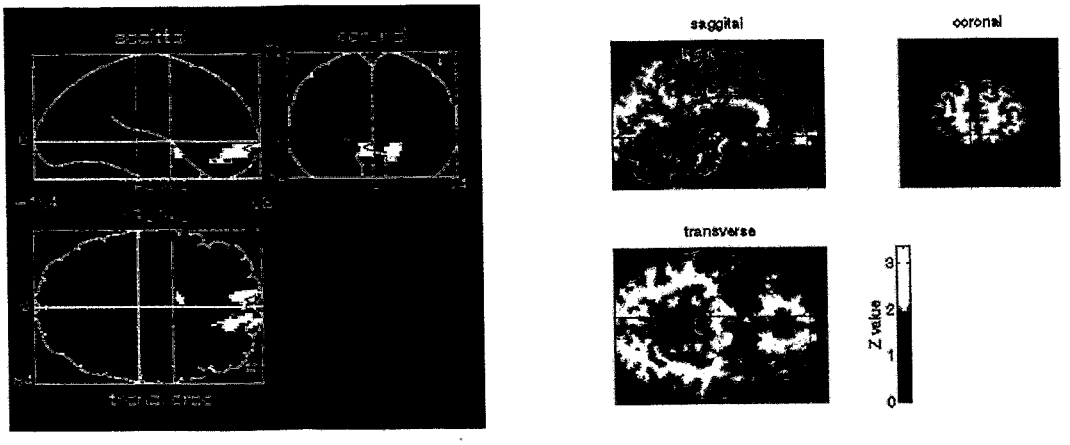

Fig. 2. Positive correlation of $rCMR_{glu}$ with the accuracy in the d2 test in patients with spasmodic torticollis, SPM projections (left) and areas with significant correlation (search threshold $p < 0.01$) matched with the MRI T1 template (right)

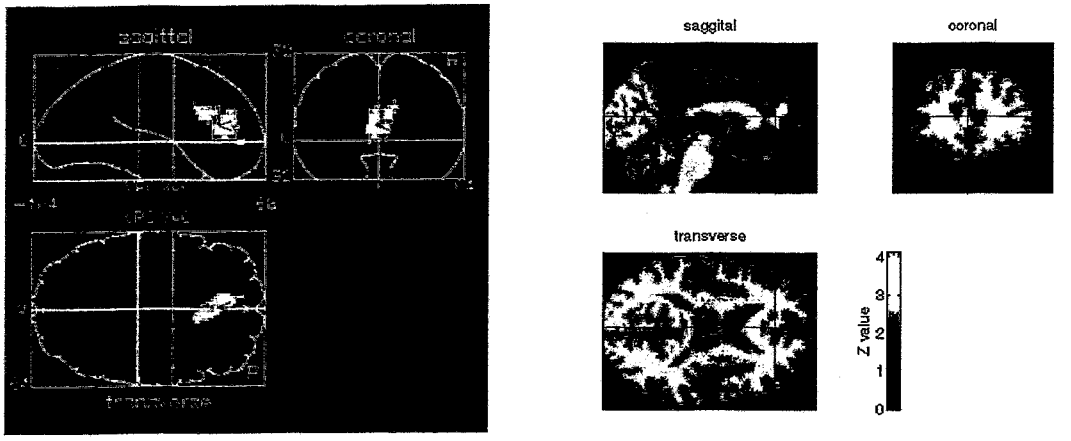

Fig. 3. Negative correlation of $rCMR_{glu}$ with the error rate in the d2 test in patients with spasmodic torticollis, SPM projections (left) and areas with significant correlation (search threshold $p < 0.01$) matched with the MRI T1 template (right)

References

[1] Ripke B., Gerdsen I., Fötzsch R., Pinkert J., Galley N., Israel M. and Richter A. (1999) Aspects of temporal behavior in spasmodic torticollis and normal volunteers. *NeuroImage* **9**, S159.

[2] Pinkert J., Gerdsen I., Fötzsch R., Oehme L., Ripke B., Missimer J., Galley N. and Franke W.-G. (1999) Functional correlates of Macro Square Wave Jerks in patients with spasmodic torticollis - A SPECT study with ^{99m}Tc-ECD. XIXth International Symposium on Cerebral Blood Flow and Metabolism, June 13-17, Copenhagen, Denmark.

[3] Fötzsch R., Pinkert J. and Gerdsen I. (1998) Functional responses of smooth tracking in patients with spasmodic torticollis. *Neuro-Ophthalmology* **20**, 12.

[4] Hinse P., Leplow B., Humbert T., Lamparter U., Junge A. and Emskotter T. (1996) Impairment of visuospatial function in idiopathic spasmodic torticollis. *J. Neurol.* **243**, 29-33.

[5] Brickenkamp R. (1962) Test d2 – Aufmerksamkeits-Belastungstest. Handanweisung. Hogrefe Verlag, Göttingen.

[6] Brickenkamp R. (1994) Test d2. Aufmerksamkeits-Belastungs-Test. Handanweisung. 8. Erweiterte und neu gestaltete Auflage. Hogrefe Verlag, Göttingen.

[7] Magyar-Lehmann S., Antonini A., Roelcke U., Maguire R. P., Missimer J., Meyer M. and Leenders K. L. (1997) Cerebral glucose metabolism in patients with spasmodic torticollis. *Mov. Disord.* **12**, 704-708.

RADIOPHARMACEUTICAL CHEMISTRY

10. Two-Step Synthesis of 16α-[^{18}F]Fluoroestradiol-Disulphamate

J. Römer, F. Füchtner, J. Steinbach

Introduction

The development of new specific oncological ^{18}F-labelled tracers for the positron emission tomography (PET) is an emerging area [1], especially for diagnosing endocrine-dependent breast cancer [2] and breast cancer metastases [3], 16α-[^{18}F]fluoroestradiol ([^{18}F]FES) has proved to be the PET tracer of choice [4]. In order to make the new PET tracer accessible to the nuclear physicians at our location, a synthesis, elaborated in the USA [5], was modified at our PET centre [6] and integrated into an automatic module [7]. Thus, [^{18}F]FES can be reliably produced in GBq amounts of high specific radioactivity.

Recently, we have found that estradiol-3,17β-disulphamate and first of all 16α-halogen-estradiol-3,17β-disulphamates are highly active steroid sulphatase inhibitors. Estrogen sulphatases *in vivo* are responsible for the deconjugation of estrogen sulphates. This deconjugation is necessary because only free estrogen can exercise its biological function. Free estrogens are mitogens and promote the growth of endocrine-dependent tumours. As steroid sulphatase is particularly prevalent in breast cancer tissue [8], sulphatase inhibitors that prevent the formation of free estrogen should be suitable for chemotherapeutic intervention in breast cancer [9]. When using 16α-[^{18}F]fluoroestradiol-3,17β-disulphamate ([^{18}F]FESDS) on the other hand, there should be the chance to image sites of high sulphatase activity. For such studies [^{18}F]FESDS had to be made available. The access to [^{18}F]FES by a rapid and reliable production method [7] was a good starting point to accomplish such a project.

In this paper we describe the conditions which are suited to convert [^{18}F]FES successfully into chemically and radiochemically pure [^{18}F]FESDS.

Results and Discussion

A simple phase-transfer method for the preparation of unsubstituted sulphamate esters , $H_2N\text{-}SO_2\text{-}OR$, where R can be aliphatic or aromatic, was described by Spillane *et al.* [10]. These authors were the first to use solid sodium carbonate as a deprotonating medium. We transferred this successful method for the first time to steroid alcohols [11].

Sulphamoyl chloride ($H_2N\text{-}SO_2\text{-}Cl$, SCl) [12], a solid moisture-sensitive compound, was used as reagent. It formed three sulphamates with 16α-fluoro-estradiol (FES). These new compounds - 16α-fluoro-estradiol-3-sulphamate (FES3S), 16α-fluoro-estradiol-17β-sulphamate (FES17S), and 16α-fluoro-estradiol-3,17β-disulphamate (FESDS) - were first synthesized and characterized in our laboratory [11].

The sulphamoylation reaction of FES or other 3,17ξ-diols yielded mixtures of sulphamates but in all the cases investigated the formation of the 17ξ-sulphamate was favoured. When using excess SCl, almost all the diol could be converted into diol-3,17ξ-disulphamate.

To separate a sulphamoylation mixture, preparative reversed-phase (RP) HPLC was used. Usually, pure acetonitrile was the eluent [11]. But, 55 % aqueous ethanol proved to be a better eluent capable of separating FES and all the sulphamates of FES in an excellent manner. Because the diol-monosulphamate is more polar than the diol, and the dioldisulphamate is more polar than a monosulphamate, FESDS was eluted from an RP column before the monosulphamates. The retention times of FES, FES3S, FES17S, and FESDS are listed in Table 1.

The new sulphamates were characterized by melting point, mass, UV, and ^{13}C NMR spectroscopy, and by thin-layer chromatography (TLC) [11]. TLC was also used in the radioactive experiments described here. Therefore, R_f values were also noted in Table 1.

An automated synthesis should be straightforward. Liquid-liquid extractions and the addition of solids are difficult in a module-assisted procedure. Therefore, we tested the usefulness of the soluble 2,6-di-tert.butyl-4-

methyl pyridine (DBMP) instead of sodium carbonate as a base.

Table 1. Retention times and R_f values of FES, FES-monosulphamates and FES-disulphamate

Compound [a]	Retention Time [min] [b]	R_f Value [c]
FES	30.5	0.32
FES3S	22.5	0.17
FES17S	21.0	0.27
FESDS	17.0	0.21

a) Abbreviations see text

b) SP 250/10 NUCLEOSIL 100-7C_{18} from Macherey & Nagel; 55% ethanol as eluent at a flow of 1.5 mL/min

c) Silica gel; toluene/ethyl acetate (3:1) as solvent

The usefulness of DBMP had already been established in non-radioactive experiments [11]. DBMP worked even if used in sub-stoichiometric amounts in relation to FES. Milligram amounts of FES in absolute acetonitrile were converted into FESDS at room temperature by using a twentyfold excess of SCl in the presence of sub-stoichiometric amounts of DBMP, the reaction being complete in a few minutes.

Conversion of [^{18}F]FES in the presence of DBMP

In the radioactive experiments, solutions of DBMP (1 mg) and SCl (10 mg) in acetonitrile were added to column-purified dry [^{18}F]FES. The solution was stirred at room temperature. Samples were taken from time to time and analysed, using analytical radio-HPLC. But contrary to the optimum non-radioactive conditions mentioned above, no conversion of [^{18}F]FES was detected. Only some negligible conversion was observed after the temperature had been increased.

However, complete conversion of the [^{18}F]FES was shown by analytical radio-HPLC when the reaction batch was evaporated to dryness at 70 °C and ethanol was added to the residue. Mainly polar products (about 75 %), but only about 25 % of the desired [^{18}F]FESDS were found in the analytical radio-chromatogram. Further experiments confirmed these results and proved that complete conversion of [^{18}F]FES had taken place in the process of evaporation.

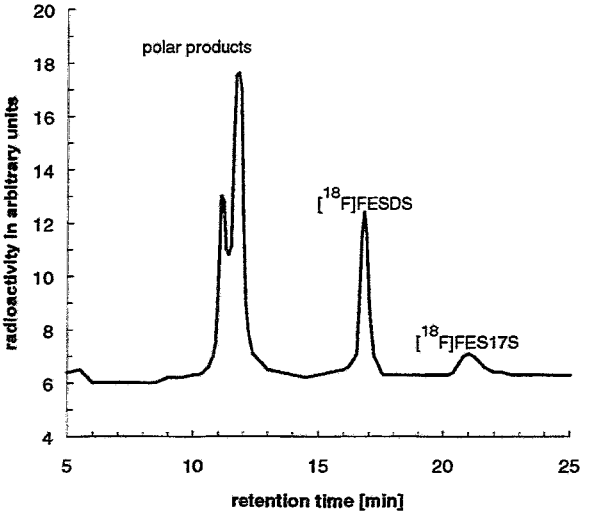

Fig. 1. The semipreparative radiochromatogram of a reaction mixture prepared by sulphamoylation of [18F]FES in the presence of DBMP

If a reaction batch treated in this way was injected into a semi-preparative RP column and then eluted with 55 % aqueous ethanol, a typical radiochromatogram was obtained as shown in Fig. 1. Peak collection,

radioactivity measurement and decay correction provided precise data on the radioactivity distribution: polar products (69.6 %), [^{18}F]FESDS (25.9 %), and another product with a retention time of 21 min, probably [^{18}F]FES17S (4.5 %). A check of the collected eluate of the [^{18}F]FESDS peak showed a radiochemical purity of >99 %.
Contrary to non-radioactive experiments, in radioactive experiments DBMP cannot be used in substoichiometric amounts. We tried to reduce the formation of polar by-products by lowering the amount of DBMP to 0.1 mg. Even with this small amount, [^{18}F]FES was completely converted without increasing the yield of [^{18}F]FESDS. Further reduction of DBMP finally led to [^{18}F]FES not being converted at all.

Conversion of [^{18}F]FES in the presence of other bases
Dimethyl formamide was recommended in the literature [13] as a good solvent for sulphamoylation because it also acts as a base. We investigated the sulphamoylation reaction of [^{18}F]FES in a solvent mixture of acetonitrile and dimethyl formamide, first at room temperature, then at 60 °C. No conversion of [^{18}F]FES occurred. Removal of the solvent at 100 °C and adding ethanol to the residue resulted in the quantitative conversion of [^{18}F]FES into polar products. No trace of [^{18}F]FESDS could however be detected.

Quantitative conversion of [^{18}F]FES into polar products also occurred when only small amounts of sodium carbonate or potassium carbonate were used. This result showed that the occurrence of undesirable by-products in the previously described experiments cannot be attributed to any special property of DBMP. It was surprising, on the other hand, that in the non-radioactive experiments for the preparation of FESDS [11] no polar product was formed in the presence of excess sodium carbonate.

Conversion of [^{18}F]FES in the presence of Kryptofix 2.2.2 / K_2CO_3
Mixtures of Kryptofix 2.2.2. (K222) and potassium carbonate in absolute acetonitrile have proved to be useful in nucleophilic fluorination reactions [14-16]. For preparing [^{18}F]FDG [17] and [^{18}F]FES [7], we have made use of a solution containing 40 µmol K222 and 20 µmol K_2CO_3 per mL (K222/K_2CO_3). Now we examined whether this moderately basic solution can be also successfully applied in the sulphamoylation reaction of [^{18}F]FES.

K222/K_2CO_3 solution (1.5 mL) was added to column-purified [^{18}F]FES. After careful evaporation of the solvent to dryness, a solution of SCl in acetonitrile was added, and this reaction mixture was stirred at 70°C. Surprisingly, a sample taken after 5 min already showed a 75 % conversion of [^{18}F]FES. After work-up, [^{18}F]FESDS and polar products were present in a ratio of about 1 : 1 as demonstrated by analytical HPLC. The same ratio was found after separation on a semi-preparative RP column. A radiochromatogram is shown in Fig. 2. The reproducible preparation of [^{18}F]FESDS was confirmed by further experiments. The conversion level was between 50 and 60 %.

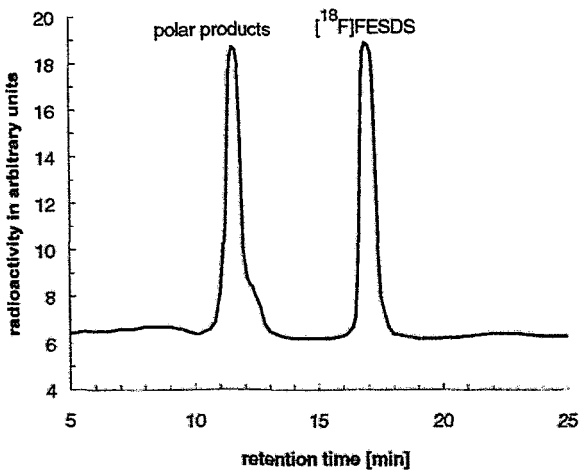

Fig. 2. The semipreparative radiochromatogram of a reaction mixture prepared by sulphamoylation of [^{18}F]FES in the presence of K222/K2CO3

The method with $K222/K_2CO_3$ was then transferred into an automatically operating module. The experiments were carried out at a higher radioactivity level. The same module was used as for preparing [^{18}F]FES. After synthesis and purification of [^{18}F]FES according to [7], the module had to be cleaned and prepared for the sulphamoylation reaction which was then carried out as described above. Finally, the reaction mixture was separated on a semipreparative RP-HPLC column.

The results of three typical module-assisted experiments are summarized in Table 2. The decay-corrected yield of [^{18}F]FESDS related to [^{18}F]FES was about 50%. The maximum yield of [^{18}F]FESDS related to the starting radioactivity at t = 0 was 6% (real yield) and 20% (decay-corrected), respectively. The total time for producing [^{18}F]FESDS was about 3 h. At the end of the synthesis [^{18}F]FESDS was available in a quantity of up to 1000 MBq.

Table 2. Results of three module-assisted experiments

Expt.	Irradiation time [min]	Starting activity [MBq] a)	[^{18}F]FES		[^{18}F]FESDS	
			Time [min] b)	$Y_{corr.}$ [%] c)	Time [min] b)	$Y_{corr.}$ [%] c)
1	15	13150	66	39.8	187	19.7
2	30	29500	62	33.8	189	16.5
3	20	22150	62	37.0	190	19.2

a) Radioactivity at the start of the synthesis (t = 0)
b) Time between t = 0 and the moment of availability of the radiotracer
c) Yield of the radiotracer related to t = 0

Chemical and radiochemical purity, specific radioactivity
The high chemical and radiochemical purity of [^{18}F]FES and its high specific radioactivity had already been shown by analytical HPLC [7]. Now, the purity of the [^{18}F]FESDS had to be determined.

Some results from Expt. 2 (Table 2) are represented in Fig. 3. There are four analytical chromato-grams; a UV chromatogram of a reference solution containing FES and FESDS (Fig. 3A), a radio-chromatogram of the raw product before it was injected into the semi-preparative RP column to be separated (Fig. 3B), a radiochromatogram of the collected eluate of the [^{18}F]FESDS peak (Fig. 3C), and a UV chromatogram of the same solution (Fig. 3D).

According to Fig. 3A the retention times of FESDS and FES were 15.7 min and 19.0 min, resp. When the raw product was analysed (Fig. 3B), a peak representing polar products (30 %) was found at 10.6 min, a large peak (58 %) was eluted at 16.0 min, and a small peak (7 %) at 19.2 min,. In Fig. 3C, the successful HPLC separation was demonstrated with the peak at 16.0 min representing [^{18}F]FESDS of high chemical and radiochemical purity (>99 %).

The named distribution and the radiochemical purity of [^{18}F]FESDS were confirmed by radio-TLC. The impure product showed three spots and the following radioactivity distribution: polar products (29 %), [^{18}F]FESDS (65 %), [^{18}F]FES (6 %). The R_f values found were 0.18 for [^{18}F]FESDS and 0.32 for [^{18}F]FES. The pure [^{18}F]FESDS solution showed one and only peak (R_f = 0.18) with a radiochemical purity of >99 %.

The specific radioactivity of the ^{18}F-labelled compound was higher the greater the starting radioactivity used [7]. Only solutions of pure [^{18}F]FESDS from the experiments in Table 2 were investigated. We injected 100 µl into the analytical HPLC system. A small peak due to FESDS was found at 216 nm (Fig. 3D). The peak mass was determined, and values for the specific radioactivity of between 150 and 200 GBq/µmol were obtained. The identity of reference FESDS and the product synthesized in the module was confirmed by mass spectroscopy (m/z 448).

Experimental

Chemicals
Sulphamoyl chloride was synthesized according to a modified procedure of Appel and Berger [12]. The synthesis of FESDS is described in [11]. Kryptofix 2.2.2 and DBMP were purchased from Merck.

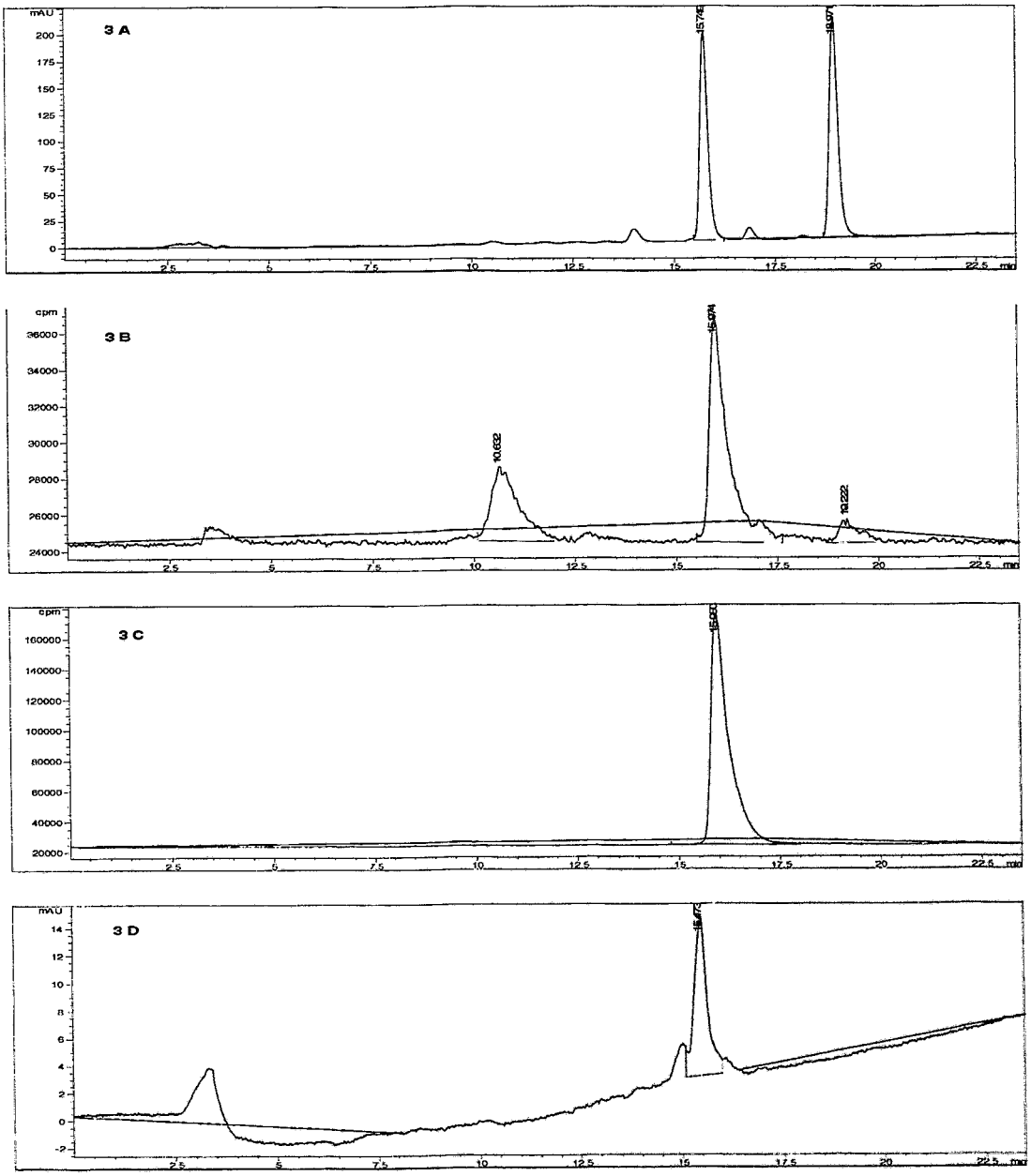

Fig. 3. Analytical HPLC chromatograms
3A – UV chromatogram of a reference solution containing FES and FESDS
3B – Radiochromatogram of the impure product of Expt. 2 in Table 2
3C – Radiochromatogram of the column-purified [^{18}F]FESDS
3D – UV chromatogram of the column-purified [^{18}F]FESDS

Preparing the no-carrier-added (n.c.a.) [^{18}F]HF

The Rossendorf PET Centre is equipped with an IBA CYCLONE 18/9 cyclotron. [^{18}F]HF is produced by the ^{18}O(p,n)^{18}F reaction using enriched [^{18}O]H_2O (1.5 mL, 95 %) as target. For the optimization experiments only limited amounts of [^{18}F]HF were necessary. Therefore, the following irradiation conditions were usually used:

- Ion beam current on the target: 30 µA (18 MeV protons)
- Irradiation time: 5 minutes

After end of bombardment, the irradiated water was transferred from the target to the module, and here the starting radioactivity at t = 0 was measured

Preparing the n.c.a. [^{18}F]FES

The synthesis was carried out in a module (Nuclear Interface, Germany) which was modified in terms of program and hardware [7]. A semi-preparative RP column (SP 250/10 Nucleosil 120-7 C_{18}, Macherey & Nagel, Germany) served for separation of [^{18}F]FES. Aqueous ethanol (55%) was used in order to transfer the impure radioactive product from the reaction vessel into the column and then to elute [^{18}F]FES isocratically at a flow of 1.5 mL/min.

Optimization experiments to synthesize [^{18}F]FESDS

N.c.a.[^{18}F]FES (about 100 – 500 MBq) dissolved in about 2 mL 55% aqueous EtOH was placed in a bulb. After adding a solution of a base (either DBMP: 0.1 mg in 0.5 mL MeCN or K222/K_2CO_3: 22.5 mg K222 and 4.2 mg K_2CO_3 in 1.5 mL MeCN), the solvent was removed on a rotary evaporator. A solution of 10 mg SCl in 2 mL MeCN was added to the absolutely dry reaction batch. The bulb was stirred at room temperature or a higher temperature (up to 70 °C). Samples of 10 µl each were investigated in an analytical HPLC system (Hewlett-Packard, series 1050, diode array detector 1040 M, radio-activity detector A 100 from Canberra Packard. Column: ET 125/8/4 NUCLEOSIL 120-5 C_{18} from Macherey & Nagel. EtOH-water mixtures were the mobile phase at a flow of 0.5 mL/min with a linear gradient: 0 min – 30 % EtOH, 20 min – 60 % EtOH, 30 min – 100 % EtOH). To work up the reaction batch, the solvent was removed on a rotary evaporator and 55 % aqueous EtOH (0.6 mL) was added. The clear solution (0.5 mL) was injected into a semi-preparative HPLC system (Merck-Hitachi, pump L-6200A, a Rheodyne injector with a 0.5 mL loop, an RP column SP 250/10 NUCLEOSIL 100-7C_{18} (Macherey & Nagel, Germany) and a diode array detector L-4500 DAD). The column was eluted with 55 % aqueous EtOH at 1.5 mL/min. After UV measurement at λ = 275 nm , the eluted solution was measured in a radioactivity detector (Canberra Packard A 120). Each solvent peak was collected and the radioactivity measured in an ionisation chamber (Nuklear Medizintechnik Dresden, Germany).

Module-assisted experiments to synthesize n.c.a.[^{18}F]FESDS

[^{18}F]FES was synthesized as described above. After cleaning the module, the collected eluate of [^{18}F]FES (1 - 3 GBq in 3 - 5 mL of 55 % aqueous EtOH) was transferred into the reaction vessel of the module in which the following four solutions were already stored in four vials:

Solution I	K222 (22.5 mg) and K_2CO_3 (4.2 mg) in 1.5 mL 86 % aqueous MeCN
Solution II	SCl (15 – 20 mg) in 1.5 mL absolute MeCN
Solution III	22% aqueous EtOH (4 mL)
Solution IV	absolute MeCN (12 mL)

The following operating steps were carried out:

- Addition of solution I and 4 mL of solution IV and drying the reaction mixture at 100 °C for 4 min.
- Addition of only 4 mL of solution IV and drying the reaction mixture at 100 °C for 4 min.
- Repetition of the last drying process and temperature reduction to 70 °C.
- Addition of solution II. The reaction mixture is stirred for 5 min at this temperature.
- Evaporation of the solvent within 1 min. Heating is switched off.
- Addition of solution III and waiting for 1 min.
- Transferring the solution into the injection loop.
- Injection of the solution into the column. Elution using 45 % aqueous EtOH.
- Collection of the eluate of the [^{18}F]FESDS peak (RT = 25 min).
- Measuring the radioactivity of [^{18}F]FESDS.

Radio-TLC

Samples of the impure product solution and the collected eluate of the [^{18}F]FESDS were developed on a silica-gel plate (MERCK) in toluene/ethyl acetate (3:1). For visualizing the chromatogram, the TLC plate was contacted with an imaging plate (IP-BAS-III, 20x25, Fuji) for 15 s . The distribution of radioactivity on the plate was recorded by an imaging analyzer (BAS 2000, Fuji).

Conclusions

Sulphamoylation of [^{18}F]FES in the presence of K222/K_2CO_3 is a rapid and reproducible procedure. It is also applicable as a module-assisted procedure. The whole synthesis of [^{18}F]FESDS in a module-assisted way is composed of five steps:

- Module-assisted synthesis of [^{18}F]FES according to [7].
- Purifying [^{18}F]FES by RP-HPLC (see also [7]).
- Cleaning the module.
- Module-assisted synthesis of [^{18}F]FESDS.
- Purifying [^{18}F]FESDS by RP-HPLC.

Starting with high levels of radioactivity, [^{18}F]FESDS can be prepared in amounts up to 5 GBq using this way.

Acknowledgements

We wish to express our gratitude to the Deutsche Forschungsgemeinschaft for its grant in support of this work. We also thank Dr. U. Pleiß (BAYER AG) for his interest and helpful discussion.

References

[1] Stöcklin G. (1998) Is there a future for clinical fluorine-18 radiopharmaceuticals (excluding FDG)? *Eur. J. Nucl. Med.* **25,** 1612-1616.

[2] Mintun M. A., Welch M. J., Siegel B. A., Mathias C. J., Brodack J. W., Mc Guire A. H. and Katzenellen bogen J. A. (1988) Breast cancer: PET imaging of estrogen receptors. *Radiology* **169,** 45-48.

[3] Mc Guire A. H., Dehtashti F., Siegel B. A., Lyss A. P., Brodack J. W., Mathias C. J., Mintun M. A., Katzenellenbogen J. A. and Welch M. J. (1991) Positron tomographic assessment of 16α-[^{18}F]fluoro-17β-estradiol uptake in metastatic breast carcinoma. *J. Nucl. Med.* **32,** 1526-1531.

[4] Bombardieri E., Crippa F., Maffioli L. and Greco M. (1997) Nuclear medicine techniques for the study of breast cancer. *Eur. J. Nucl. Med.* **24,** 809-824.

[5] Lim J. L., Berridge M. S. and Tewson T. J. (1994) Preparation of [^{18}F]16α-fluoro-17β-estradiol by selective nucleophilic substitution. *J. Labelled Compd. Radiopharm.* **35,** 176-177.

[6] Römer J., Steinbach J. and Kasch H. (1996) Studies on the synthesis of 16α-[^{18}F]fluoroestradiol. *Appl. Radiat. Isot.* **47,** 395-399.

[7] Römer J., Füchtner F., Steinbach J. and Johannsen B. (1999) Automated productionof 16α-[^{18}F]-fluoroestradiol for breast cancer imaging. *Nucl. Med. Biol.* **26,** 473-479.

[8] Anderson C. J., Lucas L. J. H. and Widlanski T. S. (1995) Phosphate esters versus sulfate esters and the mechanism of action of steroid sulfatases. *J. Am. Chem. Soc.* **117,** 3889-3890.

[9] Purohit A., Howarth N. M., Potter B. V. L. and Reed M. J. (1994) Inhibition of steroid sulphatase activity by steroidal methylthiophosphonates: Potential therapeutic agents in breast cancer. *J. Steroid Biochem. Mol. Biol.* **48,** 523-527.

[10] Spillane J., Taheny A. P. and Kearns M. M. (1982) Versatile synthesis of sulphamate esters by phase-transfer methods. *J.Chem.Soc. Perkin I,* 677-679.

[11] Römer J., Steinbach J., Kasch H. and Scheller D. (1999) Herstellung und Charakterisierung der Sulfamate von Estra-3,17ξ-diolen. *J. prakt. Chem.* **341,** 574-587.

[12] Appel R. and Berger G. (1958) Über das Hydrazodisulphamid. *Chem. Ber.* **91,** 1339-1341.

[13] Schwarz S. and Elger W. (1996) Estrogen sulphamates, a novel approach to oral contraception and hormone replacement therapy. *Drugs Future* **21,** 49-61.

[14] Johnström P. and Stone-Elander S. (1995) The ^{18}F-labelled alkylating agent 2,2,2-trifluoroethyl triflate: Synthesis and specific activity. *J. Labelled Compd. Radiopharm.* **36,** 537-547.

[15] Lang L. and Eckelman W. C. (1994) One-step synthesis of ^{18}F labeled [^{18}F]-N-succinimidyl 4-(fluoromethyl)benzoate for protein labeling. *Appl. Radiat. Isot.* **45,** 1155-1163.

[16] Taylor M. D., Roberts A. D. and Nickles R. J. (1996) Improving the yield of 2-[^{18}F]fluoro-2-deoxyglucose using a microwave cavity. *Nucl. Med. Biol.* **23,** 605-609.

[17] Hamacher K., Coenen H. H. and Stöcklin G. (1986) Efficient stereospecific synthesis of no-carrier-added 2-[^{18}F]fluoro-2-deoxy-D-glucose using aminopolyether supported nucleophilic substitution. *J. Nucl. Med.* **27,** 235-238.

11. One-Pot Synthesis of 16α-[^{18}F]Fluoroestradiol-Disulphamate

J. Römer, F. Füchtner, J. Steinbach, H. Kasch [1]
[1]Hans-Knöll-Institut Jena

Introduction

In the preceding paper [1] the successful preparation of 16α-[^{18}F]fluoroestradiol-disulphamate ([^{18}F]FESDS) in a two-step synthesis was reported. After elaborating the two-step synthesis [2], we tried to prepare [^{18}F]FESDS in a module-assisted one-pot procedure. The experiments were carried out with the intention of shortening the synthesis time and increasing the real yield of [^{18}F]FESDS. Instead of five steps in the previous procedure [1], the one-pot procedure consists of in three steps:

- Module-assisted synthesis of 16α-[^{18}F]fluoroestradiol ([^{18}F]FES)
- Module-assisted synthesis of [^{18}F]FESDS
- Purifying [^{18}F]FESDS by reversed-phase high performance liquid chromatography (RP-HPLC)

Experimental

The [^{18}F]FESDS module
One of the modules (Nuclear Interface, Münster, Germany) for synthesis of 2-[^{18}F]fluoro-2-deoxy-D-glucose ([^{18}F]FDG) was modified in terms of program and hardware. Designed as the [^{18}F]FESDS module, it is shown in Fig. 1.

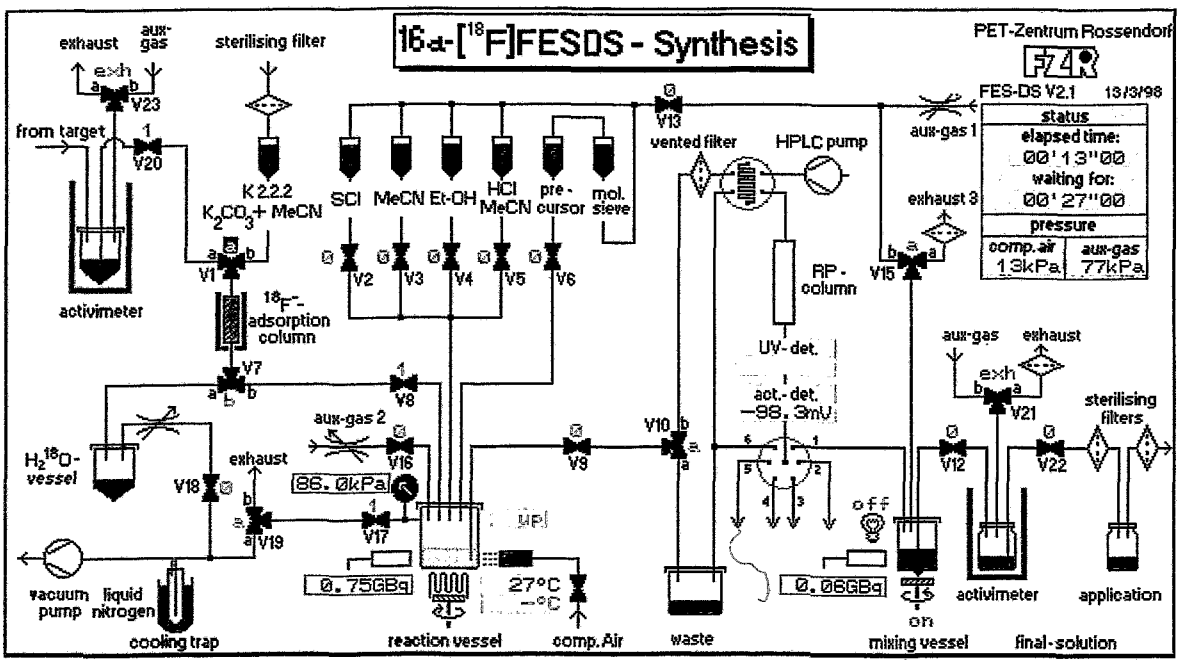

Fig. 1. Schematic diagram of the [^{18}F]FESDS module for synthesizing 16α-[^{18}F]fluoroestradiol-3,17β-disulphamate

The [^{18}F]FESDS module is an automatically operating, remote-controlled closed system. It is installed in a hot cell and makes it possible to process up to 200 GBq [^{18}F]fluoride. Evacuation is performed via a cooling trap (blue in Fig. 1) with liquid nitrogen. Volatile radioactive substances are thus trapped. The reaction vessel is made from glassy carbon and closed with a PEEK cover. It is connected via thin hose pipes (Teflon) and valves (V_1 – V_8, V_{20}) with the storage vessel for the target water (red in Fig. 1, the radioactivity A_0 at the time 0 is measured) and further storage vessels (1 – 6, blue) for storing the reagent solutions or solvents. These reservoirs are closed by septa. The solutions and solvents are moved within the module by vacuum or auxiliary gas (nitrogen). The reaction mixture in the reaction vessel can be

stirred, heated or cooled. A radioactivity detector controls the radioactivity of the reaction mixture. The reaction vessel is connected to an HPLC system (JASCO) consisting of an injection loop (5 mL), a semipreparative column (SP 250/10 Nucleosil 120-7 C_{18}, Macherey & Nagel, Germany), a UV/VIS detector, a radioactivity detector and a distribution system for the final solution (path 1, red), for other fraction collections (paths 2 – 5) and for waste (path 6, green). The column is eluted with ethanolic solutions at a flow of 1.5 mL/min.

Chemicals
The necessary precursor, 3-O-methoxymethyl-16,17-O-sulphuryl-16-epiestriol (1), was prepared according to the formula given in [3]. Sulphamoyl chloride (SCl) was prepared from commercial N-carbonylsulphamoyl chloride [4]. The synthesis of the reference substances FES and FESDS was described in [3] and [5]. Solvents and reagents were products of Sigma-Aldrich and were used as supplied. Kryptofix 2.2.2 was purchased from Merck.

Preparing the no-carrier-added (n.c.a.) [^{18}F]HF
The Rossendorf PET Centre is equipped with an IBA CYCLONE 18/9 cyclotron. [^{18}F]HF is produced by the $^{18}O(p,n)^{18}F$ reaction, using enriched [^{18}O]H_2O (1.5 mL, 95 %) as the target. To prepare ^{18}F for the [^{18}F]FESDS synthesis, the following irradiation conditions were used:
- Ion beam current on the target: 30 µA (18 MeV protons)
- Irradiation time: 30 or 60 minutes
At 60 min irradiation time, a target yield of 75 GBq was achieved. After end of bombardment, the irradiated water was transferred from the target to the module by a pneumatic transport system and measured there (A_0).

Synthesis preparation
Before starting the one-pot synthesis, the module was cleaned and supplied with all the solutions mentioned below. After storing the irradiated water in the reaction vessel of the module, the program was started. The program consisted of only four partial steps. Hydrolysis was followed by sulphamoylation. As a result the one-pot procedure was significantly shorter than the two-step synthesis.

The following solutions were needed in the one-pot synthesis of [^{18}F]FESDS:

Solution I	K222 (15 mg) and K_2CO_3 (2.77 mg) pro mL 86 % aqueous MeCN (3 mL)
Solution II	1 (2 mg) in 1 mL absolute MeCN
Solution III	0.1 M hydrochloric MeCN (6 mL) prepared by mixing 9 parts of MeCN with 1 part of 1 M HCl
Solution IV	SCl (10 – 15 mg) in 1.5 mL absolute MeCN
Solution V	22.5 % EtOH (4 mL)

Absolute MeCN (12 mL) was also required for drying processes.

The procedure for preparing [^{18}F]FESDS in a one-pot synthesis is shown in FIG. 2.

Measuring instruments and auxiliaries
An HPLC system (Hewlett Packard) with a diode array detector, a radioactivity detector and an analytical column (ET 125/8/4 Nucleosil 120-5 C_{18} from Macherey & Nagel, Germany) was used to keep check on the purity of the final product. EtOH-water mixtures were the mobile phase (flow rate: 0.5 mL/min) with a linear gradient (0 min: 30 % EtOH, 20 min: 60 % EtOH, 30 min: 100 % EtOH). The HPLC system was also used for determining [^{18}F]FESDS as an impure product and the specific activity of [^{18}F]FESDS.

Radioactivity measurements for determination of yields and specific radioactivity
In all experiments the starting radioactivity (A_0) at t = 0 and the radioactivity of [^{18}F]FESDS after HPLC purification (A_t(^{18}FESDS)) were determined.. These values were used to evaluate the yield of [^{18}F]FESDS. The yield was expressed as the real yield Y_{real}(%) and the decay-corrected yield $Y_{corr.}$(%) with the calculated value $A_{t,corr.}$ being the measured value A_t related from the measuring time t to t = 0.

$$Y_{real}(\%) = 100 \frac{A_t(^{18}FESDS)}{A_0}, \quad Y_{corr.}(\%) = 100 \frac{A_{tcorr.}(^{18}FESDS)}{A_0}$$

Furthermore, the specific activity of [^{18}F]FESDS was determined. For this purpose the FESDS concentration of the [^{18}F]FESDS solution was measured, using the analytical HPLC system (see [1]).

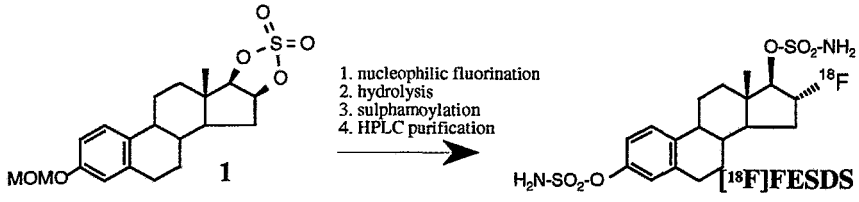

Fig. 2. One-pot synthesis of 16a-[^{18}F]fluoroestradiol-3,17b-disulphamate ([^{18}F]FESDS)

Explanation of the way of preparation of [^{18}F]FESDS with reference to Table 1
All the individual steps included in the preparation of chemically and radiochemically pure [^{18}F]FESDS are listed in Table 1. Twelve of these steps took place in the module, three during HPLC purification.

Table 1. Summary of Operations and Parameters in the Module-Assisted One-Pot Synthesis of [^{18}F]FESDS

Step	Operations and parameters
A [a)]	Add solution I (1,5 mL) [b)] and completely evaporate the solvent [c)]
B	Add solution II
C	Fluorinate at 100 °C for 10 min
D	Remove the solvent
E [d)]	Add 1,5 mL of solution III, and dry the reaction mixture at 100 °C for 3 min
F [d)]	Repeat step E twice
G	Add solution I (1.5 mL) and 2 ml MeCN and dry the reaction mixture at 100 °C for 4 min [e)]
H	Add only 2 mL MeCN and dry the reaction mixture at 100 °C for 4 min [e)]
J	Repeat step H and lower the temperature to 70 °C
K	Add solution IV and keep the reaction vessel for 5 min at this temperature
L	Evaporate the solvent within 1 min and switch the heating off
M [f)]	Add 4 mL of solution V
N	Transfer the solution from step M into the injection loop and inject into the HPLC system [g)]
O [h)]	Elute using 45 % EtOH; flow: 1.5 mL/min; detection: UV (275 nm), RA
P [f)]	Collect the radioactive peak of [^{18}F]FESDS, the retention time of which is 30 min. Measure the radioactivity of [^{18}F]FESDS

a) Before starting the one-pot synthesis, the cleaning program had been carried out, and [^{18}F]HF in [^{18}O]H_2O was placed in the module's reaction vessel and all the required solutions had been stored in the vials of the module.
b) In this moment, the fed-in radioactivity was bound as [^{18}F]KF.
c) Careful drying is necessary. Therefore, after the first drying (at 100 °C and reduced pressure), 2 ml MeCN were added, and a second drying process was performed.
d) In the steps E and F, nonbonded ^{18}F, i.e., unconverted [^{18}F]KF, was eliminated from the reaction vessel as [^{18}F]HF. The producer obtains a first information about the yield to be expected (see [6]).
e) The solvent was removed by using vacuum and auxiliary gas (2 min), then by using vacuum alone (2 min).
f) A sample of the solution from this step was checked in the analytical HPLC system.
g) HPLC = high performance liquid chromatography.
h) EtOH = ethanol; UV = ultraviolet; RA = radioactivity

Results and Discussion

The results of the first five synthesis experiments carried out in the [^{18}F]FESDS module are compiled in columns 4 - 9 of Table 2. The irradiation time and the resulting starting radioactivity are listed in columns 2 and 3.

We found that the starting radioactivity is linearly dependent on the irradiation time. A longer irradiation time proved to be advantageous for the specific activity (A_{sp}, column 9). For the results in [1] the A_{sp} values at 30 min were found between 50 and 200 GBq/µmol and at 60 min between 200 and 300 GBq/µmol.

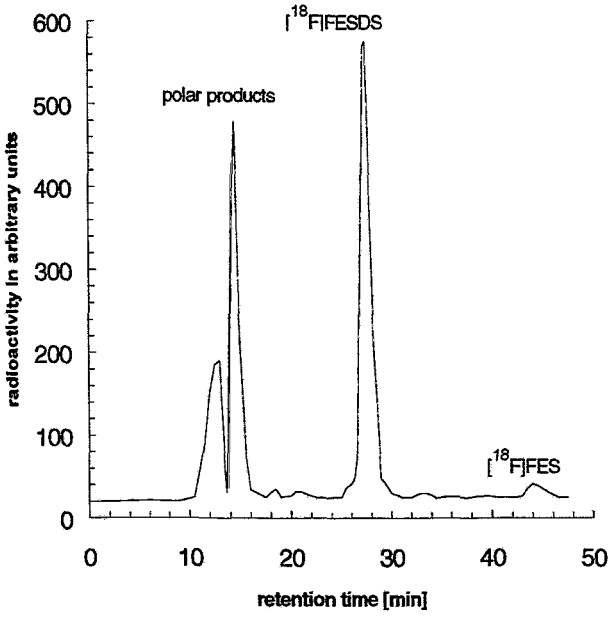

Fig. 3. A typical column radiochromatogram of the 16α-[^{18}F]fluoroestradiol-3,17β-disulphamate

Compared with the synthesis time of the two-step procedure [1], the synthesis time of the one-pot procedure was halved. Thus, the real yield (i.e. the [^{18}F]FESDS available after HPLC purification) was significantly higher. All the operations of the one-pot program (see Table 1, steps A - N) needed about 1 h. In the following HPLC purification (Table 1, steps O and P) [^{18}F]FESDS was eluted after about 25 min in a volume of about 2.5 - 3 mL. Thus, the total synthesis time was about 1.5 h.

The decay-corrected yield of about 20 % in the two-step procedure corresponds to a real yield of 6.5 %. But, the real yield of [^{18}F]FESDS found here is between 11 and 15 %. In terms of radioactivity, there are amounts of more than 10 GBq [^{18}F]FESDS which can be made available to the users.

In all the experiments between 10 and 30 mg of sulphamoyl chloride dissolved in 1.5 mL acetonitrile was used. Increasing the reagent to more than 30 mg had no effect on the yield. But the yield of [^{18}F]FESDS was lower, when less than 10 mg SCl was used for the sulphamoylation reaction.

We were pleasantly surprised at the good reproducibility of the one-pot procedure. This becomes evident from the values of real yield Y_{real} or the decay-corrected yield $Y_{corr.}$ in Table 2, which are all to be found within rather narrow limits. It also becomes evident from the fact that each successful experiment resulted in a column radiochromatogram as shown in Fig. 3. In this radiochromatogram, there are two peaks of polar products with about 50 % of the total radioactivity and the [^{18}F]FESDS peak with about 45 %, and only a small amount of unconverted [^{18}F]FES. The radiochemical purity of the collected [^{18}F]FESDS peak was >99 %.

It is important to note that the sulphamoylation reaction in the one-pot procedure is hardly susceptible to any influences. This is due to the presence of kryptofix 2.2.2 [7]. The procedure worked well even with sulphamoyl chloride which due to long storage contained a distinct amount of sulphamoyl acid.

Conclusions

Pure [^{18}F]FESDS of high quality can also be prepared in a one-pot procedure. As this procedure is more rapid than the two-step synthesis larger amounts of radioactivity can be supplied to the users. The specific activity found after 60 min irradiation time was between 200 and 300 GBq/µmol. In order to increase the specific activity, we will increase the irradiation time in the nearest future.

Table 2. Results of five one-pot syntheses in the [^{18}F]FESDS module

1	2	3	4	5	6	7	8	9
Expt.	Irradiation time [min]	Starting activity [MBq]	Synthesis time [min]	A_t(^{18}FESDS) [MBq] a)	Y_{real} [%] b)	$A_{t,corr.}$(^{18}FESDS) [MBq] c)	$Y_{corr.}$ [%] d)	A_{sp}(^{18}FESDS) [GBq/µmol] e)
1	30	34000	89	4475	13.2	7851	23.1	58.9
2	30	28100	89	3950	14.1	6930	24.7	90.8
3	60	63500	90	9350	14.7	16490	26.0	226
4	60	54800	101	7125	13.0	13467	24.6	248.2
5	60	59500	92	6870	11.5	12290	20.7	280

a) Really available Radioactivity of [^{18}F]FESDS at that Time given in Column 4
b) Real Yield of [^{18}F]FESDS
c) Radioactivity of Column 5 at Time t = 0
d) Decay-corrected Yield of [^{18}F]FESDS
e) Calculated Specific Activity of [^{18}F]FESDS

Acknowledgements

We wish to express our gratitude to the Deutsche Forschungsgemeinschaft for its grant in support of this work. We also thank Dr. U. Pleiß (BAYER AG) for his interest and helpful discussion.

References

[1] Römer J., Füchtner F. and Steinbach J. (!999) Two-step synthesis of 16α-[^{18}F]fluoroestradiol-disulphamate. *This report*, pp. 38-45.

[2] Römer J., Füchtner F. and Steinbach J. (1999) Synthesis of 16α-[^{18}F]fluoroestradiol-3,17β-disulphamate. *J. Labelled Compd. Radiopharm.* (in press).

[3] Römer J., Steinbach J. and Kasch H. (1996) Studies on the synthesis of 16α-[^{18}F]fluoroestradiol. *Appl. Radiat. Isot.* **47**, 395-399.

[4] Appel R. and Berger G. (1958) Über das Hydrazodisulfamid. *Chem. Ber.* **91**, 1339-1341.

[5] Römer J., Kasch H., Steinbach J. and Scheller D. (1999) Herstellung und Charakterisierung der Sulfamate von Estra-3,17β-diolen. Schnelle Umsetzung von 16α-Fluorestradiol zum 16α-Fluorestradiol-3,17β-disulfamat. *J. prakt. Chem.* **341**, 574-587.

[6] Römer J., Füchtner F., Steinbach J. and Johannsen B. (1999) Automated production of 16α[^{18}F]fluoroestradiol for breast cancer imaging. *Nucl. Med. Biol.* **26**, 473-479.

[7] Römer J., Füchtner F. and Steinbach J. (2000) Synthesis of 16α-fluoroestradiol-3,17β-disulphamate. *J. Labelled Compd. Radiopharm.* (in press).

12. Steroidal 16,17-Cyclic Carbonates as Key Products for Cyclic Sulphites and Sulphates

H.Kasch[1], U.Dintner[1], J.Römer, J.Steinbach
[1]Hans-Knöll-Institut für Naturstoff-Forschung Jena

Introduction

We recently described the synthesis of the 16β,17β-cyclic carbonates (**1**, cis-β,β), starting from 17β-hydroxy,16α-bromo-steroids of the androstane and estrane series [1]. The isomeric 16α,17α-cyclic carbonates (**1** , cis-α,α) can be similarly synthesized from the 17α-hydroxy, 16ß-bromo derivatives through the intra-molecular ring closure reactions to the intermediate 16α,17α dioxolanimines [2] (Scheme 1).

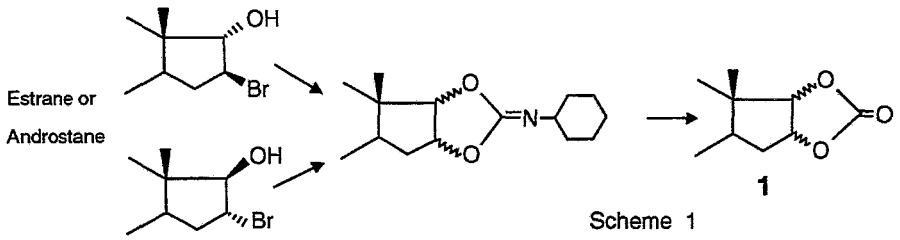

Scheme 1

Cyclic carbonates are good tools for preparing cis-diols (**2**) which can be converted via the surprisingly stable cyclic sulphites (**3**) into cyclic sulphates (**4**) (Scheme 2). The reaction sequence **1 → 2 → 3 → 4** described here is a new approach to the cis-16ξ-O,17ξ-O-sulphonyl steroids which are important precursors for nucleophilic fluorination reactions.

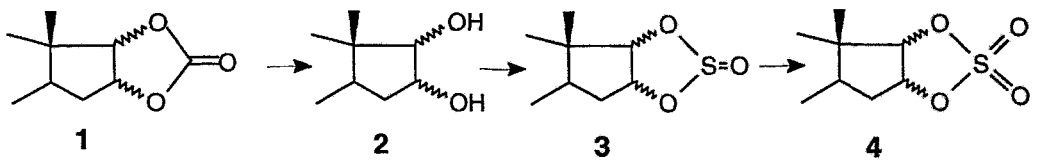

Scheme 2

Experimental

16α,17α- or 16β,17β-diols (2)
The corresponding 3-O-protected cyclic carbonate (**1**) (1 mmol) was suspended in methanol (15 ml) containing water (1 ml) and potassium carbonate (2 mmol). The solution was heated to 50 °C and stirred until the saponification was completed. The 3-O-protected diols **(2)** were precipitated by adding water to the methanolic solution.

(R) and (S) - 16α,17α- or 16β,17β-cyclic sulphites (3)
Dry 3-O-protected-16ξ,17ξ-diol (**2**) (0.3 mmol) was dissolved in tetrahydrofuran. Pyridine (0.5 mmol) and thionyl chloride (0.5 mmol) were intermittantly added to the stirred solution at temperatures below 0°C. After stirring for 15 minutes, the solution was evaporated to dryness and the residue suspended in water. The mixture of the diastereomeric sulphites was separated by column chromatography on silica gel, using toluene (estrane-series) or toluene / n-hexane (androstane-series).
The minor unpolar components of the sulphites showed „R"- configuration of the oxothiodioxolan-function in the α,α- and „S" in the β,β-series, while the polar main components showed „S"-configuration in the α,α- and „R" in the β,β-series.

16α,17α- or 16β,17β-cyclic sulphates (4)
The above mixture of sulphite preparations (0.3 mmol) was dissolved in a two phase methylenchloride/water solution containing potassium permanganate (0.5 mmol) and tetrabutyl-ammoniumbromide (0.1 mmol). The solution was vigorously stirred until the oxidation was complete, controlled by thin-layer chromatography (TLC)

on silica gel using toluene. After adding sodium sulphite, the steroid was extracted with methylene chloride and recrystallized after evaporating the solvent.

Structure determination
MS, ^{1}H NMR, 2D ^{13}C NMR, IR, and UV were used for structure determination. The absolute configuration of the cyclic sulphites was determined by circular dichroism (CD) and correlation with NMR data, chromatographic characteristics and MM2-calculations.

Results and Discussion

Cyclic carbonates are stable to acids, for example, to diluted hydrochloric acid or hydrobromic acid / acetic acid, but they are easily cleaved under basic conditions in protic and aprotic solvents. In this process cis-diols are quantitatively synthesized by saponification, using a diluted aqueous-methanolic potassium carbonate solution. The cyclic carbonates are easier saponified than the 3-acetates. Thus, the 3-protective group can be partially saved in the saponification process.
The reaction **2** → **3** was optimized. It was found that the cyclic sulphites (**3**) are best prepared by using thionyl chloride in tetrahydrofuran in the presence of pyridine as a proton-accepting base. The resulting sulphites were purified and characterized. The results are summarized in Table 1.

Table 1. Melting points and chromatographic properties of some new cyclic sulphites **3** α

Cyclic sulphites **3** prepared according to the reaction **2** → **3**	R_F-value a)	Retention time [min] b)	M. p. [°C]
3ß-Acetoxy-[(R)-16α,17α-dioxysulfinyl]-androst-5-ene **(3a)**	0.30	5.2	173-176
3ß-Acetoxy-[(S)-16α,17α-dioxysulfinyl]-androst-5-ene **(3b)**	0.26	5.6	175-181
3ß-Acetoxy-[(S)-16β,17β-dioxysulfinyl]-androst-5-ene **(3c)**	0.28	5.2	192-197
3ß-Acetoxy-[(R)-16β,17β-dioxysulfinyl]-androst-5-ene **(3d)**	0.20	6.2	172-180
3-Methoxy- [(R)-16α,17α-dioxysulfinyl]-estra-1,3,5(10)-triene **(3e)**	0.43	4.2	129-134
3-Methoxy- [(S)-16α,17α-dioxysulfinyl]-estra-1,3,5(10)-triene **(3f)**	0.34	4.9	157-159
3-Methoxy- [(S)-16β,17β-dioxysulfinyl]-estra-1,3,5(10)-triene **(3g)**	0.37	4.0	140-147
3-Methoxy- [(R)-16β,17β-dioxysulfinyl]-estra-1,3,5(10)-triene **(3h)**	0.28	4.3	130-133

a) TLC was performed using silica gel 60 $_{F254}$ aluminium sheets (Merck) and toluene (for estrane derivatives) or toluene / n-hexane (androstane series) as eluents.
b) HPLC was performed using a RP18 Purosphere column, 5 µm, 125/4 (Merck) and acetonitrile : 1% aqueous diisopropylamine = 90 : 10 as eluent.

In each reaction, no matter whether 16α,17α- or 16β,17β-dihydroxysteroid was used as a starting material, two isomeric sulphites were formed. These two sulphites (e.g. **3a** and **3b** in Table 1) were easily separated from each other by TLC and HPLC.
The Valence Shell Electron Pair Repulsion Theory [3] offers a simple explanation for the formation of diastereomeric sulphites in the reaction **2** → **3**. The electron pair on the sulphur of the cyclic sulphites is perceived to be functioning as substituents. Because of the various configuration possibilities of the electron pair, the sulphites are formed in two different „R" and „S" configurations according to the rule stipulated by Cahn, Ingold and Prelog [4].
MM2-calculations showed that sulphite is thermodynamically favoured, the more polar it is, which was indeed the case. The product relationships depended on the reaction conditions. Working at room temperature and using only small amounts of pyridine, more of the thermodynamically unfavoured product was formed.
TLC performance and the NOE (NMR) method revealed the interactive effects of the oxothiodioxolane rings with the neighbouring substituents; thus proving the polarity of the diastereomers (R / S), and likewise the thermodynamically favourable connection.
Additional confirmation has been seen in these data through CD measurements in methanol. Within appropriate short wave parameters, the CD curves of the substance pairs of the 16β,17β (or 16α,17α) sulphites occurred as epimeres, which means that the Cotton effects are reversed. Since the estratriene derivative of

the CD curves are clearly seen, due to the additional chromophors in the A-rings at 205 and 212 nm, the significant CD bands of the androstene derivatives are at 205, or 195 nm.
In Fig. 1, the epimeric 16β,17β-sulphites of the 16-epiestriol-3-methyl ethers are shown. On the right, the interaction of the sulphinyl group with the 13-methyl group in **3g** is represented. But no interaction between sulphinyl and 13-methyl group exists in **3h** on the left side.

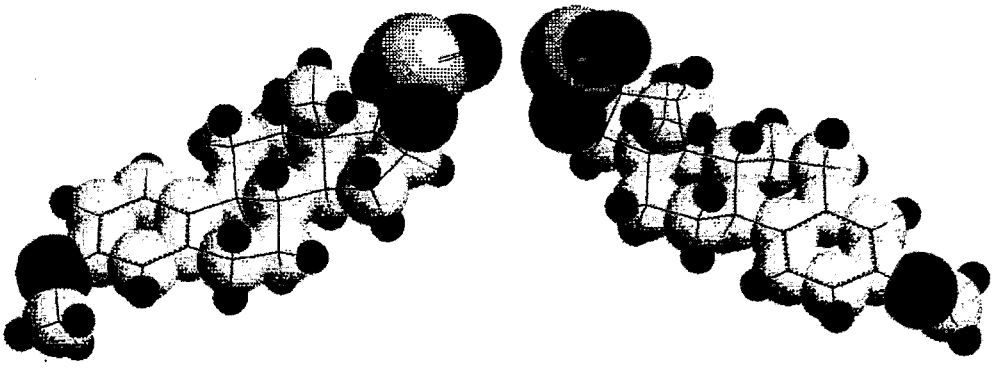

3-Methoxy- [(R)-16β,17β-dioxysulfinyl]-estra-1,3,5(10)-triene **(3h)**

3-Methoxy- [(S)-16β,17β-dioxysulfinyl]-estra-1,3,5(10)-triene **(3g)**

Fig. 1. Three-dimensional structure of the epimeric 16β,17β-sulphites of the epiestriol-3-methylether

In general, the reaction **3 → 4** is carried out according to the Sharpless method [5], in which the freshly prepared cyclic sulphites are oxidized with rhodium-III-chloride/$NaJO_4$. But oxidation with permanganate under phase transfer conditions proved to be a better method, because it was able to overcome the intermittent solubility problems of the steroids. The epimeric sulphites can be used as a substrate. This is because the asymmetric centre on the sulphur was removed by oxidation, forming the symmetric cyclic sulphates. This saves the purification of the epimeric sulphites and the resulting sulphates.
Recently the cyclic cis-16ξ-O,17ξ-O-sulphonyl steroids have played an important part as precursors for preparing the vicinal trans-16-substituted 17-hydroxy steroids [6]. Because of their electrophilic properties the cis-16ξ-O,17ξ-O-sulphonyl steroids are more reactive than the corresponding cis-16ξ-O,17ξ-O-sulphinyl steroids.

Conclusions

Steroidal 16ξ,17ξ-cyclic carbonates which are available from 17-keto steroids are good tools for preparing cis-16ξ,17ξ-diols. The following reactions open up possibilities of synthesizing 16ξ,17ξ-cyclic sulphites and 16ξ,17ξ-cyclic sulphates. The latter represent important precursors for the nucleophilic ^{18}F-fluorinations. After successful preparation of 16α-[^{18}F]fluoroestradiol our investigations will be extended to the androstane-series.

References

[1] Kasch H., Dintner U., Römer J. and Steinbach J. (1997) Preparation of androst-5-ene-3β,16β,17β-triol derivatives as precursors for rapid synthesis of 16α-[^{18}F]fluoro-androst-5-ene-3β,17β-diol. *Annual Report 1997*, Institute of Bioinorganic and Radiopharmaceutical Chemistry, FZR-200, pp 193 – 195.
[2] Kasch H., Dintner U., Steinbach J. and Römer J. *Publication in preparation.*
[3] Gillespie R. J. (1967) Elektronenpaar-Abstoßung und Molekülgestalt. *Angew.Chem.* **79**, 885-896.
[4] Cahn R. S., Ingold Ch. and Prelog V. (1966) Spezifikation der molekularen Chiralität. *Angew. Chem.* **78**, 413-447.
[5] Gao Y. and Sharpless K. B. (1988) *J. Am. Chem. Soc.* **110**, 7538.
[6] Berridge M. S., Franceschini M. P., Rosenfeld E. and Tewson T. J. (1990) Cyclic sulfates: Useful substrates for selective nucleophilic substitution. *J. Org. Chem.* **55**, 1211.

13. In Vitro Selection of Sulphatase Inhibitors for Tumour Diagnosis with PET and for Tumour Therapy

H. Kasch[1], J. Römer, J. Steinbach
[1]Hans-Knöll-Institute für Naturstoff-Forschung Jena

Introduction

Steroids play a significant role as mediators in cellular communication. As hormones which affect enzymes and components of cell membranes, they are seen as responsible for a number of functions. Steroid hormones, especially estrogens, are frequently responsible for the development of breast cancer [1, 2].
Over the last 15 years various concepts of drug treatment of estrogen-dependent tumours (for example with Tamoxifen) have been successfully tested. The main focus was directed on the elimination of estrogens such as estrone, estradiol and androstenediol. The estrogen action was minimized by application of receptor antagonists, on the one hand, and inhibition of the transformation of steroid precursors, such as estrone sulphate, dehydroepiandrosterone (DHEA) sulphate or androstenedione, into estrogens, on the other. The targets to achieve these aims are enzymes, such as 17-steroid dehydrogenase, esterase, aromatase, estrone sulphatase, and estrogen receptors. All these enzymes and receptors are enriched in estrogen dependent tumour cells [3].
The combination of the estrogen receptor blockers and inhibitors of aromatase, 17-steroid dehydrogenase and estrone sulphatase holds out good prospects for the therapy of estrogen-dependent mammary tumours.
We recently reported on synthesis of new sulphamates (**2**, **3**, **4**) of estradiol (**1a**) and its 16α-compounds as potential inhibitors of sulphatase [4]. In this paper we describe the search for such sulphatase inhibitors, using human placenta microsomes [5]. Our goal was to select suitable compounds which can be useful for tumour, utilizing ^{18}F-labelled compounds and the PET-technique and also for therapy. For PET purposes we intended to image the sulphatase target in mamma tumours.

Chemical and biological experiments

General
The sulphamates (**2**, **3**, **4**) were prepared by sulphamoylation of the 3,17-diols (**1**) with sulphamoyl chloride in DMF or in methylenchloride / K_2CO_3 in the presence of tetrabutylammonium bromide. The sulphamoylation reaction is not regioselective, i.e. all the sulphamates are formed. To determine their biological behaviour the sulphamates have to be prepared in > 99 % purity. In order to ensure high purity a combined purification procedure using flash chromatography on silicagel and HPLC was used. In this way contamination of the biologically weaker compound by traces of a more active 3- or 3,17-sulphamate was ruled out.

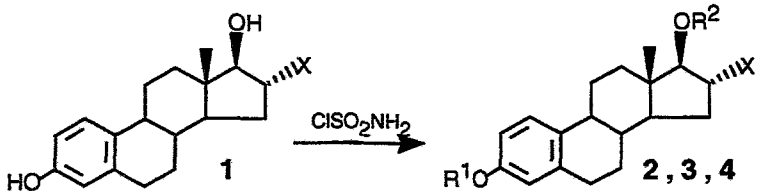

	X	R^1	R^2
1a	H		
1b	Br		
1c	F		
2a	H	H_2N-SO_2	H
2b	Br	H_2N-SO_2	H
2c	F	H_2N-SO_2	H
3a	H	H	SO_2-NH_2
3b	Br	H	SO_2-NH_2
3c	F	H	SO_2-NH_2
4a	H	H_2N-SO_2	SO_2-NH_2
4b	Br	H_2N-SO_2	SO_2-NH_2
4c	F	H_2N-SO_2	SO_2-NH_2

In vitro - testing with human placenta microsomes

Estrone sulphatase can release estrone or dehydroepiandrosterone (DHEA) from estrone sulphate or DHEA-sulphate. The enzyme is ubiquitously distributed within the body and is especially enriched in the leukocytes, macrophages, the brain, and the placenta. It can further be seen in the estrogen-dependent MCF-7 cell lines.

For the in vitro analysis of the sulphatase-inhibiting effect, placenta microsomes taken from a fresh placenta were used according to the Reed procedure [6]. At –20 °C the microsomes are preserved from any significant loss of activity for six months. Further experiments with rat liver microsomes yielded comparable results.

The incubation experiments were carried out using [6,7-^{3}H]estrone sulphate potassium salt. Free [6,7-^{3}H]-estrone released by sulphatase was measured after extraction with toluene.

Procedure

In a 5 ml test tube estrone sulphate potassium [6,7-^{3}H], estrone sulphate ammonium salt (altogether 20mM) as well as a solution of the sulphatase inhibitors to be tested (1 – 2 mg / ml basic solution, concentration between 0.01 and 5 µM) were mixed in a tris-HCl buffer. In a second vial human placenta microsomes (0.1 – 0.5 mg protein, determined by Bradford's method) were prepared in a tris buffer.

The chilled enzyme-containing solution was added to the substrate solution. After warming to 37 °C and incubation for 20 minutes, the enzyme was destroyed by adding 1.5 ml of toluene, and the steroid was extracted (Vortex, 1 min.). To measure the radioactivity in a liquid scintillation analyzer (Packard), 50 µl of toluene extract was withdrawn and mixed with 3 ml of scintillator solution (Vortex, 10 s). For comparison of the IC_{50} values, known compounds such as estrone sulphamate and dehydroepi-androsterone sulphate were used as standards. This measurement was carried out two or three times.

With new substances the initial experiment was geared towards ascertaining the IC_{50} values. In sulphatase inhibiting effects, the values ranged from 0.01 to 25 µM.

Results and Discussion

We were interested in finding substances with high sulphatase-inhibiting effects. Such substances are useful for diagnostic purposes, where the drug and the labelled compound are nearly identical in structure and activity. In the present case of fluoroestradiol-3,17β-disulphamate or bromoestradiol-3,17β-disulphamate the diagnostics (^{18}F- or ^{75}Br,^{76}Br-labelled compound) and therapeutics are fortunately identical.

The sulphatase inhibition effect of all the sulphamates **2**, **3**, and **4** was determined. The IC_{50} values obtained are compiled in Table 1.

Table 1. IC_{50} values for sulphatase inhibition by estrone sulphamate and the sulphamates **2**, **3**, and **4**

Substances	3-Monosulphamates (2) [µM]	17-Monosulphamates (3) [µM]	3,17-Disulphamates (4) [µM]
Estrone	0,07		
Estradiol (1a)	0.09 (2a)	25 (3a)	0.035 (4a)
16α-Bromoestradiol (1b)	0.09 (2b)	7 (3b)	0.020 (4b)
16α-Fluoroestradiol (1c)	0.08 (2c)	2.5 (3c)	0.025 (4c)

Fig. 1 shows the relative values for sulphatase inhibition by the 3-, 3,17- and 17-sulphamates with estrone sulphamate (activity = 1) being the reference compound.

The results demonstrate that the disulphamates (**4a**, **4b**, **4c**) are essentially more active than estrone sulphamate. The inhibitor activities of estradiol-3-sulphamates (**2a**, **2b**, **2c**) are moderate in comparison with estrone sulphamate, those of estradiol-17-sulphamates (**3a**, **3b**, **3c**) are weak.

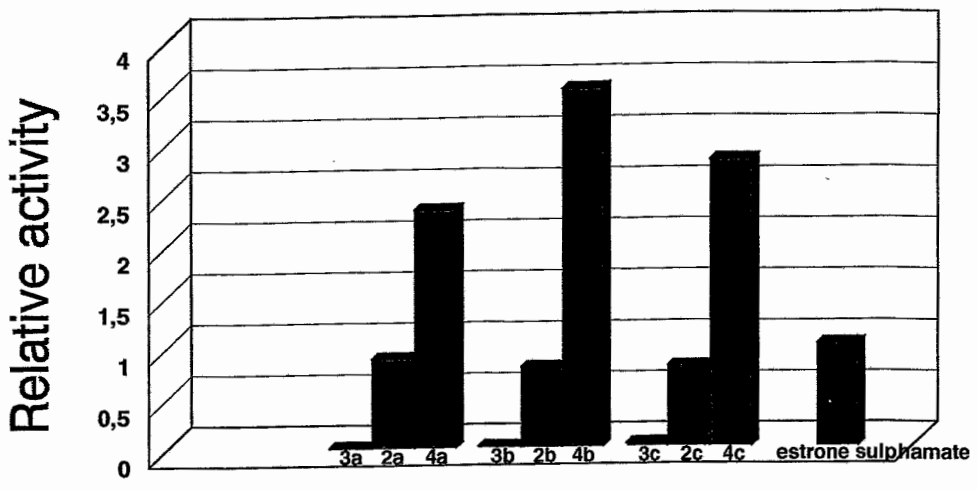

Fig. 1. Sulphatase inhibition by 17-monosulphamates **3** (green), 3-monosulphamates **2** (red), and 3,17-disulphamates **4** (blue). The values are related to estrone sulphamate activity of which is set = 1.

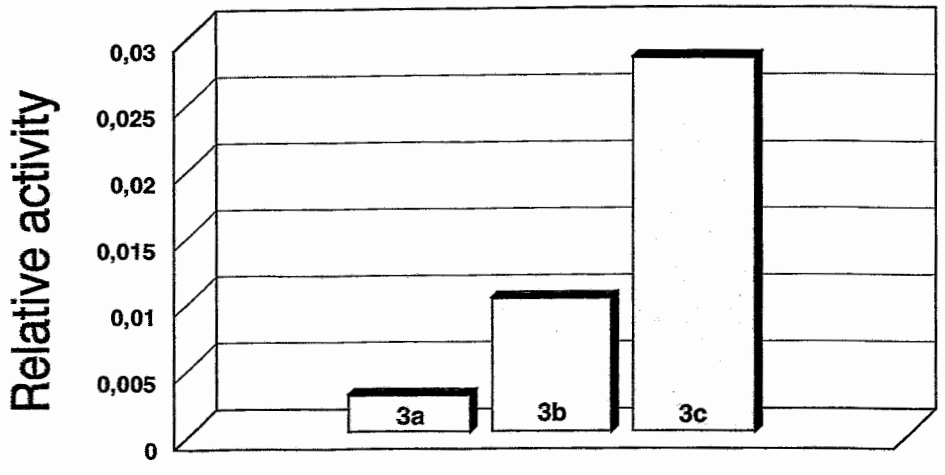

Fig. 2. Increase of the sulphatase inhibitory effect within the 17-monosulphamates **3a**, **3b**, and **3c**. The values are related to estrone sulphamate activity of which is set = 1.

Conclusions

A series of novel sulphatase inhibitors which are more active than the well-known steroid sulphatase inhibitors were selected. The introduction of an additional sulphamate group in the 17 position was combined not only with a decrease in estrogenic activity, but also with an enormous increase in the inhibition of estrone sulphatase [7].
Because 16α-fluoroestradioldisulphamate belongs to the most active sulphatase inhibitors, there are good prospects of ist being used as a diagnostic in [^{18}F] labelled form as well as for therapy.

Acknowledgements

The technical assistance of H.Hicke (HKI) with the sulphatase test is gratefully acknowledged. We wish to express our gratitude to the Deutsche Forschungsgemeinschaft for its grant in support of this work.

References

[1] Duncan L., Purohit A., Potter B. V. L. and Reed M. J. (1993) Inhibition of steroid sulphatase activity by estrone-3-methylthiophosphonate, *Cancer Res.* **53**, 298–303.

[2] Selcer K. W. and Li P.-K. (1995) Estrogenicity, antiestrogenicity and estrone sulphatase inhibition of estrone-3-amine and estrone-3-thiol. *J. Steroid Biochem. Mol. Biol.* **52**, 281-286.

[3] Anderson C. J., Lucas L. J. H. and Widlanski T. S. (1995) Molecular recognition in biological systems: Phosphate esters vs sulphate esters and the mechanism of action of steroid sulphatase. *J. Am. Chem. Soc.* **117**, 3889-3890.

[4] Römer J., Steinbach J., Kasch H. and Scheller D. (1999) Preparation and characterization of the sulphamates of estra-3,17-diols. Rapid conversion of 16α-fluoroestradiol-3,17β-disulphamates. *J. Prakt. Chem.* **341**, 574-583.

[5] Purohit A., Williams G. J., Howarth N. M., Potter B. V. L. and Reed, M. J (1995) Inactivation of steroid sulphatase by an active site-directed inhibitor, estron-3-sulphamate. *Biochemistry* **34**, 11508–11514.

[6] Reed K. C. and Ohno S. (1976) Kinetic properties of human placental aromatase. Application of an assay measuring $^{3}H_2O$ release from 1β,2β-^{3}H-androgens. *J. Biol. Chem.* **251**, 1625-1631.

[7] Kasch H., Dintner U., Härtl A., Römer J. and Steinbach J. (1999) [^{18}F]-PET-tracer- effective tools for disclosing ways of signal transduction. *Annual Report 1998.* HKI-Jena, pp. 33-36.

14. One-Pot Synthesis of N-Succinimidyl 4-[^{18}F]Fluorobenzoate

P. Mäding, M. Scheunemann, H. Kasper, J. Steinbach

Introduction

We have been using N-succinimidyl 4-[^{18}F]fluorobenzoate ([^{18}F]SFB) for labelling peptides by [^{18}F]fluorobenzoylation [1]. [^{18}F]SFB is prepared according to [2] by a three-step synthesis, which is a time-consuming and labour-intensive procedure. We are interested in a simplification and improvement of the synthesis of [^{18}F]SFB and therefore tried to produce the [^{18}F]SFB in a one-pot process.

Experimental

Materials
4-Dimethylaminobenzoic acid, trimethyloxonium tetrafluoroborate, Kryptofix 222 and dibenzo-18-crown-6 were purchased from Merck and had for synthesis quality. Di-(N-succinimidyl) carbonate (purum, 97 %), ethylene carbonate (puriss., 99 %) and sulfolane (99.5 %) were obtained from Fluka, Bu_4NOH (1 M solution in methanol) and methyl triflate (99 %) from Aldrich, and 18-crown-6 from Janssen Chimica.

Analysis
To determine the extent of conversion and the radiochemical purity and to identify the labelled products, an HPLC system (JASCO) was used, including a pump, a Rheodyne injector with a 20 µl loop, a LiChrospher WP300 RP-18 column (5 µm, 250 mm x 3 mm, Merck) and a UV detector coupled in series with a radioactivity detector FLO-ONE\Beta 150TR (Canberra Packard). The HPLC analyses were carried out at a flow rate of 0.5 ml/min with mixtures of MeCN and water containing 0.2 % TFA. The gradient of the eluents was: 0 min - 10 % MeCN/ 90 % water; 10 min - 60 % MeCN/ 40 % water; 14 min - 100 % MeCN/ 0 % water; 20 min - 100 % MeCN/ 0 % water.

Synthesis of the precursors
N-Succinimidyl 4-dimethylaminobenzoate (1)
Di-(N-succinimidyl) carbonate (2.56 g; 10 mmol) was added to a suspension of 4-dimethylaminobenzoic acid (1.65 g; 10 mmol) in 25 ml MeCN. After dropwise addition of NEt_3 (1.01 g; 10 mmol) in MeCN (5 ml) a clear solution of the reaction mixture was obtained. The mixture was heated at 50 °C for 1 h and then evaporated. The residue was dissolved in CH_2Cl_2 (60 ml). The organic solution was washed with aqueous $NaHCO_3$ and then with HCl (0.01 M). The organic phase was dried with Na_2SO_4. Evaporation of the filtered extract left a solid residue which was recrystallized from isopropanol. Light grey crystals, melting point: 205 - 207 °C, yield: (1.5 g, 57 %).

Tetrafluoroborate salt of N-succinimidyl 4-trimethylammonium benzoate (2)
Trimethyloxonium tetrafluoroborate (0.19 g; 1.28 mmol) was dissolved in nitromethane (1 ml) under argon. A solution of **1** (0.33 g; 1.26 mmol) in nitromethane (4 ml) was added drop by drop to the oxonium salt The reaction mixture was stirred for 4 h. Then dry diethyl ether (20 ml) was added while stirring, with a pink oil separating. The ether was decanted off and the procedure was twice repeated. In this way the oil slowly changed into a pink solid. It was recrystallized from a mixture of ethanol and isopropanol (4 : 7). Colourless crystals, melting point: 185 - 188 °C, yield: (0.18 g, 39 %).

Triflate salt of N-succinimidyl 4-trimethylammonium benzoate (3)
A solution of methyl triflate (0.19 g; 1.16 mmol) in CH_2Cl_2 (1 ml) was added to a stirred solution of **1** (0.3 g; 1.14 mmol) in CH_2Cl_2 (4 ml). The reaction mixture was stirred for 8 h with a pink oil separating. Then the solvent was decanted off. Addition of dry diethyl ether (10 ml) changed the oil into a colourless solid. After filtration of the hygroscopic solid through a frit glass filter it turned pink. The product was recrystallized from a mixture of THF and ethanol (2 : 1). Colourless crystals, melting point: 160 - 162 °C, yield: (0.11 g, 22 %).

Radiosyntheses
Experiments for the synthesis of [^{18}F]SFB
A solution of a phase-transfer catalyst (15 mg Kryptofix 222 or 10.6 mg 18-crown-6 or 14.4 mg dibenzo-18-crown-6; 40 µmol) and K_2CO_3 (2.77 mg; 20 µmol) in aqueous MeCN (1.5 ml; 86 %) or only Bu_4NOH (1 M, 40 µl, 40 µmol) in MeCN (1 ml) was added to a mixture of irradiated [^{18}O]H_2O containing n.c.a.

[^{18}F]HF. This reaction mixture was dried by means of a nitrogen stream at 90 - 95 °C using a cooled trap. The residue was carefully dried by repeated addition and evaporation of abs. MeCN (3 x 1 ml). After addition of the precursor **2** or **3** in a solvent, the reaction mixture was heated either at 90 - 95 °C or in a microwave oven.
For detailed reaction conditions see Table 1.

Results and Discussion

Prerequisites for the one-step procedure of preparing [^{18}F]SFB was a suitable precursor which already included the activated ester function of the benzoic acid and, in p-position, a leaving group for the nucleophilic substitution. Such a precursor was prepared by a two-step synthesis according to Scheme 1 starting from 4-dimethylaminobenzoic acid.
The esterification of the benzoic acid using di-(N-succinimidyl) carbonate yielded N-succinimidyl 4-dimethylaminobenzoate (**1**). The corresponding salt of N-succinimidyl 4-trimethylammonium benzoate (**2** = tetrafluoroborate; **3** = triflate) was obtained by methylation of the dimethylamino group of (**1**) with trimethyloxonium tetrafluoroborate or methyl triflate.

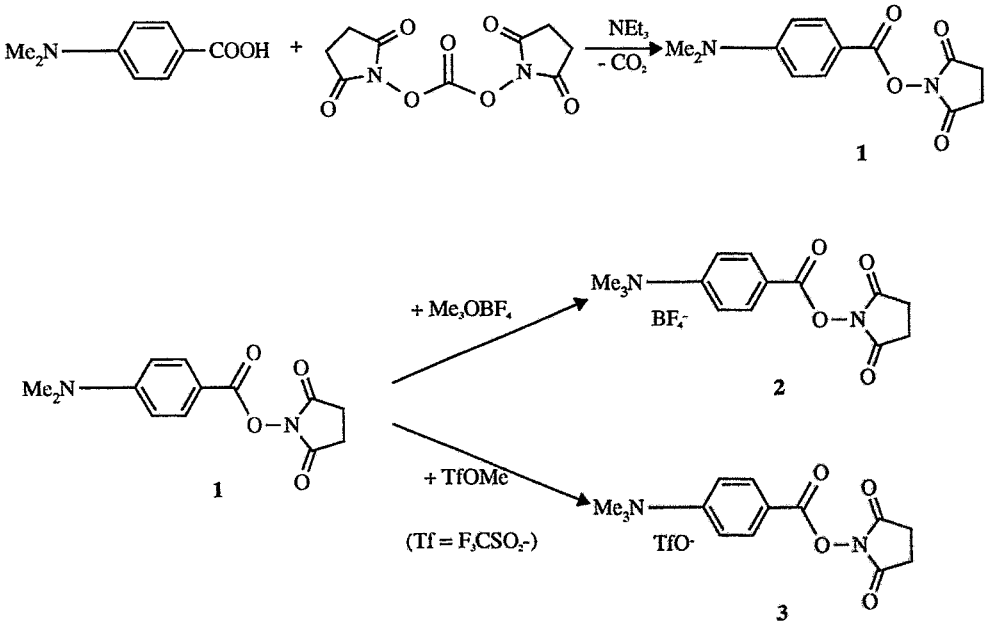

Scheme 1

The structures of the compounds **1**, **2** and **3** were confirmed by their ^{1}H and ^{13}C NMR data.
The one-pot synthesis of [^{18}F]SFB by nucleophilic substitution of [^{18}F]fluoride for the trimethylammonium group of the precursors **2** or **3** according to Scheme 2 was tested under various reaction conditions: several phase-transfer catalysts, various solvents, reaction temperatures and reaction times (see Table 1). The phase-transfer catalysts Kryptofix 222, 18-crown-6 and dibenzo-18-crown-6 were combinded with K_2CO_3 in a molar ratio of 2 : 1. Tetrabutylammonium hydroxide was also tested as a phase-transfer catalyst.

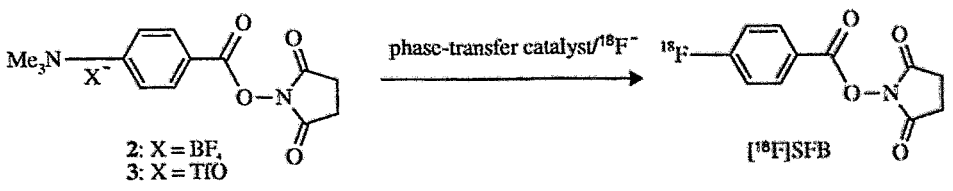

Scheme 2

Table 1. Results of experiments for synthesizing [^{18}F]SFB under various reaction conditions

Expt.	Precursor	Phase-transfer catalyst	Solvent	Reaction time	Reaction temperature or microwave power	[^{18}F]SFB Total yield [%]
1	**2**	K 222	250 µl MeCN	10 min	90 °C - 95 °C	0
2	**2**	K 222	250 µl DMSO	10 min	90 °C - 95 °C	0
3	**2**	18-crown-6	125 µl MeCN	10 min	90 °C - 95 °C	0
4	**2**	K 222[1)]	125 µl MeCN	10 min	90 °C - 95 °C	0
				2 min	600 W	0
				5 min	900 W	0
5	**2**	K 222	150 µl MeCN	5 min	900 W	0
6	**2**	18-crown-6	150 µl MeCN	5 min	900 W	2
7	**2**	Bu_4NOH	125 µl MeCN	10 min	90 °C - 95 °C	0
				5 min	900 W	0
8	**2**	Bu_4NOH	125 µl DMSO	5 min	900 W	0
9	**2**	18-crown-6	150 µl DMSO	2 min	900 W	0
				3 min	600 W	
10	**2**	18-crown-6	150 µl MeCN	4 min	900 W	
				6 min	440 W	
				10 min	600 W	2
11	**3**	18-crown-6	150 µl MeCN	10 min	900 W	9
12	**2**	18-crown-6	150 µl HMPT	10 min	90 °C - 95 °C	2
13	**3**	18-crown-6	1 ml MeCN	10 min	90 °C - 95 °C	
				5 min	600 W	4
14	**2**	18-crown-6	1 ml MeCN	10 min	90 °C - 95 °C	
				5 min	600 W	21
15	**2**	18-crown-6[2)]	1 ml MeCN	10 min	90 °C - 95 °C	10
16	**2**	18-crown-6	1 ml MeCN	10 min	140 °C	15
17	**2**	K 222	1 ml MeCN	10 min	90 °C - 95 °C	0
18	**2**	18-crown-6	1 ml MeCN	20 min	90 °C - 95 °C	14
19	**2**	18-crown-6	1 ml acetone	10 min	90 °C - 95 °C	4
20	**2**	18-crown-6	0.5 ml MeCN	40 min[3)]	90 °C - 95 °C	21
21	**2**	dibenzo-18-crown-6	1 ml MeCN	10 min	90 °C – 95 °C	11
				15 min	600 W	
22	**2**	18-crown-6	300 µl MeCN 500 µl ethylene carbonate	10 min	90 °C – 95 °C	1
23	**2**	18-crown-6	500 µl sulfolane	10 min	90 °C - 95 °C	0

[1)]reduced amount of K_2CO_3 (0.69 mg; 5 µmol)
[2)]double amount of 18-crown-6 (21.2 mg; 80 µmol)
[3)]while stirring and ultrasonicating

It was shown that the Kryptofix 222/K_2CO_3 mixture, which is often used for nucleopilic substitutions, was unsuitable for the one-pot synthesis of [^{18}F]SFB according to Scheme 2. The best results (yields of 21 % [^{18}F]SFB) were obtained using an 18-crown-6/K_2CO_3 mixture in 0.5 - 1 ml MeCN (see Expt. 14 and 20). But the use of [^{18}F]SFB as a labelling agent requires a pure substance. Purification procedures which were not investigated increase the preparation time and decrease the yields. The advantage of the one-pot synthesis of [^{18}F]SFB over the three-step synthesis according to [2] cannot be assessed at the moment. Further investigations in this field are necessary.

References

[1] Scheunemann M., Mäding P., Bergmann R., Steinbach J., Johannsen B. and Tourwé D. (1999) Reaction of neurotensin(8-13) and its partially reduced congener with unlabelled and ^{18}F-labelled N-succinimidyl 4-fluorobenzoate (SFB). *Report January 1998 – June 1999*, Institute of Bioinorganic and Radiopharmaceutical Chemistry, FZR-270, pp. 26-28.

[2] Wester H.J., Hamacher K. and Stöcklin G. (1996) A comparative study of n.c.a. fluorine-18 labeling of proteins via acylation and photochemical conjugation. *Nucl. Med. Biol.* **23**, 365-372.

15. The Utilization of [^{18}F]N-Succinimidyl 4-Fluorobenzoate ([^{18}F]SFB) for Labelling Bombesin Derivatives

M. Scheunemann, P. Mäding, R. Bergmann, J. Steinbach, B. Johannsen

Introduction

Bombesin as well as its closely related congener, human gastrin-releasing peptide (GRP), are produced and secreted by human small-cell lung cancers (SCLC) [1]. It was disclosed that both peptides act as autocrine growth factors for various cell lines of this tumour type [2]. Moreover it was found that specific receptors for peptides related to GRP are expressed on the surface of various other tumour cell types as well, such as human prostate [3] and human breast cancer [4]. The obvious physiological if not pharmacological role of bombesin in the proliferation of these tumour types has triggered a wide search for new antagonists with a high affinity and selectivity for the appropriate binding sites. In addition to these efforts, there is a general interest in the development of new radiopharmaceuticals for the visualisation and radiotherapy of bombesin receptor positive tumours.

Pyr-Gln-Arg-Leu-Gly-Asn-Gln-Trp-Ala-Val-Gly-His-Leu-Met-NH_2 **bombesin**, (three-letter code)
pEQRLGNQWAVGHLM-NH_2 (one-letter code)

H-Ala-Pro-Val-Ser-Val-Gly-Gly-Gly-Thr-Val-Leu-Ala-Lys-Met-Tyr-Pro-Arg-Gly-Asn-His-Trp-Ala-Val-Gly-His-Leu-Met-NH_2
APVSVGGGTVLAKMYPRGNHWAVGHLM-NH_2 **human GRP**

Our motivation consists in the appropriate ^{18}F labelling of bombesin(6-14) derivatives, which represent the minimal structures associated with full biological activity [5].

Results and Discussion

Because peptide structures bearing a variety of various H-acidic functions each attempt to introduce the [^{18}F]fluoride anion directly by nucleophilic substitution would fail due to the high basicity of the fluoride ions. The use of a prosthetic group is therefore a requirement for selective labelling of a peptide such as bombesin BN(6-14) or its analogues. As for the corresponding labelling procedures of several neurotensins, such as NT(8-13) [6], we chose again the 4-[^{18}F]fluoro benzoyl moiety as prosthetic group. N-Succinimidyl-4-[^{18}F]fluorobenzoate ([^{18}F]SFB), which in our experiments serves as the molecule carrying the positron emitter fluorine-18, was prepared in a three-step procedure as described in the literature [7]. In view of the fact that peptides derived from the bombesin(6-14) class might display a chemical behaviour widely differing from NT(8-13) derivatives, we started our experiments with smaller analogues of BN(6-14). Thus, we selected the dipeptide Phe-Trp (FW) as well as the tetrapeptide Phe-Gln-Gly-Pro (FQGP). In each of these model peptides phenylalanine serves as the N-terminal amino acid.

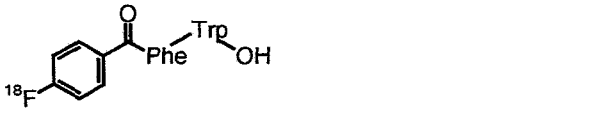

(1)

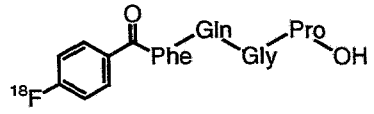

(2)

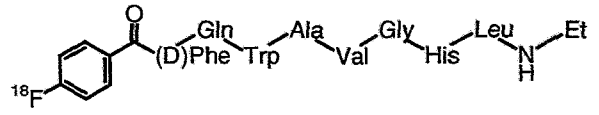

(3)

Studying the steric influence of the benzyl substituent of phenylalanine (Phe; F) on the reactivity with SFB, the absolute configuration of the N-terminal amino acid is expected to be of less importance due to the absence of a stereogenic centre in the labelling agent.
For the synthesis of the nonradioactive analogues of **1**, **2** and **3** we tested protic solvents, such as an aqueous buffered medium (borate-phosphate buffer, pH 8.3), as well as aprotic mixtures, such as DMF or acetonitrile, in each case with triethyl amine as the proton acceptor. Generally it can be said that an

aqueous buffered system tends to provide more favourable reaction conditions for a complete and better chemoselective conversion of the starting peptide. But the addition of a small amount of DMF is advisable, especially for the synthesis of the nonradioactive analogues of **1** and **3**, for complete dissolution of the highly lipophilic peptide precursor.
In the course of our studies we turned our attention to experiments using [^{18}F]SFB on the n.c.a. level. Thus, the two derivatives **2** and **3** were synthesised and biologically tested. The results of the radiolabelling of the tetrapeptide FQGP and the bombesin derivative (D)-FQWAVGHL-NHEt are listed in Table 1.

Table 1. Results of ^{18}F-fluoro-benzylation of two Phe peptides

Peptide	No.	r.c.y. [1] (decay corrected)	specific [2] radioactivity [GBq/µmol]	mol weight [3] of product
Phe-Gln-Gly-Pro [FQGP]	**2**	65 %	≈ 5	569.6
(D-Phe^{6},Leu^{13}, des-Met^{14}-NHEt) BN(6-14) [(D)-FQWAVGHL-NHEt]	**3**	2.3 %	≈ 5	1106.3

[1]: r.c.y. = radiochemical yield
[2]: starting from approx. 3.5 GBq [^{18}F]F$^-$
[3]: as indicated by mass spectrometry of the unlabelled derivative (electro spray, ES$^+$)

To confirm the suggested structure of the labelled peptides we synthesised the nonradioactive analogues. The mass spectrum (electrospray, ES(+)) of each nonradioactive analogue indicates a compound showing a molpeak as calculated for the fluorobenzoylated compound.
Both independently prepared unlabelled derivatives coelute fairly well with the ^{18}F-labelled peptides.
In order to determine the definite position of the 4-fluoro benzoyl group, we used the ninhydrin test, a standard method for identification of molecules bearing secondary or primary amino groups, such as amino acids or simple amino alcohols. By using this test system we obtained a negative result for the unlabelled analogues of **1**, **2** and **3**. Their parent peptides, on the other hand, show a positive result which clearly demonstrates the successful coupling of the prosthetic group to the α-amino group of the *N*-terminal amino acid.

The authors wish to thank Dipl.-Chem. K. Fischer for recording the electrospray mass spectra.

This work was supported by the European Union (BMH4-CT98-3198).

References

[1] Carney D. N., Cuttitta F., Moody T. W. and Minna J. D. (1987) Selective stimulation of small cell lung cancer clonal growth by bombesin and gastrin-releasing peptide *Cancer Research* **47**, 821–825.
[2] Moody T. W., Pert C. B., Gazdar A. F., Carney D. N. and Minna J. D. (1981) High levels of intracellular bombesin characterize human small-cell lung carcinoma. *Science* **214**, 1246–1248.
[3] Bologna M., Festuccia C., Muzi P., Biordi L. and Ciomei M. (1989) Bombesin stimulates growth of human prostatic cancer cells in vitro. *Cancer* **63**, 1740–1720.
[4] Giachetti S., Gauville C., de Cremoux P., Bertin L., Berthon P., Abita J.-P., Cuttitta F. and Calvo F. (1990) Characterization in some human breast cancer cell lines of gastrine-releasing peptide-like receptors which are absent in normal breast epithelial cells. *Int. J. Cancer* **46**, 293–298.
[5] Kroog G. S., Jensen R. T. and Battey J. F. (1995) Mammalian bombesin receptors. *Med. Res. Rev.* **15**, 389–417.
[6] Scheunemann M., Mäding P., Bergmann R., Steinbach J., Johannsen B. and Tourwe D. (1999) Reaction of neurotensin (8-13) and its partially reduced congener with unlabelled and ^{18}F-labelled N-succinimidyl 4-fluorobenzoate (SFB), *Report January 1998 – June 1999*, Institute of Bioinorganic and Radiopharmaceutical Chemistry, FZR–270, pp 26–28.
[7] Wester H.-J., Hamacher K. and Stöcklin G. (1996) A comparative study of n.c.a. fluorine-18 labeling of proteins via acylation and photochemical conjugation *Nucl. Med. Biol.* **23**, 365–372.

16. Co-Labelling Experiments for the Synthesis of [1-^{11}C/^{13}C]Phenol

P. Mäding, H. Kasper, M. Scheunemann, K. Fischer, J. Steinbach

Introduction

The synthesis of [1-^{11}C]phenol (**6a**) is described in [1]. As the identity and the position of the label of ^{11}C-labelled compounds cannot be directly determined, we carried out ^{13}C/^{11}C co-labelling experiments according to Scheme 1, making use of the opportunities provided by mass spectrometry and ^{13}C NMR spectroscopy. Two HPLC systems were used for analytical control.

Scheme 1

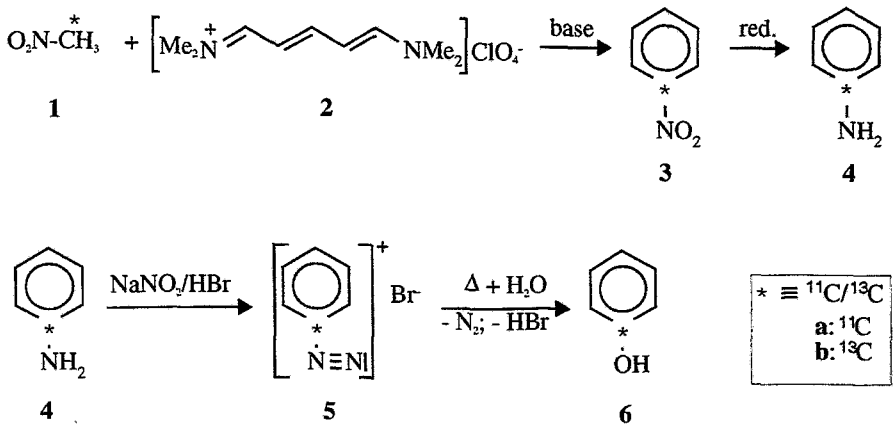

1 2 3 4 4 5 6

Experimental

General

Analytical HPLC was used to determine the extent of reaction conversion and the radiochemical purity of the reaction products and to identify the products. HPLC was performed with an HPLC system from Merck-Hitachi, including a gradient pump (L-6200A), a Rheodyne injector with a 20 µl loop and a diode array detector (L-4500 DAD) coupled in series with a radioactivity detector FLO-ONE\Beta A500 (Canberra Packard). Two analytical HPLC systems were used: a gradient system [1] and an isocratic system.

Gradient system:

The column used was a Merck LiChrospher 100 RP-18 endcapped, 5µm, 150 mm x 3.3 mm. The mobile phase consisted of phosphate buffer pH 7.0 (c[NaH_2PO_4] = 0.26 mM; c[Na_2HPO_4] = 0.51 mM) and acetonitrile at a flow rate of 0.5 ml/min, with the following linear gradient of the eluents: 0 min - 100 % buffer/ 0 % MeCN; 20 min - 0 % buffer/ 100 % MeCN.

Isocratic system:

These analyses were performed with a NUCLEOSIL 120 RP-18 column (5 µm, 125 mm x 4 mm, Macherey-Nagel) isocratically eluted with isopropanol/water (20/80) containing 0.1 M ammonium formate at a flow rate of 0.5 ml/min. Retention times: 22.77 min for **3**, 6.35 min for **4**, 7.81 min for **6**. Reagent-grade nitrobenzene (Fluka, Switzerland), reagent-grade aniline (Fluka, Switzerland) and reagent-grade phenol (Berlin Chemie, Germany) were used as reference substances. Nitro-[^{13}C]methane (**1b**) (99 atom % ^{13}C) was purchased from Aldrich.

^{13}C NMR spectra were recorded on a Varian INOVA 400 spectrometer at 100.6 MHz with $CDCl_3$ as an internal standard.

Mass spectrometric analyses were carried out on a Micromass tandem quadrupole mass spectrometer (Quattro LC) operated in the MS mode. Mass spectral data were recorded in the negative ESI mode using a cone voltage of 35 V. A solution of phenol or [1-^{13}C]phenol (**6b**) in MeOH was infused at a flow rate of 5 µl/min.

*Nitro-[1-^{11}C/^{13}C]benzene (**3a/b**)*

Nitro-[^{11}C]methane (**1a**) was trapped in a cooled 2 ml vessel (10 °C) containing HMPT (250 µl), 5-dimethylaminopenta-2,4-dienylidene-dimethylammonium perchlorate (**2**) (8 mg, 32 µmol) and t-BuOK

(3.5 mg, 31 µmol). Nitro-[^{13}C]methane (**1b**) (1 µl, 18.5 µmol) was added. Cyclization/ aromatization into **3a/b** was achieved by heating the well-sealed vessel at 170 °C for 7 min.

[1-^{11}C/^{13}C]aniline (4a/b)
The reduction of **3a/b** to obtain **4a/b** was performed by adding an excess of $Na_2S{\cdot}9H_2O$ (28 mg, 117 µmol) in water (100 µl) to the above reaction mixture and heating at 170 °C for 30 min.
Then the reaction mixture was diluted with water (1 ml) and passed through an activated polystyrene cartridge (LiChrolut EN, Merck). After washing the cartridge with water (20 ml) and with aqueous HBr (2 ml, 10 %), **4a/b** was eluted with ethanol (2 ml).
The acidic ethanolic solution of **4a/b** was diluted with water (8 ml) and passed through a cartridge filled with cation exchange resin DOWEX 50 WX 8 (SERVA, 100-200 mesh, H^+ form, neutral). The resin was washed with water to make it neutral. Pure **4a/b** was eluted with ammonia (2 M).

[1-^{11}C/^{13}C]Phenol (6a/b)
The ammoniacal solution (3 ml) was acidified with HBr (1 ml, 40 %) and cooled to 0 °C. Compound **4a/b** was diazotized by adding $NaNO_2$ (10 mg, 145 µmol) in water (100 µl) to the cooled solution. After 5 min at 0 °C the reaction mixture was heated at 100 °C for 5 min. The [1-^{11}C/^{13}C]benzenediazonium bromide (**5a/b**) formed was then concentrated and **6a/b** was obtained. It was analysed by the two HPLC systems mentioned above.
After decay of the ^{11}C radioactivity, the acid solution was passed through an activated polystyrene cartridge (LiChrolut EN, Merck). The cartridge was washed with water to make the resin neutral. Then the polystyrene cartridge was dried by means of a nitrogen stream (3 l/h). [1-^{13}C]Phenol (**6b**) was eluted from the cartridge with $CDCl_3$ (1 ml) and analysed by ^{13}C NMR. Part of the $CDCl_3$ solution of **6b** was evaporated for MS investigations in MeOH.

Results and Discussion

The synthesis of nitro-[1-^{11}C/^{13}C]benzene (**3a/b**) by reaction of 5-dimethylaminopenta-2,4-dienylidene-dimethylammonium perchlorate (**2**) with **1a/b** and the subsequent reduction of **3a/b** to [1-^{11}C/^{13}C]aniline (**4a/b**) were carried out in a similar way as the ^{11}C procedure described in [2]. The amount of sodium sulphide and the reduction time had to be increased in comparison with the pure ^{11}C synthesis for a satisfactory reduction of **3a/b** to **4a/b**. [1-^{11}C/^{13}C]Phenol (**6a/b**) was obtained by diazotization of purified **4a/b** and subsequent concentration of the [1-^{11}C/^{13}C]benzenediazonium salt **5a/b** formed by analogy with [1]. Compound **6a/b** was identified by two HPLC systems using a reference standard.
After decay of the ^{11}C radioactivity of **6a**, [1-^{13}C]phenol (**6b**) was purified by solid-phase extraction on a polystyrene cartridge. The position of the label was confirmed by analysis of the ^{13}C-NMR spectrum of **6b**. The strong ^{13}C signal of **6b** at δ = 156.0 ppm corresponded to the ^{13}C signal of the C-1 of authentic phenol. Compound **6b** was also analysed by MS, indicating a molecular ion peak at m/z 94 (M-1), which corresponded to the molecular ion peak at m/z 93 (M-1) observed with authentic phenol.

References

[1] Mäding P. and Steinbach J. (2000) Synthesis of [1-^{11}C]phenol. *J. Labelled Compd. Radiopharm.* (in press).

[2] Steinbach J., Mäding P., Füchtner F. and Johannsen B. (1995) N.c.a. ^{11}C-labelling of benzenoid compounds in ring positions: Synthesis of nitro-[1-^{11}C]benzene and [1-^{11}C]aniline. *J. Labelled Compd. Radiopharm.* **36**, 33-41.

17. $^{11}C/^{13}C$-Ring-Labelling of Nitrobenzenes by Condensation of Pyrylium Salts with Nitro-[$^{11}C/^{13}C$]Methane

P. Mäding, H. Kasper, M. Scheunemann, K. Fischer, J. Steinbach

Introduction

The synthesis of the nitro-[1-^{11}C]benzenes **5a-7a** by condensation of the corresponding pyrylium salts **2-4** with nitro-[^{11}C]methane (**1a**) was described in [1, 2]. It had previously been presented and published in an abstract form [3, 4]. In preparation of a publication in this field [5] we decided to rigorously confirm the identity of the ^{11}C-ring-labelled nitrobenzenes and the position of the label. Accordingly $^{13}C/^{11}C$ co-labelling experiments were carried out as represented in Scheme 1. The potentials of mass spectrometry and ^{13}C-NMR spectroscopy were additionally made use of. Two HPLC systems were used for analytical purposes.

Scheme 1

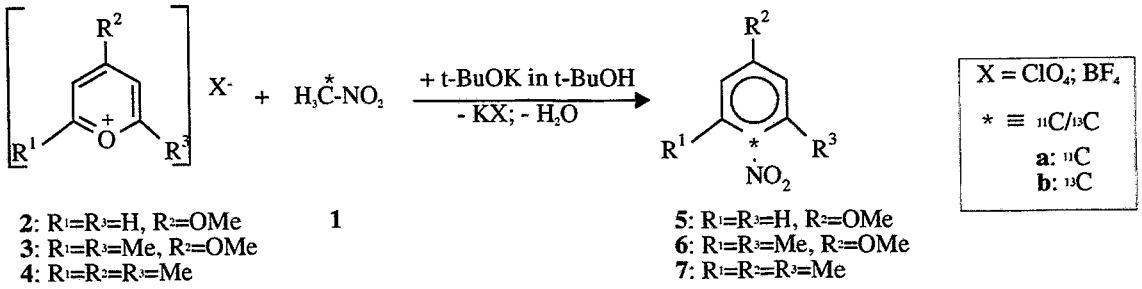

2: R^1=R^3=H, R^2=OMe
3: R^1=R^3=Me, R^2=OMe
4: R^1=R^2=R^3=Me

1

5: R^1=R^3=H, R^2=OMe
6: R^1=R^3=Me, R^2=OMe
7: R^1=R^2=R^3=Me

Experimental

General

HMPT, t-BuOK and BuLi (1.6 M in hexane), all of synthesis quality, were purchased from Merck. $Bu_4NF{\cdot}3H_2O$ (purum) was obtained from Fluka. Nitro-[^{13}C]methane (**1b**) (99 atom % ^{13}C) was purchased from Aldrich.

Nitromethane 99 %, 4-nitroanisole 97 % (Aldrich), 2-nitromesitylene 99 % (ABCR GmbH &. Co., Germany) and 2,6-dimethyl-4-methoxy-nitrobenzene (synthesized according to [6]) were used as refe-rence substances.

The ^{13}C NMR spectra of the ^{13}C-ring-labelled nitrobenzenes were recorded on a Varian INOVA 400 spectrometer at 100.6 MHz with $CDCl_3$ as an internal standard.

Mass spectrometric analyses were carried out on a Micromass tandem quadrupole mass spectrometer (Quattro LC) operated in the MS mode. Mass spectral data were recorded in the positive ESI mode using a cone voltage of 20 V or 30 V. A solution of the particular nitrobenzene or the corres-ponding ^{13}C-ring-labelled nitrobenzene in MeOH was infused at a flow rate of 5 µl/min.

To determine the extent of reaction conversion and the radiochemical purity of the reaction products, an HPLC system (JASCO) was used, including a pump, a Rheodyne injector with a 20 µl loop, a LiChrospher 100 RP-18 endcapped column (5 µm, 150 mm x 3.3 mm, Merck) and a UV detector coup-led in series with a radioactivity detector FLO-ONE\Beta 150TR (Canberra Packard). The HPLC analyses were carried out at a flow rate of 0.5 ml/min with the following linear gradient of the eluents: 0 min - 70 % buffer/ 30 % MeCN; 10 min - 0 % buffer/ 100 % MeCN; 20 min - 0 % buffer/ 100 % MeCN; buffer = phosphate buffer pH 7 (c[NaH_2PO_4] = 0.26 mM; c[Na_2HPO_4] = 0.51 mM).

A second HPLC system was used to confirm the identity of the synthesized compounds **5** (6.44 min), **6** (10.09 min) and **7** (14.98 min). These analyses were performed with a NUCLEOSIL 120 RP-18 column (5 µm, 125 mm x 4 mm, Macherey-Nagel) isocratically eluted with isopropanol/water (40/60) containing 0.1 M ammonium formate at a flow rate of 0.5 ml/min.

*4-Nitro-[4-$^{11}C/^{13}C$]anisole (**5a/b**)*

The gaseous nitro-[^{11}C]methane (**1a**) was trapped in a cooled 2 ml vessel (10 °C) containing HMPT (250 µl), 4-methoxypyrylium perchlorate (**2**) (8 mg, 38 µmol) and $Bu_4NF{\cdot}3H_2O$ (12 mg, 38 µmol). Nitro-

[^{13}C]methane (**1b**) (2 µl, 37 µmol) was added. After addition of t-BuOK (1 M in t-BuOH, 38 µl, 38 µmol) and t-BuOH (250 µl), the well-sealed vessel was heated at 120 °C for 30 min.
Using a syringe, the reaction mixture was diluted with water (10 ml) and passed through an activated RP-18 cartridge (Chromafix C18 ec, Macherey-Nagel). After washing the cartridge with water (10 ml), **5a/b** was eluted with acetonitrile (2 ml) and analysed by HPLC.
After decay of the ^{11}C radioactivity of 4-nitro-[4-^{11}C]anisole (**5a**), the solvent was evaporated. 4-Nitro-[4-^{13}C]anisole (**5b**) was purified by flash chromatography, using a silica gel column (i.d. 1 cm, length 4.3 cm) and a mixture of petroleum ether and ether (9 : 1). The separated fractions (each 1 ml) of **5b** were combined and evaporated. The purified solid product was dissolved in $CDCl_3$ (0.7 ml) and analysed by ^{13}C-NMR. Part of this $CDCl_3$ solution was evaporated for MS investigations in MeOH.

*2,6-Dimethyl-4-methoxy-nitro-[1-^{11}C/^{13}C]benzene (**6a/b**)*
The gaseous **1a** was trapped in a 2 ml vessel containing t-BuOH (250 µl) and 2,6-dimethyl-4-methoxypyrylium perchlorate (**3**) (9 mg, 38 µmol). **1b** (2 µl, 37 µmol) was added. After addition of t-BuOK (1 M in t-BuOH, 40 µl, 40 µmol) the well-sealed vessel was heated at 120 °C for 30 min. The reaction mixture was analysed by HPLC.
After decay of the ^{11}C radioactivity of 2,6-dimethyl-4-methoxy-nitro-[1-^{11}C]benzene (**6a**), the reaction mixture was evaporated. 2,6-Dimethyl-4-methoxy-nitro-[1-^{13}C]benzene (**6b**) was purified by flash chromatography, using a silica gel column (i.d. 1 cm, length 3.8 cm) and a mixture of petroleum ether and ether (9 : 1). The separated fractions (each 1 ml) of **6b** were combined and evaporated. The purified solid product was dissolved in $CDCl_3$ (0.7 ml) and analysed by ^{13}C NMR. Part of this $CDCl_3$ solution was evaporated for MS investigations in MeOH.

*2-Nitro-[2-^{11}C/^{13}C]mesitylene (**7a/b**)*
The gaseous **1a** was trapped in a 2 ml vessel containing t-BuOH (250 µl) and 2,4,6-trimethylpyrylium tetrafluoroborate (**4**) (8 mg, 38 µmol). **1b** (2 µl, 37 µmol) was added. After addition of t-BuOK (1 M in t-BuOH, 40 µl, 40 µmol) the well-sealed vessel was heated at 120 °C for 30 min. The reaction mixture was analysed by HPLC.
After decay of the ^{11}C radioactivity of 2-nitro-[2-^{11}C]mesitylene (**7a**), the reaction mixture was evaporated. 2-Nitro-[2-^{13}C]mesitylene (**7b**) was purified by flash chromatography, using a silica gel column (i.d. 1 cm, length 2.5 cm) and petroleum ether. The separated fractions (each 1 ml) of **7b** were combined and evaporated. The purified solid product was dissolved in $CDCl_3$ (0.7 ml) and analysed by ^{13}C-NMR. Part of this $CDCl_3$ solution was evaporated for MS investigations in MeOH.

Results and Discussion

The synthesis of the nitro-[1-^{11}C/^{13}C]benzenes **5a/b-7a/b** by reaction of the corresponding pyrylium salts **2-4** with **1a/b** was carried out in a similar way as the ^{11}C procedures described in [1, 2]. Nitro-[^{13}C]methane (**1b**) was added immediately after nitro-[^{11}C]methane (**1a**) had been trapped in the reaction mixture. Because of the molar ratios of the pyrylium salts **2-4** and **1b**, the reaction times had to be increased compared with the pure ^{11}C syntheses to obtain **5a/b-7a/b** in satisfactory yields. The compounds **5a/b-7a/b** were identified by two HPLC systems. An additional purification step using an RP-18 cartridge had to be carried out after the synthesis of **5a/b**. In this way the high-boiling HMPT and other impurities were removed.
After decay of the ^{11}C radioactivity of **5a-7a**, the ^{13}C-ring-labelled nitrobenzenes **5b-7b** were purified by flash chromatography.
The position of the label was confirmed by analysis of the ^{13}C NMR spectra of 4-nitro-[4-^{13}C]anisole (**5b**), 2,6-dimethyl-4-methoxy-nitro-[1-^{13}C]benzene (**6b**) and 2-nitro-[2-^{13}C]mesitylene (**7b**). The strong ^{13}C signal of **5b** (δ = 141.5 ppm), **6b** (δ = 145.5 ppm) and **7b** (δ = 149.7 ppm) corresponded to the ^{13}C signal of the authentic unlabelled compound. MS analyses of **5b** (m/z = 155 (M+1)), **6b** (m/z = 183 (M+1)) and **7b** (m/z = 167 (M+1)) indicated a molecular ion peak which differed from the correspon-ding molecular ion peak of the authentic unlabelled compound by 1.

References

[1] Mäding P., Steinbach J. and Kasper H. (1997) Substances labelled in metabolically stable posi-tions: The conversion of pyrylium salts with nitro-[^{11}C]methane - a new method for the synthesis of n.c.a. ^{11}C-ring labelled nitroaromatics. *Annual Report 1996,* Institute of Bioinorganic and Radiopharmaceutical Chemistry FZR-165, pp. 162-165.

[2] Mäding P., Steinbach J. and Kasper H. (1997) Substances labelled in metabolically stable posi-tions: The synthesis of n.c.a. 2,6-dimethyl-4-methoxy-nitro-[1-^{11}C]benzene. *Annual Report 1997,* Institute of Bioinorganic and Radiopharmaceutical Chemistry FZR-200, pp. 179-182.

[3] Mäding P., Steinbach J. and Johannsen B. (1997) ^{11}C-Ring-labelling of nitroaromatics by condensation of pyrylium salts with nitro-[^{11}C]methane. *J. Labelled Compd. Radiopharm.* **40**, 738-739.

[4] Mäding P., Steinbach J., Zessin J., Chebani, K. and Johannsen B. (1997) ^{11}C-Labelling of benzenoid and N-heteroaromatic compounds in ring positions. *J. Labelled Compd. Radiopharm.* **40**, 740-742.

[5] Mäding P., Steinbach J. and Johannsen B. (2000) No-carrier-added ^{11}C-labelling of benzenoid compounds in ring positions by condensation of nitro-[^{11}C]methane with pyrylium salts. *J. Labelled Compd. Radiopharm.* (in press).

[6] Dimroth K. (1960) Neuere Methoden der präparativen organischen Chemie III. 3. Aromatische Verbindungen aus Pyryliumsalzen. *Angew. Chem.* **72**, 331-342.

18. Repeated Charging of Automated Synthesis Modules with Liquid Starting Materials for the Preparation of PET Tracers by an Ultrasonic Fill Height Sensor

J. Zessin, F. Füchtner, J. Steinbach, B. Jung, P. Mäding, E. Will, E. Lösel, N. Dohn, H. Krug[1]
[1]Zentralabteilung Forschungs- und Informationstechnik

Introduction

The synthesis of PET tracers requires a high level of starting radioactivity due to the short half-life of the radionuclides. The radiotracer preparation has therefore to be carried out in shielded hot cells with automated synthesis modules. The growing number of PET investigations requires the use of the synthesis modules several times a day. The residual radioactivity after radiotracer preparation makes it necessary to automate cleaning processes and fill-up procedures of starting materials. The latter can be performed with multiple dosing of liquids from a reservoir vessel.
In this paper we described a device for multiple charging of synthesis modules with liquids based on fill height measurement by an ultrasonic sensor.

Experimental

Charging unit
The charging unit was used for the addition of hydroiodic acid in the synthesis of [^{11}C]methyl iodide. The device is based on the ultrasonic sensor Sonometer 10 for filling level measurment (SONOTEC, Halle/Sa., Germany). The hydroiodic acid reservoir is a graduated glass cylinder (height: 180 mm, inner diameter: 10 mm) sealed with a silicone rubber septum. The outer diameter of this vessel is similar to the diameter of the ultrasonic sensor. An improved contact between the sensor and the ground bottom of the reservoir is achieved by using of a coupling paste. Teflon tubing is used for connecting the reservoir and the reaction vessel.

Automated preparation of [^{11}C]methyl iodide
[^{11}C]Methyl iodide was prepared from [^{11}C]carbon dioxide in an automated synthesis module, which was described in a former report [1].

Results and Discussion

The device for repeated charging of the reaction vessel with liquid starting materials consists of a reservoir and an ultrasonic sensor for filling level measurement. The fill height was determined by measuring the running time of the echo from the liquid surface. Parameters to be adjusted at the sensor are the sonic speed in the liquid and a dead time for elimination of troublesome echos both from the bottom and the wall of the vessel. Due to this dead time the minimum fill height was 30 mm.
At first we checked the precision of the charging procedure for various volumes. The results are summarized in Table 1.

Table 1. Precision and time required by the automated filling process

Set volume (ml)	Filled volume (ml)	Time required by the filling process[1)] (s)
0.1	0.1 ± 0.03	12
0.2	0.2 ± 0.05	16
0.5	0.5 ± 0.1	27
1.0	1.2 ± 0.1	16
1.5	1.5 ± 0.1	19
2.0	2.1 ± 0.2	21

1) 8 s of this value was needed for switching the valves, the filling processes was carried out, using an optimized overpressure value

The liquid was transported from the reservoir to the reaction vessel by overpressure. The transfer time depended on the level of the gas overpressure. In the tests the overpressure was optimized to reach minimum transfer times combined with maximum precision. Volumes from 0.1 up to several millilitres can be dosed with this charging device, which covers all the volumes commonly used in PET tracer syntheses. After these initial tests the described charging unit was used for the addition of hydroiodic acid in the synthesis of [^{11}C]methyl iodide. The set volume of hydroiodic acid for the conversion of lithium aluminium [^{11}C]methylate into [^{11}C]methyl iodide was 1.7 ml. The volume measured by the charging unit was 1.8 ± 0.1 ml. The whole charging process took about 30 s.

The radiochemical yields and the synthesis times of [^{11}C]methyl iodide preparation were not influenced by this charging device. Starting from 3.9 GBq (105 mCi) [^{11}C]CO_2, 1.5 ± 0.2 GBq [^{11}C]methyl iodide (not decay-corrected) was obtained after synthesis, which corresponds to a decay-corrected radiochemical yield of 67 ± 4 %. The radiochemical purity of [^{11}C]methyl iodide was greater than 98 %. Under these conditions the specific radioactivity at the end of the synthesis varied from 3.3 to 6.3 GBq/µmol (90 – 170 mCi/µmol).

We also tried to use such a charging unit for addition of the lithium aluminium hydride solution. The automated addition of this solution was not possible due to blockages in the valves, which may have been caused by hydrolysis of the lithium aluminium hydride.

Conclusion

We demonstrated that the charging unit based on an ultrasonic filling level sensor can be used for repeated charging of reaction vessels with liquids in the synthesis of PET radiotracers. In this way synthesis modules can be used several times a day without filling up reagents. This was demonstrated by the use of such a charging unit in an automated synthesis module for dosing of hydroiodic acid in the preparation of [^{11}C]methyl iodide. The reliability of this charging device was confirmed in more than 50 syntheses.

References

[1] Zessin J., Mäding P., Jung B., Krug H., Gommlich S., Lösel E., Dohn N., Füchtner F. and Steinbach J. (1999) Automated production of [^{11}C]methyl iodide. *Report January 1998 – June 1999*, Institute of Bioinorganic and Radiopharmaceutical Chemistry, FZR-270, pp. 137-138.

19. Installation of Surge Protective Devices for the "CYCLONE 18/9" PLC System

St. Preusche, H. Ross, H. Krug[1]
[1]Forschungszentrum Rossendorf, Zentralabteilung Forschungs- und Informationstechnik

Introduction

At the Rossendorf PET Center the PET cyclotron and the radiochemical laboratories are 500 meters apart. Due to this fact our CYCLONE 18/9 PLC configuration consists of two PLC modules. The main PLC unit (SIMATIC S135U) at the cyclotron site controls the cyclotron. The chemistry PLC unit (SIMATIC S95U) at the site of the radiochemical laboratories controls the chemistry modules. The two PLC units communicate via a SINEC L2 bus cable 500 meters in length.

Problem

The control system worked without any problems for more than three years.
But after a heavy thunderstorm at the end of June 1999 we were unable to operate the cyclotron. The following problems appeared in the control system:

- no communication between PC/PLC (S135U)
- PC login was not possible either at the cyclotron or at the radiochemistry terminals
- bus failure in the chemistry PLC (S95U)

Solution

The SIMATIC S95U was repaired at Rossendorf. The final stage circuit was replaced and the bus failure thus overcome.
An intervention by an IBA specialist was necessary to locate the problem of the SIMATIC S135U. It was impossible to deal with it at Rossendorf and thus the main PLC unit, the bus terminals RS485 and the two PC were shipped to IBA and were repaired there. The PLC communication processor, which manages the communication both between the PLC units and between the PLC units and PC was found to be malfunctioning. The problems were obviously caused by excess voltage in the SINEC L2 bus cable during the heavy storm.

After reinstallation of the system at Rossendorf we additionally protected the entrances of the two bus terminals at either end of the SINEC L2 bus cable with a so-called BLITZDUCTOR CT (DEHN + SÖHNE GmbH + Co. KG, Elektrotechnische Fabrik, Neumarkt, Germany), which is a two-piece surge protective device for the protection of information technology systems. It consists of a base (feed-through terminal) and the protection module.

To prevent the same problems occurring in the control system of the radionuclide transport system (RATS), the BLITZDUCTOR CT system was also inserted to protect the RATS bus cable.

20. Operation of the Rossendorf PET Cyclotron "CYCLONE 18/9" in 1999

St. Preusche, J. Steinbach

Routine operation

Our standard radionuclides produced in routine operation are $[^{18}F]F^-$, $[^{18}F]F_2$ and ^{11}C, which are applied for radiotracers, radiopharmaceuticals and for various experimental uses.

Since November this year the cyclotron has been used for radiopharmaceutical production from Monday to Friday, reducing the initial service day per week to one per month. This is due to the great demand for the radiopharmaceuticals, both for the in-house use and for the distribution outside the institute. The daily operation time is two to four hours.

Table 1 gives an overview of the 1999 radionuclide production and the typical irradiation conditions. The radionuclide ^{13}N was produced to optimize the irradiation and extraction conditions and to introduce $[^{13}N]$ammonia as radiopharmaceutical.

Table 1. Radionuclide production in 1999

RN	Radionuclide production		Typical irradiation conditions			
	Number of Irradiations	$SumA_{EOB}$ [GBq]	Irrad. Time [min]	I_T [μA]	$Yield_{EOB}$ [GBq]	Sat. Yield [GBq/μA]
$[^{18}F]F^-$	227	13300	60	30	70	7.8
$[^{18}F]F_2$	107*)	467	120	18	11	1.2
^{11}C	74	1138	40	25	80	4.3
^{13}N	24	144	10	10	5	1.2

*) including pre-irradiations

Fig. 1 shows the number of irradiations of our standard radionuclides and Fig. 2 the total amount of activity produced from 1997 to 1999. Due to the reconstruction of our radiopharmaceutical laboratories it has not been possible to work with ^{11}C-labelled compounds from late spring to the end of November.

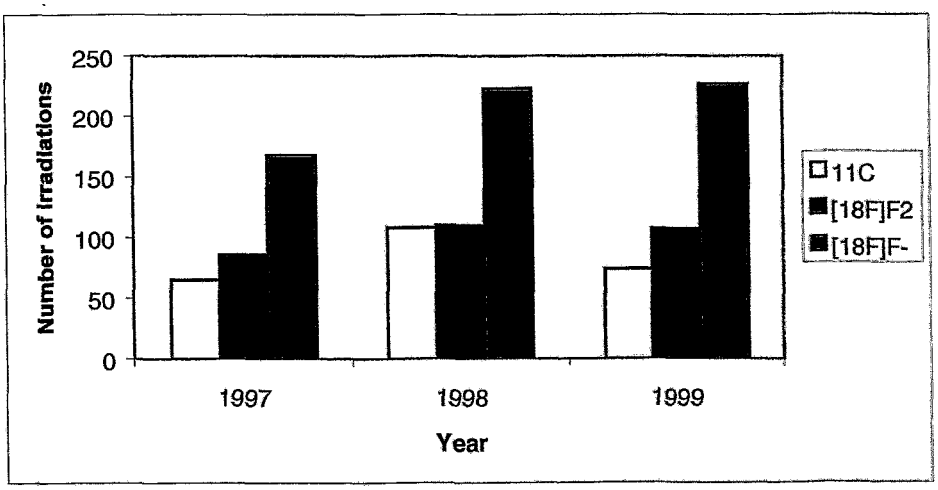

Fig.1. Number of irradiations of standard radionuclides produced.

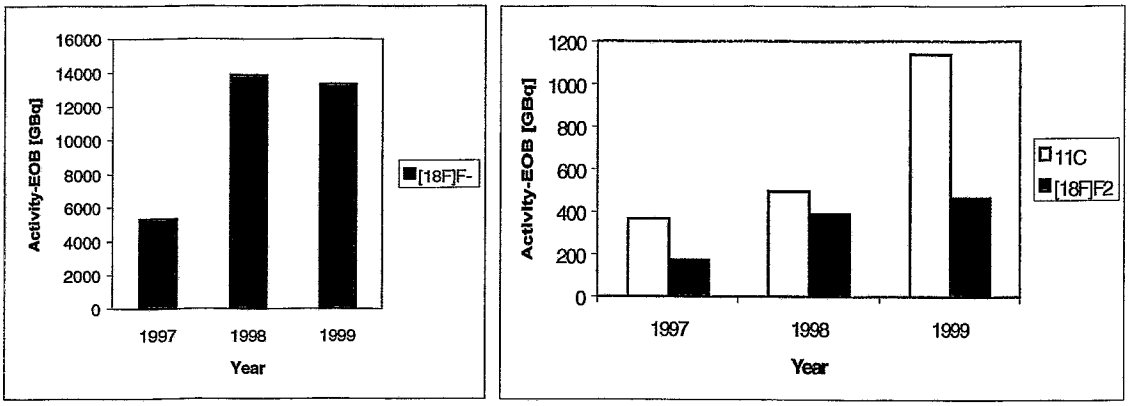

Fig. 2. Total amount of activity produced

Improvements at the cyclotron

Installation of surge protective devices for the "CYCLONE 18/9" PLC system
Resulting from problems caused by a heavy thunderstorm at the end of June [1, 2], we decided to better protect the CYCLONE 18/9 PLC system. The entrances of the two bus terminals at either end of the SINEC L2 bus cable are now equipped with a so-called BLITZDUCTOR CT (DEHN + SÖHNE GmbH + Co. KG, Elektrotechnische Fabrik, Neumarkt, Germany). This is a two-piece surge protective device for the protection of information technology systems. It consists of a base (feed-through terminal) and the protection module.
To prevent the same problems occurring in the control system of the radionuclide transport system (RATS), the BLITZDUCTOR CT system was also inserted to protect the RATS bus cable.

Maintenance and service

The cathodes of both ion sources, both puller electrodes and all the strippers were replaced during the half-yearly maintenance of the inner parts of the cyclotron in late summer.
Preventive changes of the target and vacuum windows are carried out every 2500 µAh at each target [3]. For the $[^{18}F]F^-$ water target this is every five to six months. We changed the windows at the beginning of May and the end of September 1999.

Radiation protection

- Emission of radionuclides with the exhaust air
The emission of radionuclides with the exhaust air is monitored. As shown in Table 1 it is far below the limit.

Table 2. Emission of radionuclides 1999 with the exhaust air resulting from operation of the CYCLONE 18/9 and U-120 cyclotrons

Radionuclide	Emission [Bq/a]
^{41}Ar	3.2E09
^{18}F	2.3E09
^{13}N	6.9E09
^{11}C	3.3E10
Sum	4.6E10
Percent of the annual limit	0.7

- *Exposure to radiation of the cyclotron staff*

The cyclotron staff belong to category A of occupational exposed persons. The average exposure to radiation was 1.8 mSv in 1997, 2.9 mSv in 1998 and 2.7 mSv in 1999 (Jan. to Sep.).

References

[1] Preusche St. and Steinbach J. (1999) Operation of the Rossendorf PET cyclotron "CYCLONE 18/9" in 1998/1999. *Report January 1998 – June 1999*, Institute of Bioinorganic and Radiopharmaceutical Chemistry, FZR-270, pp. 215-218.

[2] Preusche St., Ross H. and Krug H. (1999) Installation of surge protective devices for the CYCLONE 18/9" PLC system. *This report*, p 69.

[3] Preusche St., Füchtner F. and Steinbach J. (1998) The Rossendorf PET cyclotron `CYCLONE 18/9" facility - two years of operation - CYCLONE 18/9 + 10/5 USER COMMUNITY, second workshop, Leuven, Belgium, Dec. 10 – 11.

21. Synthesis and Characterization of Novel Mixed-Ligand Technetium(III) Complexes Containing Tridentate/Monodentate Thiol Ligands and Monodentate Phosphines

H.-J. Pietzsch, S. Seifert, A. Drews, P. Leibnitz[1], H. Spies
[1]Bundesanstalt für Materialforschung- und prüfung, Berlin

Introduction

"3+1" mixed-ligand oxotechnetium(V) complexes with tridentate/monodentate thiolate coordination [TcO(SES)(SR)] ($HS\text{-}CH_2CH_2\text{-}E\text{-}CH_2CH_2\text{-}SH$, E = O, S, NR'), constitute a well-documented group of compounds which are used in radiotracer design [1, 2]. Extensive studies have been carried out to add to the variety of such complexesin which a monodentate ligand is combined with a chelating agent as a tool for introducing technetium into biologically relevant molecules.

Alternatively, coordination of the tripodal NS_3-chelator 2.2'.2"-nitrilotris(ethanthiol) with technetium(III), combined with a monodentate isonitrile or phosphine ligand, produces weakly polar "4+1"-complexes, in which the metal is more strongly shielded than in the square-pyramidal oxo complexes [3, 4].
Here we describe the reaction of "3+1" complexes of the general composition [TcO(SES)($S\text{-}C_6H_4\text{-}COCH_3$)] (E = O, $N(CH_3)$, S) with dimethylphenylphosphine to produce oxo-free Tc(III) species with SES/S/P coordination. This reaction can be considered a prototypical example of the reduction of "3+1" oxotechnetium(V) complexes by tertiary phosphines.

Results and Discussion

Oxotechnetium(V) complexes as the starting material were prepared by the common reaction of Tc(V) gluconate with mixtures of the appropriate tridentate ligand and 4-methoxybenzenethiol as described elsewhere[2]. They were reduced by dimethylphenylphosphine in acetone/acetic acid (1:1) at ambient temperature, which was indicated by the change in colour of the reaction mixtures to a deep violet (Fig. 1).

The products were isolated as microcrystalline powders and recrystallized from $CHCl_3$/methanol as violet crystals suitable for X-ray diffraction analysis.

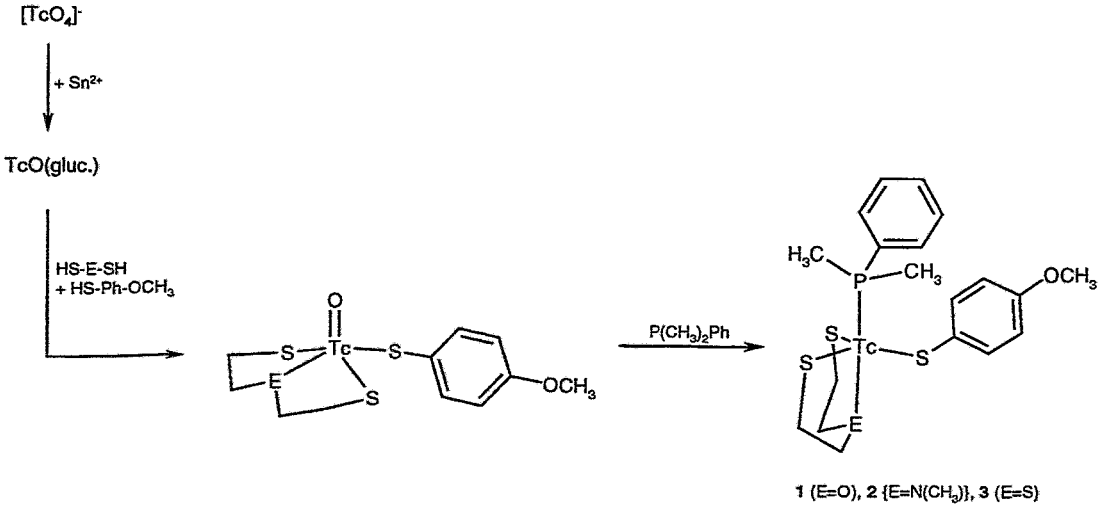

Fig 1. Reduction of oxotechnetium(V) mixed-ligand complexes by dimethylphenyl phosphine

The analytical data of the complexes correspond to the general formula [Tc(Me_2PhP)(SES)(S-C_6H_4-$COCH_3$)]. This formulation was confirmed by ^1H NMR spectroscopic data. The signal groups can be clearly assigned to the individual ligands. A ligand ratio in the complexes of 1:1:1:1 follows from the integrals.
As illustrated in Fig. 2 the complexes adopt the trigonal-bipyramidal geometry, thus minimizing the steric hindrance between the bulky phosphine and the thiol ligands. In this respect the compounds are comparable to the "4+1" Tc(III) complexes formed by the tripodal ligand 2.2'.2"-nitrilotris(ethanthiol) and tertiary phosphines [4].

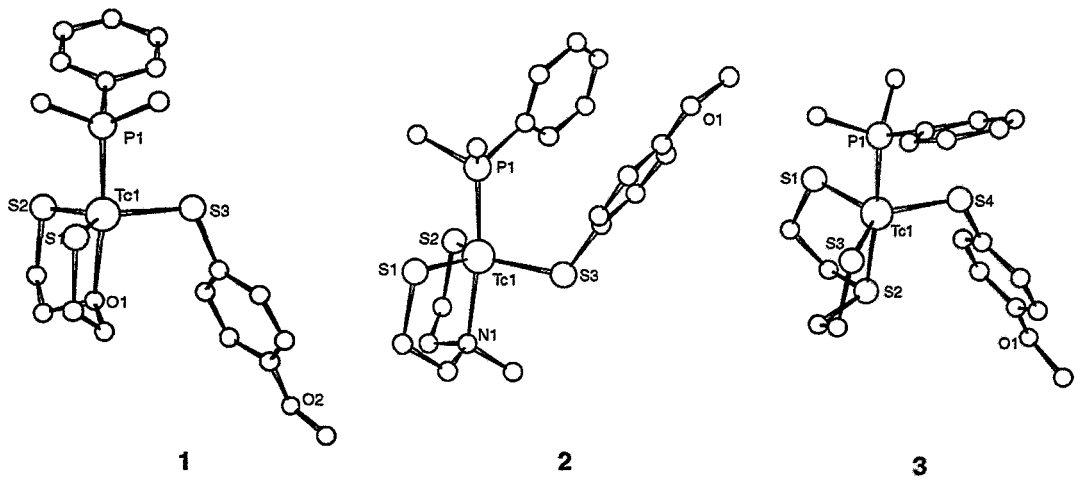

Fig. 2. Molecular structures of Tc(III) mixed-ligand complexes containing tridentate/monodentate thiol ligands and monodentate phosphines.

The reaction is not limited to dimethylphenylphosphine. PPh_3, PBu_3 and $P(CH_2CH_2CN)_3$ react in a similar manner with the oxotechnetium(V) complexes, as was shown earlier by the UV/Vis data of the reaction products [5].

References

[1] Pietzsch H.-J., Spies H. and Hoffmann S. (1989) Lipophilic Tc Complexes VI. Neutral oxotechnetium(V) complexes with monothiol/tridentate dithiol coordination. *Inorg. Chim. Acta* **165**, 163-166.

[2] Spies H., Pietzsch H.-J. and Johannsen B. (1999) The "n+1" approach in the design of specific Tc radiopharmaceuticals: Potentials and Problems. In: *Technetium and Rhenium in Chemistry and Nuclear Medicine* **5**, (M. Nicolini, U. Mazzi Eds.) SGEditoriali, Padova, pp. 101-108.

[3] Spies H., Glaser M., Pietzsch H.-J., Hahn F. E., Kintzel O. and Lügger T. (1994) Trigonal-bipyramidal Tc and Re complexes with tetradentate NS_3 tripod ligands. *Angew.Chem. Intern. Ed.* (in Engl.) **33**, 1354-1356.

[4] Spies H., Glaser M., Pietzsch H.-J., Hahn F. E., Kintzel O. and Lügger T. (1995) Synthesis and reactions of trigonal-bipyramidal Re and Tc complexes with a tripopdal, tetradentate NS_3 ligand. *Inorg. Chim. Acta* **240**, 465-478.

[5] Pietzsch H.-J., Spies H. and Hoffmannn S. (1990) Lipophilic Tc complexes IX. The reduction of (3-oxapentane-1,5-dithiolato)(p-carbmethoxybenzenethiolato)-oxotechnetium(V) by tertiary phosphines. *Inorg. Chim. Acta* **168**, 7-9.

22. No Carrier Added Preparations of "3+1+1" Technetium Complexes

S. Seifert, A. Drews, A. Gupta, H.-J. Pietzsch, H. Spies

Introduction

As described in the article above, reduction of the well-known 3+1 Tc(V) complexes [TcO(SES/S)] with phosphines leads to tridentate/monodentate/monodentate coordinated "3+1+1" Tc(III) complexes of the general formula [Tc(SES/RS/P)] (E = S, NR, O; RS = monothiol; P = phosphine) [1, 2].
The preparation of these complexes at the no carrier added level was investigated to study their reactivity in aqueous solution and in biological media *in vitro* as well as *in vivo*. At first the complexes were prepared at the carrier added level in a two-step procedure via the 3+1 Tc(V) complex, followed by reduction with phosphine. Then a more "kit-like" procedure was developed, which involved the reduction of pertechnetate in the presence of all three ligands. Finally, stability studies were carried out to check the suitability of this type of complex for biological studies.

Experimental

No carrier added preparation of 3+1 technetium complexes as well as the purification and separation of ligand excess were carried out according to described methods [3, 4]. We studied the complexation reactions at n.c.a. level with the tridentate ligands 3-thiapentane-1,5-dithiol (HS-$(CH_2)_2$-S-$(CH_2)_2$-SH), 3-methylazapentane-1,5-dithiol (HS-$(CH_2)_2$-N(CH_3)-$(CH_2)_2$-SH) and 3-oxapentane-1,5-dithiol (HS-$(CH_2)_2$-O-$(CH_2)_2$-SH) and the monodentate ligand methoxythiophenol (MTP). For the following reduction of the Tc(V) complex the pH of the reaction solution and the amounts of dimethylphenylphosphine and stannous chloride were optimized. It was found that 0.2 mg of dimethylphenylphosphine are suitable for reducing the separated ^{99m}Tc(V) complex to the Tc(III) complex at pH 3 - 4 within 1 – 2 hours at room temperature.

The one-step procedure for preparing 3+1+1 ^{99m}Tc complexes was performed according to the following route:

A mixture of
0.5 ml pertechnetate solution (10 – 500 MBq generator eluate),
0.25 ml propylene glycol,
0.25 ml acetonitrile,
0.50 mg methoxythiophenol, dissolved in ethanol,
0.05 mg tridentate ligand (SSS, SOS or SNMeS ligand), dissolved in ethanol and
0.02 ml 0.1 M NaOH is reduced by addition of
20 µl $SnCl_2$ solution (1.0 – 1.5 mg $SnCl_2$/5.0 ml 0.1 N HCl).

The resulting solution is neutralized with trifluoroacetic acid to pH 5.0 - 6.0 and after that, 0.2 mg of dimethylphenylphosphine (dissolved in acetonitrile) are then added. The vial is closed and the reaction solution is heated at 50 – 60 °C for 20 min.

Yields: 90 - 95 % [^{99m}Tc(SSS/MTP/PMe_2Ph)] and [^{99m}Tc(SOS/MTP/PMe_2Ph)],
80 - 85 % [^{99m}Tc(SNMeS/MTP/PMe_2Ph)].

Results and Discussion

The possibility of preparing n.c.a. ^{99m}Tc(III) complexes of the general formula [Tc(SES)(RS)PMe_2Ph] was evaluated. A comparison of the chromatographic data of ^{99}Tc reference complexes described in the article above with the ^{99m}Tc preparations confirms the identity of SSS, SOS as well as SNMeS complexes (Table 1).

Table 1. HPLC data of 3+1+1 ^{99}Tc and ^{99m}Tc complexes

Complex	Hypersil ODS (MeOH/0.01 M PBS pH 7.4, 80/20); R_t [min]
[^{99}Tc(SSS/MTP/PMe_2Ph)]	11.9
[^{99m}Tc(SSS/MTP/PMe_2Ph)]	11.9
[^{99}Tc(SNMeS/MTP/PMe_2Ph)]	13.6
[^{99m}Tc(SNMeS/MTP/PMe_2Ph)]	13.5
[^{99}Tc(SOS/MTP/PMe_2Ph)]	9.3
[^{99m}Tc(SOS/MTP/PMe_2Ph)]	9.3

The preparation was studied using the two reaction routes shown in Scheme 1.

Scheme 1. Reaction routes to prepare the n.c.a. 3+1+1 ^{99m}Tc complexes

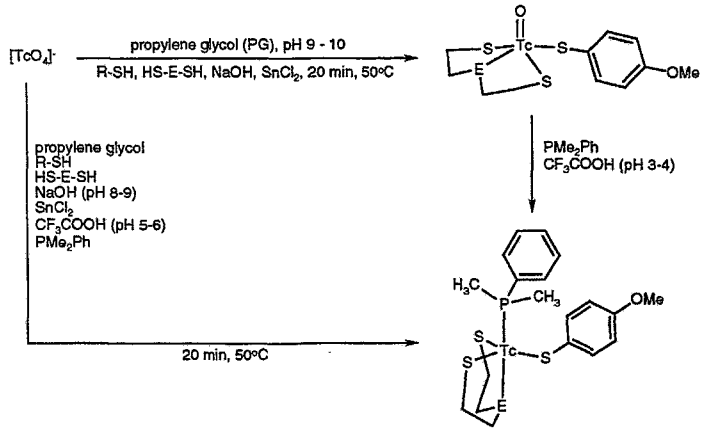

At first, the preparation of [^{99m}Tc(SSS/MTP/PMe_2Ph)] was carried out via the 3+1 ^{99m}Tc(V) complex, which was then reduced with phosphine. The 3+1 ^{99m}Tc complexes were prepared by direct reduction of pertechnetate with stannous chloride in an optimized mixture of amounts of ligand and propylene glycol (PG) and purified by HPLC. For the following reduction of the Tc(V) complex the pH of the reaction solution and the quantities of dimethylphenylphosphine and stannous chloride were optimized.
It was found that 0.2 mg of dimethylphenylphosphine dissolved in acetonitrile are the optimum amount for reduction. The reduction proceeds slowly. It takes about one hour at room temperature to complete the reaction with yields of about 70 %. The reaction is pH-dependent. Under dilute acidic conditions (pH 3 – 4) the Tc(V) complex is reduced to the desired product. The Tc(III) complex is not formed in neutral or weak alkaline solutions.

Encouraged by these results a one-pot reaction was tested to prepare the ^{99m}Tc(III) complex directly from pertechnetate. The optimized parameters (ligand amounts, reducing agent, pH) found for the preparation of ^{99m}Tc(V) complexes and the reduction to the Tc(III) complex were used for this purpose. The preparation of ^{99m}Tc(V) complexes is commonly carried out at pH 9 – 10. On the other hand, the reduction to the Tc(III) complex should take place in a weak acidic solution. This discrepancy was solved by using nearly neutral conditions for preparation of the desired complex. High yields of 90 % - >95 % can be reached, if the addition of ligands and other substances to the generator eluate follows the order mentioned above. Using the optimum parameters for preparation of the ^{99m}Tc(III) complexes, a reaction time >1 h is needed to complete the reaction. The formation of the desired complex is accelerated by heating the reaction solution to 50 – 60 °C for 20 – 30 minutes. Higher temperatures diminish the yield of the product. Without addition of stannous chloride only low yields of the desired product are obtained.

Stability studies

The ^{99m}Tc complexes are partially stable in alcoholic or acetonitrilic solutions. This behaviour was also observed for the corresponding ^{99}Tc complexes dissolved in acetonitrile. The blue colour of the 3+1+1 ^{99}Tc(III) complex solution slowly turns red after standing for days due to oxidation to the 3+1 ^{99}Tc(V) complex and small parts of other unknown products (Fig. 1)

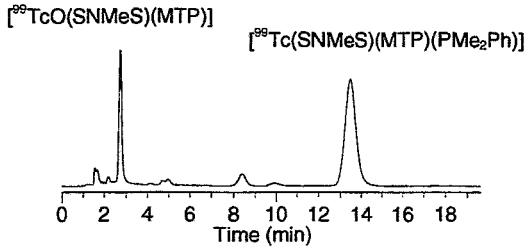

Fig. 1. HPLC pattern of [^{99}Tc(SNMeS)(MTP)(PMe_2Ph)] dissolved in acetonitrile, after 50 h at room temperature.

The rate of transformation varies for the three investigated complexes. The following order of stability was determined for the ^{99}Tc complexes:

[^{99}Tc(SOS)(MTP)(PMe_2Ph)] > [^{99}Tc(SSS)(MTP)(PMe_2Ph)] > [^{99}Tc(SNMeS)(MTP)(PMe_2Ph)]

While the ^{99}Tc complex solutions are practically stable for 3 – 4 hours and longer, the ^{99m}Tc complexes undergo a faster transformation in methanolic solution (Fig. 2). The order of stability is different from that determined for the ^{99}Tc complexes.

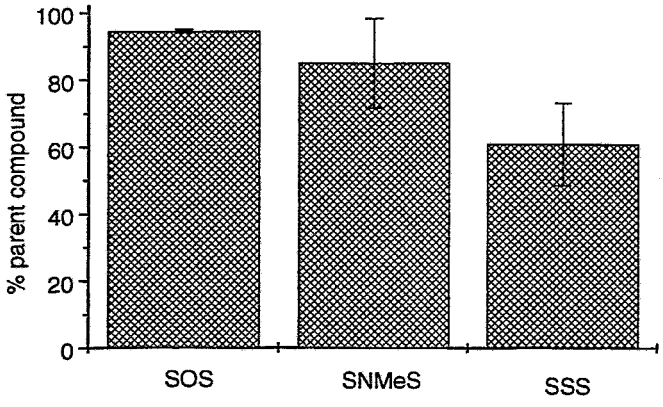

Fig. 2. Stability of purified [^{99m}Tc(SES)(MTP)(PMe_2Ph)] complexes, 2 h after HPLC separation and dissolution in methanol.

In aqueous/alcoholic solutions parallel to the oxidation a rapid decomposition of the 3+1+1 complexes to three more hydrophilic products is observed by HPLC and TLC.

A remarkable increase in stability in aqueous solution was achieved by adding β-hydroxypropyl-cyclodextrin (HPB) to the complex solution. According to results obtained by Goomer *et al.* in 1992 an improvement is in fact observed by the addition of HPB to the complex solution. Fig. 3 shows the stability of the SSS complex in aqueous solution with and without addition of HPB.

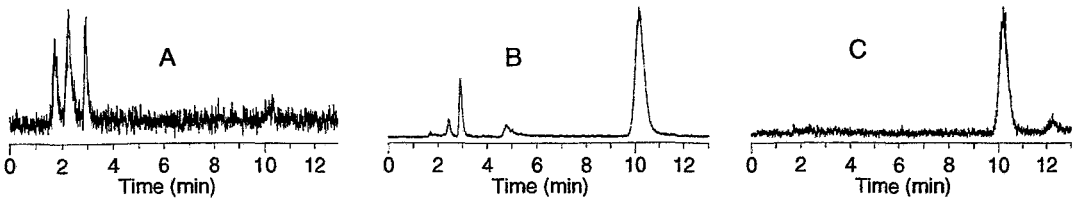

Fig. 3. Stabilization of [^{99m}Tc(SSS)(MTP)(PMe_2Ph)] complex (R_t = 10.1 min) by addition of β-hydroxypropylcyclodextrin (HPB). A: complex solution diluted 1:10 with water after 30 min; B: complex solution in methanol after 90 min; C: complex solution diluted 1:10 with 25 % aqueous HPB solution after 90 min.

GSH challenge

Challenge experiments with glutathione confirm also for this class of complexes the exchange of the monothiol ligand as known from the 3+1 complexes [5]. It was found that the transchelation of 3+1+1 complexes proceeds generally faster than for 3+1 complexes. In the case of SNMeS and SOS complexes the rate of exchange is much faster than the rate of decomposition. That allows clear studies of the transchelation reaction with GSH and of the reversibility of this reaction. It was possible to show that the reaction product of the [^{99m}Tc(SNMeS)(MTP)(PMe_2Ph)] complex with GSH is identical in HPLC and TLC analyses with the prepared [^{99}Tc(SNMeS)(GS)(PMe_2Ph)] complex which was characterized by elemental analysis and mass spectrometry (Fig. 4).

Besides the challenge product of the ^{99m}Tc(III) complex also the challenge product of the corresponding 3+1 ^{99m}Tc(V) complex was observed. The oxidation of Tc(III) to Tc(V) was clearly visible after addition of MTP to the challenge sample. In a reversible reaction both the 3+1+1 Tc(III) complex and the 3+1 Tc(V) complex were formed by ligand exchange of GSH against MTP (Fig. 5).
The addition of HPB to the complex solution did not influence the rate of transchelation with GSH.

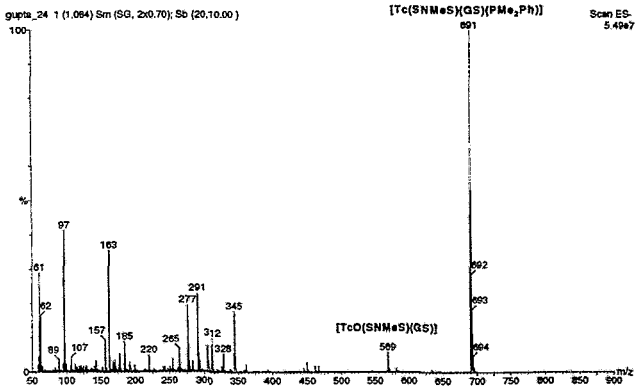

Fig. 4. Electron spray ionization mass spectrum of [^{99}Tc(SNMeS)(GS)(PMe_2Ph)]

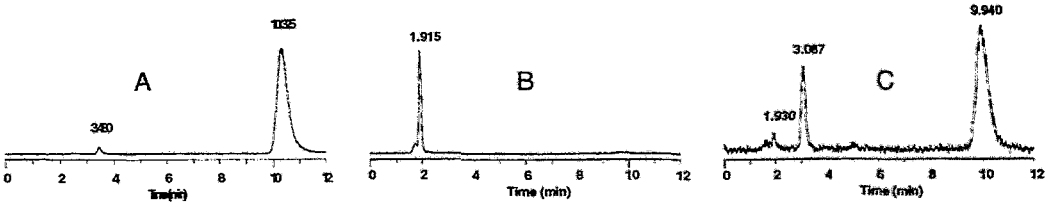

Fig. 5. HPLC chromatograms of ligand-exchange reaction of [^{99m}Tc(SOS)(MTP)(PMe_2Ph)] (A) with GSH (B) and reversible reaction after addition of MTP (C). Column: Hypersil ODS, R_t values: 1.9 min ([^{99m}Tc(SOS)(GS)(PMe_2Ph)]), 3.1 min ([^{99m}TcO(SOS)(MTP)], 9.9 min ([^{99m}Tc(SOS)(MTP)(PMe_2Ph)].

Summarizing, it can be concluded that the no carrier added preparation of technetium mixed-ligand complexes of the general formula [Tc(SXS)(RS)(PMe_2Ph)] (3+1+1 complexes) is possible in a one-step procedure starting from pertechnetate in yields of 85 – 95 % of radiochemical purity. The identity of n.c.a. preparations with the fully characterized ^{99}Tc complexes was confirmed by comparison of their chromatographic data.
In challenge experiments performed with glutathione the same exchange of the monothiolato ligands was observed as for the 3+1 complexes. The exchange was also reversible but the challenge reactions proceeded faster than with the 3+1 complexes. The complexes were moreover oxidized in solution. All these properties together do not meet the requirements of a radiotracer and lead to the conclusion that 3+1+1 technetium complexes are not an alternative to 3+1 complexes.

References

[1] Pietzsch H.-J., Spies H. and Hoffmann S. (1989) Lipophilic Tc complexes. VI. Neutral oxotechnetium(V) complexes with monothiol/tridentate dithiol coordination. *Inorg. Chim. Acta* **165**, 163-166.

[2] Pietzsch H.-J., Seifert S., Drews A., Leibnitz P. and Spies H. (1999) Synthesis and characterization of novel mixed-ligand technetium(III) complexes containing tridentate/monodentate thiol ligands and monodentate phosphines. *This report*, pp. 73-74.

[3] Seifert S., Pietzsch H.-J., Scheunemann M., Spies H. and Johannsen B. (1997) Serotonin receptor-binding technetium and rhenium complexes. 17. Different routes of nca preparation of "3+1" ^{99m}Tc complexes. *Annual Report 1997*, Institute of Bioinorganic and Radiopharmaceutical Chemistry, FZR-200, pp.10-13.

[4] Seifert S., Pietzsch H.-J., Scheunemann M., Spies H., Syhre R. and Johannsen B. (1998) No carrier added preparations of "3+1" mixed-ligand ^{99m}Tc complexes. *Appl. Radiat. Isot.* **49**, 5-11.

[5] Gupta A., Seifert S., Syhre R., Johannsen B. (1999) Challenge experiments with "3+1" mixed-ligand ^{99m}Tc complexes and glutathione: influence of structural parameters on the complex stability. *Report January 1998 – June 1999*, Institute of Bioinorganic and Radiopharmaceutical Chemistry, FZR-270, pp.167-172.

23. Oxorhenium Mixed-Ligand "3+1" and "3+2" Complexes with the 2,6-Dithiomethylpyridine Ligand. Crystal Structure of [2,6-dithiomethylpyridinato][*p*-methoxybenzenethiolato]oxorhenium(V)

B. Nock[1], H.-J. Pietzsch, F. Tisato[2], T. Maina[1], P. Leibnitz[3], H. Spies, E. Chiotellis[1]
[1]Institute of Radioisotopes - Radiodiagnostic Products, National Centre for Scientific Research "Demokritos", Athens, Greece
[2]Istituto di Chimica e Tecnologie Inorganiche e dei Materiali Avanzati, Consiglio Nazionale delle Ricerche, Padova, Italy
[3]Bundesanstalt für Materialforschung, Berlin

Introduction

Our recent work has been largely focused on the '3+1' mixed ligand systems for oxorhenium and oxotechnetium containing primarily the SNS/S or the SSS/S donor atom sets. These are neutral and lipophilic metal chelates adopting a distorted trigonal bipyramidal or square pyramidal geometry [1, 2]. Despite the fact that several examples of such mixed ligand metal chelates coupled to pharmacophore groups, like tropane, ketanserin or *o*-methoxyphenylpiperazine, have been recently proposed for the *in vivo* mapping of brain receptors [3, 4], complications related to their *in vivo* instability limit their effective application for such purposes [5 - 7]. We have recently proposed the use of '3+2' mixed ligand complexes, wherein the monothiolato coligand of the '3+1' concept has been replaced by a bidentate *o*-diphenylphosphinophenolato ligand. Thus, six-coordinate octahedral complexes, instead of five-coordinate ones, form exhibiting a closed coordination shell and, consequently, an increased stability [8].

We report herein on the synthesis and characterization of two novel oxorhenium complexes prepared each according to the '3+1' or the '3+2' mixed ligand approach and containing 2,6-dithiomethylpyridine as tridentate ligand [9].

Results and Discussion

Complex **1** was obtained in good yields by reaction of equimolar amounts of 2,6-dithio-methylpyridine and *p*-methoxybenzenethiol on the $[(n\text{-}C_4H_9)_4N][ReOCl_4]$ precursor (Scheme 1).

Scheme 1.

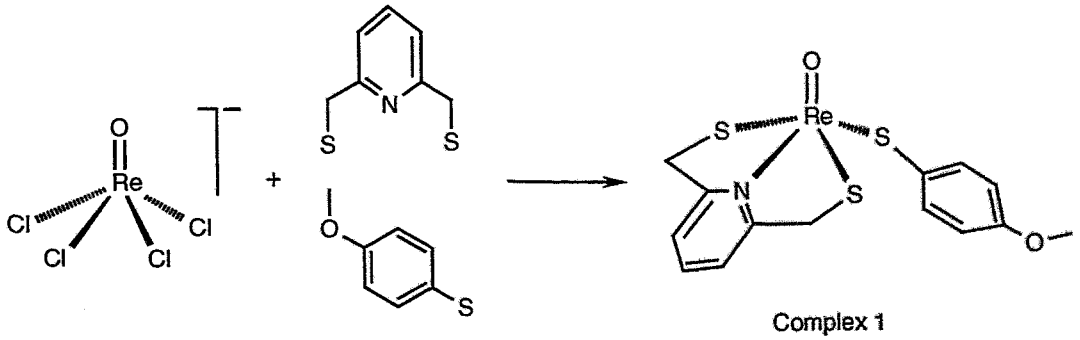

Complex 1

As shown in the ORTEP diagram of Fig. 1, complex **1** adopts the usual distorted square-pyramidal arrangment of the four donor atoms (SNS/S) around the $[Re{=}O]^{3+}$ core. The tridentate ligand, representing a novel framework of donor atoms capable of forming '3+1' mixed-ligand complexes, spans three positions in the basal plane, *via* the charged thiolate S atoms and the neutral pyridine nitrogen. The fourth position is occupied by the *p*-methoxybenzenethiolate S atom. The Re atom lies above the basal plane towards the O apex (0.83 Å).

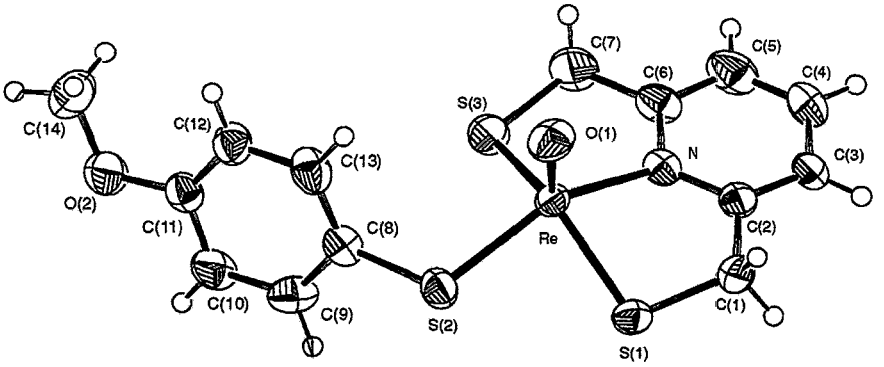

Fig. 1. Molecular structure of complex **1**

Complex **2a**, as depicted in Scheme 2, was obtained by a two step synthesis: i) equimolar amounts of *o*-diphenylphosphinophenol were reacted with $[(n\text{-}C_4H_9)_4N][ReOCl_4]$ affording the emerald intermediate $[(n\text{-}C_4H_9)_4N][ReOCl_3(PO)]$; ii) the latter was then reacted with 2,6-dithiomethylpyridine affording complex **2a** as a red solid.

Scheme 2

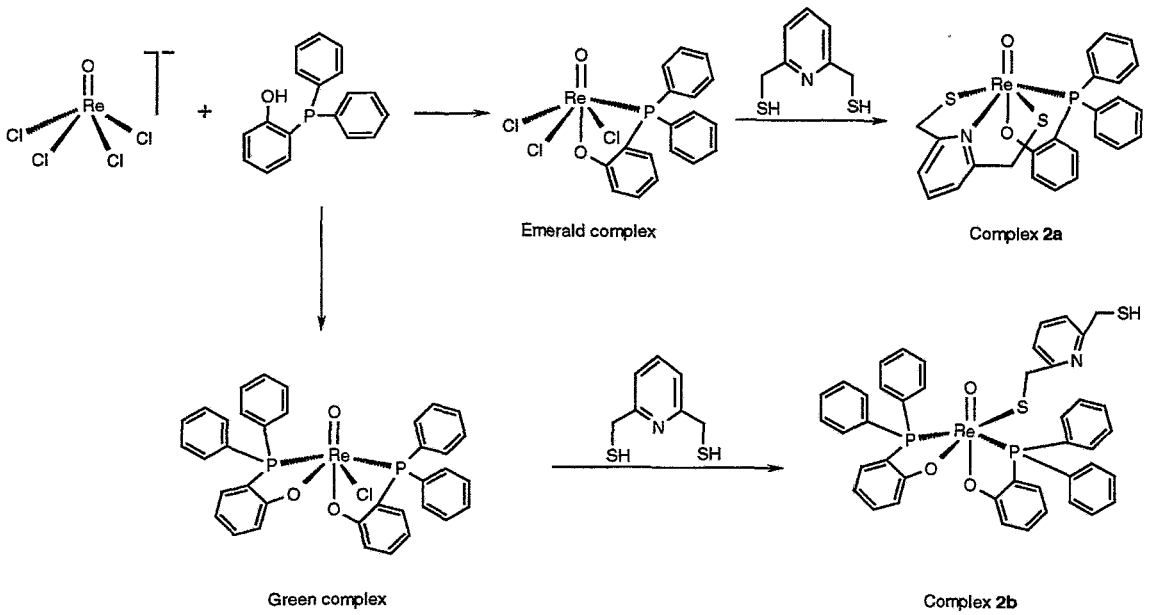

Complex **2a** is a six-coordinate neutral oxorhenium species, given that the two thiolate groups of the SNS ligand and the hydroxy group of the PO ligand are deprotonated upon coordination to the ReO^{3+} core. The IR spectrum shows an intense band at 951 cm^{-1} corresponding to the Re=O stretching vibration, found in good agreement with that of analogous six-coordinate oxorhenium complexes containing the same PO ligand [8, 10]. The UV/Vis spectrum exhibits a maximum at 313, 399 nm, like to that of similar oxorhenium compounds [8].

A complete ^{1}H, ^{13}C and ^{31}P NMR analysis confirms the formula assigned to complex **2a**. In detail, the proton spectrum displays the expected AB pattern for the methylene protons of the tridentate ligand centered at 5.29 ppm, along with signals of the pyridine ring deshielded with respect to those of the uncoordinated ligand. The aromatic protons of the phenyl ring interposed between the donors of the PO^{-} ligand display a four signal pattern consistent with the coordination spanning a position on the equatorial plane (P) and the position *trans* to the oxo linkage (O), as previously shown by the parent complex $[ReOCl_3(PO)]^{-}$ [10] and related bis-substituted P,O-oxorhenium compounds [11]. Analogously, the ^{13}C spectrum shows the aliphatic carbon at 53.8 ppm and all of the aromatic signals arising from both the pyridine and arylphosphine in the range 117.0 – 153.8 ppm. The ^{31}P spectrum exhibits a

singlet at 13.1 ppm to be compared with the signal of uncoordinated POH which falls at – 31.2 ppm [10].
During the synthesis of the mono-substituted emerald complex $[ReOCl_3(PO)]^-$, always trace amounts of the bis-substituted $[ReOCl(PO)_2]$ green compound are recovered [10]. The latter reacts also with 2,6-dithiomethylpyridine leading to the formation of a minor complex **2b**, as depicted in Scheme 2. It was isolated from a silica column during the purification of the major complex **2a**. Complex **2b** is more hydrophilic as compared to **2a**. The IR spectrum of **2b** reveals a band at 947 cm^{-1} attributed to the ν[Re=O] stretching vibration [8, 10]. The formulation of **2b** was assessed by NMR studies. The ^{31}P spectrum clearly indicates the presence of two magnetically unequivalent P nuclei giving a two doublets pattern with coupling constant of 8 Hz, in agreement with a *cis*-P configuration (see Scheme 2). These two doublets are centered at 9.6 and 4.6 ppm, values slightly different from those observed in the same solvent (11.6 and 2.3 ppm) for the parent complex $[ReOCl(PO)_2]$, indicating the substitution of the chloride ligand by the thiolate function of the dithiomethylpyridine ligand. The proton spectrum shows two multiplets in the methylene region, along with a series of overlapped multiplets in the aromatic region in the correct 4:31 integration ratio. The coordination of a thiolate group leaving outside a further uncoordinated dangling thiol is precedended [11].

References

[1] Pelecanou M., Pirmettis I. C., Papadopoulos M. S., Raptopoulou C. P., Terzis A., Chiotellis E. and Stassinopoulou C. I. (1999) Structural studies of ReO(V) mixed ligand [SNS][Cl] and [SNS][S] complexes. *Inorg. Chim. Acta* **287**, 142-151.

[2] Spies H., Fietz T., Pietzsch H.-J., Johannsen B., Leibnitz P., Reck G., Scheller D. and Klostermann K. (1995) Neutral oxorhenium(V) complexes with tridentate dithiol ligands and monodentate alkyl/aryl thiols as co-ligands. *J. Chem. Soc. Dalton Trans.* 2277-2280.

[3] Meegalla S., Plössl k., Kung M.-P., Chumpradit S., Stevenson D. A., Frederick D. and Kung H. F. (1996) Tc-99m-labeled tropanes as dopamine transporter imaging agents. *Bioconjug. Chem.* **7**, 421-429.

[4] Johannsen B., Scheunemann M., Spies H., Brust P., Wober J. and Syhre R. (1996) Technetium(V) and rhenium(V) complexes for 5-HT_{2A} serotonin receptor binding: structure-affinity considerations. *Nucl. Med. Biol.* **23**, 429-438.

[5] Nock B., Maina T., Yannoukakos D., Pirmettis I. C., Papadopoulos M. S. and Chiotellis E. (1999) Glutathione-mediated metabolism of technetium-99m SNS/S mixed ligand complexes: A proposed mechanism of brain retention. *J. Med. Chem.* **42**, 1066-1075.

[6] Pelecanou M., Pirmettis I. C., Nock B. A., Papadopoulos M. Chiotellis E. and Stassinopoulou C. I. (1998) Interaction of [ReO(SNS) (S)] and [^{99m}TcO(SNS) (S)] mixed ligand complexes with glutathione: isolation and characterization of the product. *Inorg. Chim. Acta* **281**, 148-152.

[7] Syhre R., Seifert S., Spies H., Gupta A. and Johannsen B. (1998) Stability versus reactivity of "3+1" mixed-ligand technetium-99m complexes in vitro and in vivo. *Eur. J. Nucl. Med.* **25**, 793-796.

[8] Nock B., Maina T., Tisato F., Papadopoulos M., Raptopoulou C. P., Terzis A. and Chiotellis E. (1999) Novel six-coordinate oxorhenium "3+2" mixed-ligand complexes carrying the SNS/PO donor atom set: synthesis and characterization. *Inorg. Chem.* **38**, 4197-4202.

[9] Nock B., Pietzsch H.-J., Tisato F., Maina T., Leibnitz P., Spies H. and Chiotellis E. (1999) Oxorhenium mixed-ligand '3+1' and '3+2' complexes with the 2,6-dithiomethylpyridine ligand. Crystal structure of [2,6-dithiomethylpyridinato][*p*-methoxybenzenethiolato]oxorhenium(V). *Inorg. Chim. Acta*, submitted for publication.

[10] Bolzati C., Tisato F., Refosco F., Bandoli G. and Dolmella A. (1996) Uncommon anionic dioxorhenium(V) and neutral monooxorhenium(V) mixed-ligand complexes containing heterofunctionalized phosphine ligands: syntheses and structural characterization. *Inorg. Chem.* **35**, 6221-6229.

[11] Maresca K. P., Bonavia G. H., Babich J. W. and Zubieta J. (1999) Synthesis and characterization of oxorhenium "3+1" mixed-thiolate complexes. Crystal and molecular structures of $[ReO\{3\text{-}(SCH_2CH_2)_2S\}(C_6H_4X\text{-}4\text{-}CH_2S)]$ (X = F, Cl, Br, OMe) and of the pendant thiolate compounds $[ReO\{3\text{-}(SCH_2CH_2)_2S\}(1\text{-}SCH_2CH_2SCH_2CH_2SH)]$ and $[ReO\{3\text{-}(SCH_2CH_2)_2S\}\text{-}\{1\text{-}SCH_2CH(OH)\text{-}CH(OH)CH_2SH\}]$. *Inorg. Chim. Acta* **284**, 252-257.

24. Synthesis and Characterization of Trigonal-Bipyramidal Technetium(III) Complexes with Tetradendate/Monodendate NS_3/Isocyanide Coordination: Potencies of the "4+1" Tc Chelate System for the Design of Neutral, Non-Polar and Lipophilic Complexes Stable *In Vivo*

H.-J. Pietzsch, A. Gupta, R. Syhre, H. Spies

Introduction

To date most technetium compounds suitable for coupling to biologically active molecules, e.g. CNS receptor targeted agents, are tetragonal-pyramidal complexes of the oxo ion $Tc{=}O^{3+}$. However, the properties and thus the *in vivo* behaviour of such complexes are strongly influenced by the quite polar Tc=O unit offering a free position *trans* to the oxo ligand for further reaction *in vivo*. The stricter the requirements for specific agents, the more important is the question whether such a polarity is beneficial or not. Alternatives are the oxo-free lower oxidation states, namely +1 and +3. After we reported on trigonal-bipyramidal mixed ligand rhenium(III) complexes with 2,2',2"-nitrilotris(ethanethiol) und isocyanides as co-ligands [1, 2], which are neutral and non-polar since they contain sterically well shielded oxo-free Re(III) ions, in the present paper we describe the basic chemistry of the ^{99}Tc analogues relevant for the radiotracer design. This involves the synthesis and structural analysis of ^{99}Tc complexes with simple isocyanides serving as models for functionalized derivatives. The no-carrier-added preparation of the analogous ^{99m}Tc-complexes is described as well as their stability in aqueous solution and in plasma, and their biodistribution in rats.

Results and Discussion

^{99}Tc chemistry

The ^{99}Tc complexes **^{99}Tc2** - **^{99}Tc5** were synthesized by a two step procedure starting from $[TcO_4]^-$ via the phosphine-containing precursor **^{99}Tc1** according to Scheme 1.

To a mixture of pertechnetate(VII) and 2,2',2"-nitrilotris(ethanethiol) (NS_3) an excess of dimethylphenylphosphine was added as a reducing agent and coligand to yield **^{99}Tc1**. Subsequent ligand exchange reactions of the appropriate isocyanides with **^{99}Tc1** in chloroform led to the formation of the complexes **^{99}Tc2** - **^{99}Tc5**.

Scheme 1

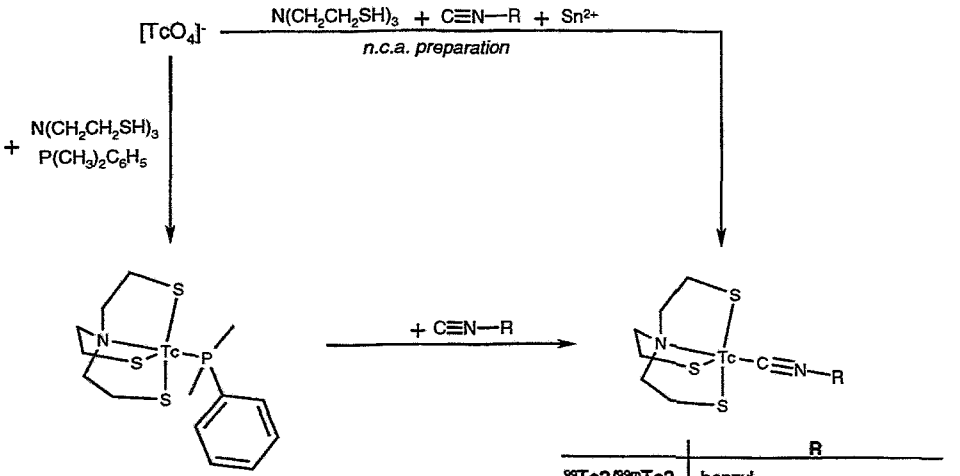

The complexes were characterized by elemental analyses as well as by NMR-, IR- and UV/Vis spectroscopy. X-ray structure analyses of some representatives confirm the triganol-pyramidal coordination geometry of this type of complexes (Figs. 1 - 5).

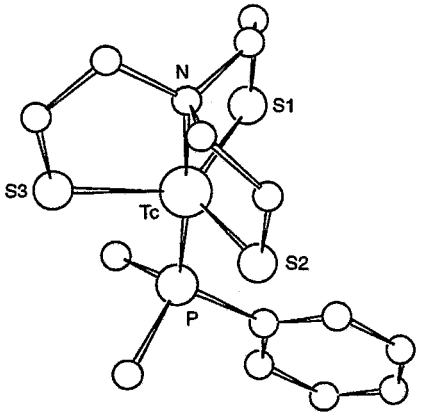

Fig. 1. Molecular structure of ^{99}**Tc1**

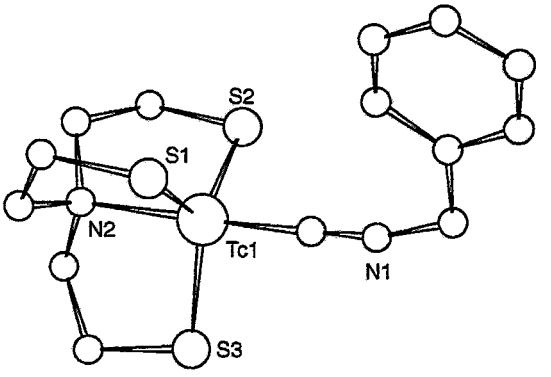

Fig. 2. Molecular structure of ^{99}**Tc2**

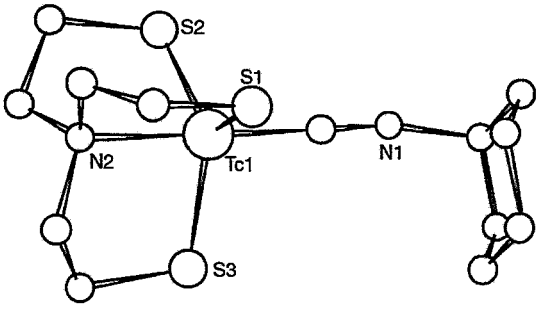

Fig. 3. Molecular structure of ^{99}**Tc3**

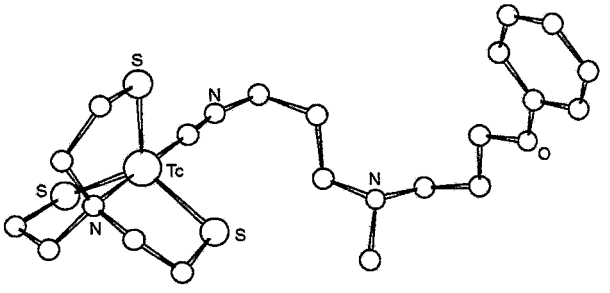

Fig. 4. Molecular structure of ^{99}**Tc4**

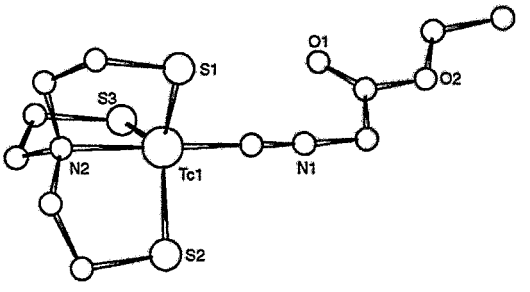

Fig. 5. Molecular structure of ^{99}**Tc5**

^{99m}Tc chemistry and biodistribution studies

No-carrier-added preparation of the ^{99m}Tc complexes

The no-carrier-added preparation of the complexes ^{99m}**Tc2** - ^{99m}**Tc4** was performed by a one-step procedure starting from $^{99m}TcO_4^-$ with stannous chloride as reducing agent. The yields were between 50 – 75 % using not optimized preparation conditions. In the appropriate reaction mixtures a by-product occurs which is not eluted from the Hypersil column. Therefore TLC has to be performed for

determining the yields of the preparation. After HPLC separation the radiochemical purity of the ^{99m}Tc(III) "4+1" complexes was determined by TLC and found to be >90 % (Fig. 6).

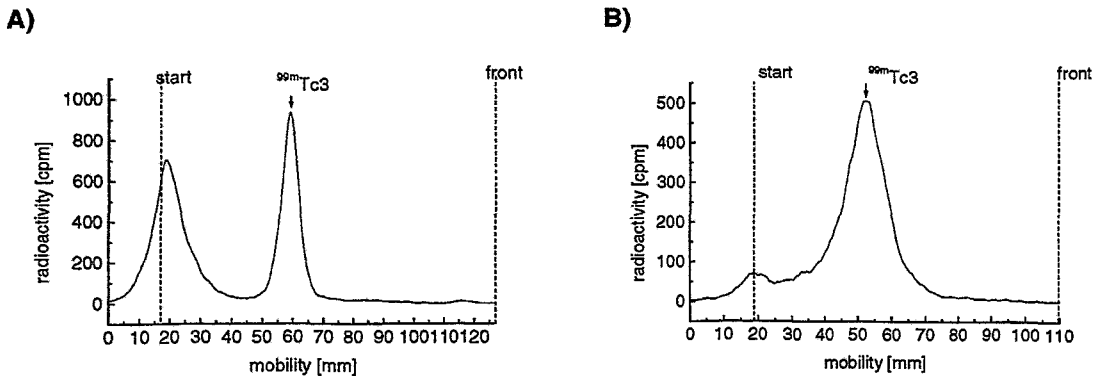

Fig. 6. TLC pattern of the ^{99m}**Tc3** complex; TLC: aluminium sheets RP-18 $_{F254s}$ (Merck) developed with methanol/water (80/20)
A)no-carrier-added preparation of ^{99m}**Tc3**, reaction mixture
B)no-carrier-added preparation of ^{99m}**Tc3** after HPLC purification

In order to establish the structure of the ^{99m}Tc complexes, comparison by HPLC with the well characterized ^{99}Tc analogues was pursued applying parallel radiometric and photometric detection. Thus, after co-injection of complexes ^{99m}**Tc2** and ^{99}**Tc2**, practically identical retention times were observed, while the recovery through the column was quantitative. Similarly, co-injections of the complex couples ^{99m}**Tc3**/^{99}**Tc3** and ^{99m}**Tc4**/^{99}**Tc4** led to identical R_t values for the respective compounds, revealing their structural analogy. R_t values of HPLC, R_f values of TLC and partition coefficients (log P) of the ^{99m}Tc complexes in the system octanol/saline are given in Table 1.

Table 1. HPLC data of ^{99}Tc and ^{99m}Tc complexes; Hypersil ODS: MeOH/0.01 M PBS pH 7.4, linear gradient 70 – 100 % A in 5 min, TLC data: TLC aluminium sheets RP-18 $_{F254s}$ (Merck) eluent: methanol/water (80/20)

Complex	R_t [min]	LogP (octanol/saline)	R_f
^{99}**Tc2**	5.8		0.4
^{99m}**Tc2**	5.9	1.5	0.4
^{99}**Tc3**	7.1		0.3
^{99m}**Tc3**	7.3	1.7	0.3
^{99}**Tc4**	7.7		0.1
^{99m}**Tc4**	7.7	1.6	0.1

Glutathione challenge experiments

Glutathione (GSH), the most abundant thiol compound in tissues, has to be considered as a potential agent for transchelating reactions *in vivo*. GSH is also responsible for the *in vivo* reactivity of so-called "3+1" mixed-ligand ^{99m}Tc(V) complexes. In view of these experiences it would be useful to explore also the behaviour of the "4+1" complexes against GSH ligand exchange reactions.

The ^{99m}Tc compounds were diluted with a 10 mM GSH solution immediately after HPLC purification and analysed after 120 minutes. In all cases no additional peaks, indicating Tc-GSH mixed ligand species, were observed in HPLC studies as well as in TLC studies. Under the conditions described above practically no ligand exchange reaction occurs between the ^{99m}Tc(III) „4+1" complexes and glutathione. Therefore we expect that no reactions of the complexes with thiol compounds in tissues as well as in blood will occur.

Stability studies in plasma and in rat blood

For stability studies the ^{99m}Tc complexes were incubated in rat blood and rat plasma for 120 minutes. After incubation the blood is centrifuged and the supernatant plasma was separated from the erythrocytes. The supernatent plasma as well as the resulting hemolysate were analysed using a Supelguard column as described above. For the complexes **^{99m}Tc2 - ^{99m}Tc4** no additional peaks were observed, indicating some kind of decomposition, modification or alteration of the complexes in HPLC studies with supelgard column. There is also no tendency of these complexes to bind on plasma components.

To confirm these results the plasma samples as well as the hemolysates were extracted with ethyl acetate. In this way approx. 85 - 95 % of the activity in the samples could be extracted. Analysing the extracts by HPLC using a Hypersil column and by TLC as described in the experimental section only the parent compounds were detected. These results indicate that the ^{99m}Tc(III) "4+1" complexes behave absolutely stable in plasma and blood of rat for at least 120 min as shown for **^{99m}Tc4** in Fig. 7.

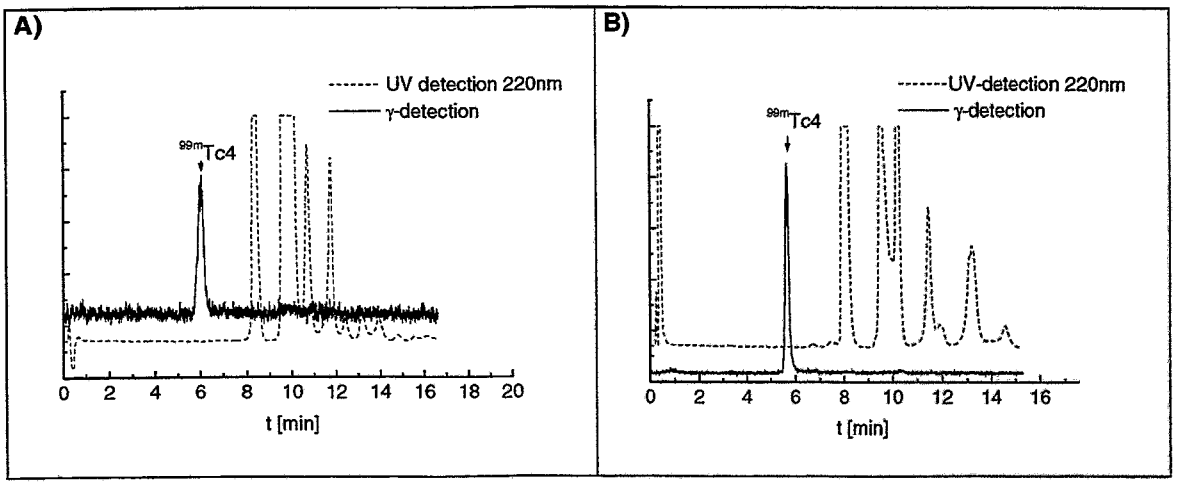

Fig 7. HPLC pattern of the **^{99m}Tc4** complex; Supelguard column (20 x 4.6 mm, 10 µm, flow rate 1.0 ml/min) using a linear gradient 95 % A to 40 % A in 15 min [A: isopropanol/0.1% trifluoroacetic acid (TFA) (10/90), B: isopropanol/0.1 % TFA (90/10)].
A: 120 minutes incubation in rat blood, hemolysate
B: 120 minutes incubation in rat blood, supernatant plasma

Biodistribution studies in rats

Biodistribution results for ^{99m}Tc complexes **^{99m}Tc2 - ^{99m}Tc4** in rats were shown in Table 2. These neutral, lipophilic complexes cross the blood-brain-barrier of the animals. They show a significant initial brain uptake up to 1.1 %, obtained for the most lipophilic cyclohexyl substituted complex **^{99m}Tc3** (logP 1.7). It was observed that the cyclohexyl as well as the benzyl substituted complex (**^{99m}Tc3** and **^{99m}Tc2)** indicate rather higher brain uptake compared to the complex **^{99m}Tc4** (max. 0.6 % ID; 2' p.i.), which contains a nitrogen-bearing side chain. Furthermore it was found that all of the complexes (**^{99m}Tc2 - ^{99m}Tc4)** were fast cleared from the blood and the brain of rats. Except the excretory organs liver and kidneys no prominent uptake and retention in the organism of rats could be observed after injection of these tracers. They were measured to be stable in whole-blood of rats and revealed no affinity to protein components of rat plasma. (Fig. 6).

Table 2. Biodistribution pattern of ^{99m}Tc complexes **2** - **4** in Wistar rats (% ID/organ except for blood as % ID/g; means ± SD; n = 5)

Complex	Time [min]	Blood/g	Brain	Heart	Lungs	Kidneys	Liver
^{99m}**Tc2**	5	0.34 ± *0.09*	0.79 ± *0.11*	0.4 ± *0.1*	1.5 ± *0.5*	2.1 ± *0.2*	31.6 ± *4.0*
	120	0.11 ±*0.04*	< 0.05	0.1 ±*0.02*	0.3 ± *0.1*	1.7 ± *0.4*	33.2 ± *5.6*
^{99m}**Tc3**	5	0.23 ± *0.11*	1.12 ± *0.31*	0.5 ± *0.2*	1.2 ± *0.3*	1.8 ± *0.2*	25.2 ± *2.1*
	120	0.13 ± *0.07*	0.05 ± *0.05*	0.1 ± *0.02*	0.4 ± *0.1*	1.5 ± *0.3*	22.5 ± *3.6*
^{99m}**Tc4**	5	0.13 ±*0.02*	0.44 ± *0.07*	0.6 ± *0.1*	1.1 ± *0.4*	5.2 ± *0.7*	13.8 ± *1.6*
	120	0.07 ± *0.01*	< 0.05	0.1 ±*0.01*	0.5 ± *0.1*	3.2 ± *1.7*	13.6 ± *2.0*

Conclusion

The tripodal, tetradendate ligand 2,2',2"-nitrilotris(ethanethiol) und isocyanides as co-ligands are able to form non-polar, lipophilic technetium complexes which contain sterically well shielded oxo-free Tc(III) ions. The monodendate isocyanide ligand enables easy functionalization in order to fine-tune physico-chemical properties of the complexes or to link the chelate unit to biomolecules. ^{99m}Tc complexes can easily be prepared at no-carrier-added level in high radiochemical yield. Challenge experiments with glutathione clearly indicate that no transchelation reaction occurs *in vivo*. This behaviour is considered to be an advantage of the ^{99m}Tc thioether carbonyl complexes over mixed-ligand ^{99m}Tc oxocomplexes in the oxidation state +5. Therefore, we believe that the complexes may be a useful tool in designing of ^{99m}Tc or ^{186}Re/^{188}Re radiopharmaceuticals.

References

[1] Spies H., Glaser M., Pietzsch H.-J., Hahn F. E., Kintzel O. and Lügger T. (1994) Trigonal-bipyramidale Technetium- und Rhenium-Komplexe mit vierzähnigen tripodalen NS_3 Liganden. *Angew.Chem.* **106**, 1416-1419.

[2] Spies H., Glaser M., Pietzsch H.-J., Hahn F. E., Kintzel O. and Lügger T. (1995) Synthesis and reactions of trigonal bipyramidal rhenium and technetium complexes with a tripodal NS_3 ligand. *Inorg. Chim. Acta* **240**, 465-478.

25. Chemical and Biological Characterization of Technetium(I) and Rhenium(I) Tricarbonyl Complexes with Dithioether Ligands Serving as Linkers for Coupling the "$Tc(CO)_3$" and "$Re(CO)_3$" Moieties to Biologically Active Molecules

H.-J. Pietzsch, A. Gupta, M. Reisgys, A. Drews, S. Seifert, R. Syhre, H. Spies, R. Alberto[1],U. Abram[2], P. A. Schubiger[1], B. Johannsen
[1]Paul-Scherrer-Institut Villigen, Abteilung für Radiopharmazie, Switzerland
[2]Forschungszentrum Rossendorf, Institut für Radiochemie

Introduction

The oxidation state +1 of technetium has been addressed only in a minor way before a new approach to inert technetium compounds on basis of Tc(I) carbonyl complexes has been elaborated [1 - 3]. Intensive investigations in the Tc carbonyl chemistry made available an organometallic Tc(I) aqua ion, $[Tc(H_2O)_3(CO)_3]^+$, from TcO_4^- under normal pressure. So, the prerequisite to exploit the small $[Tc(CO)_3]^+$ moiety for the labeling of biomolecules is given [4, 5]. Thioethers with the π-acceptor properties of the sulfur show a great potency to coordinate at the metal(I) carbonyl centre and a couple of Re carbonyl complexes with thioether ligands are known [6]. They may serve in an alternative approach to fully exploit the potential of the $[M(CO)_3]^+$ moiety (M = Tc, Re) for the design of radiotracers. In the present paper we describe the basic chemistry of the Tc(I)/Re(I) carbonyl thioethers as relevant for the radiotracer design.

Results and Discussion

Rhenium chemistry

The organometallic precursors $(NEt_4)_2[ReBr_3(CO)_3]$ and $[Re(NO_3)_3(CO)_3]^{2-}$ were reacted with bidendate dithioethers ($\mathbf{L^1}$-$\mathbf{L^5}$) of the general formula H_3C–S-CH_2CH_2-S-R (R = -CH_2CH_2COOH, CH_2-C≡CH) and R'–S-CH_2CH_2-S-R' (R' = CH_3CH_2-, CH_3CH_2-OH, CH_2COOH). The product pattern depends from the kind of the precursor complex and the reaction conditions.

In methanol $(NEt_4)_2[ReBr_3(CO)_3]$ reacts with $\mathbf{L^1}$-$\mathbf{L^5}$ to form stable rhenium(I) tricarbonyl complexes of the general composition $[ReBr(CO)_3L]$. Under these conditions the functional groups do not participate in the coordination (Scheme 1).

Scheme 1

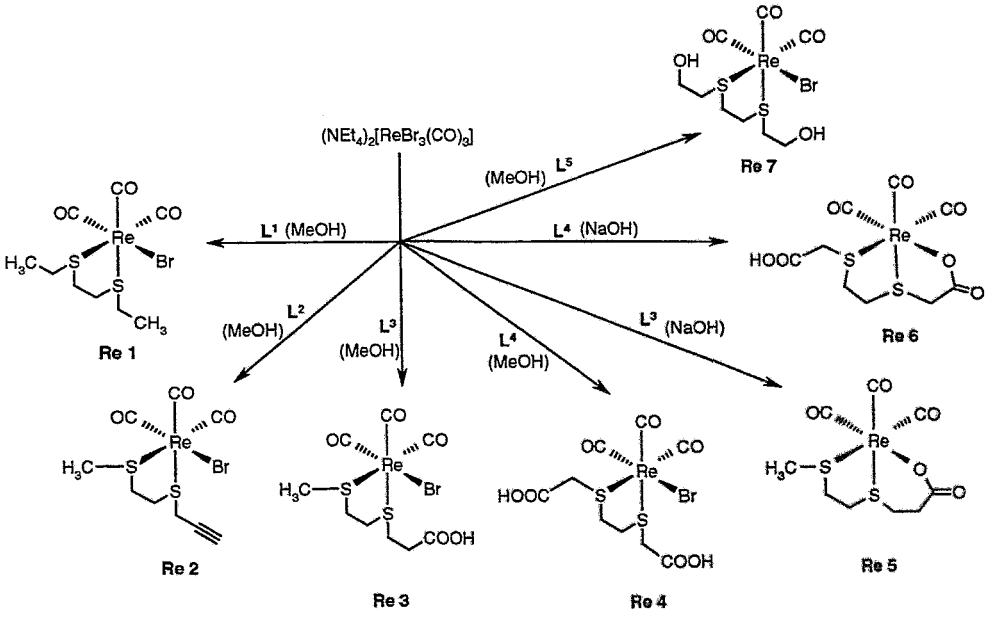

As a prototypic representative of this type of Re compounds the propargylic-group-bearing complex [$ReBr(CO_3)(H_3C$-S-CH_2CH_2-S-$CH_2C{\equiv}CH)$] **Re2** was studied by X-ray diffraction analysis (Fig.1). Its molecular structure exhibits a slightly distorted octahedron with facial coordination of the carbonyl ligands.

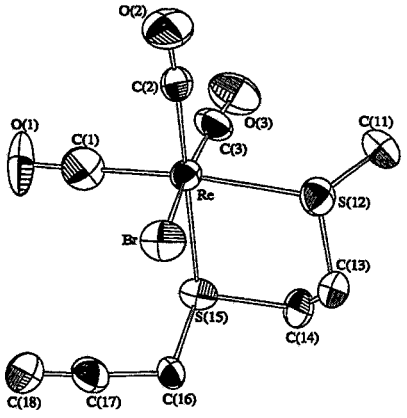

Fig. 1. Molecular structure of complex **Re2**

The potentially tetradentate ligand HO–CH_2CH_2–S-CH_2CH_2-S-CH_2CH_2-OH was reacted with the trinitrato precursor $[Re(NO_3)_3(CO)_3]^{2-}$ to yield a cationic complex [$Re(CO)_3$(HO–CH_2CH_2–S-CH_2CH_2-S-CH_2CH_2-OH)]NO_3 **Re8** which shows the coordination of one hydroxy group (Scheme 2). **Re8** has been characterized by correct elemental analysis, infrared spectroscopy, capillary electrophoresis and X-ray diffraction analysis.

Scheme 2

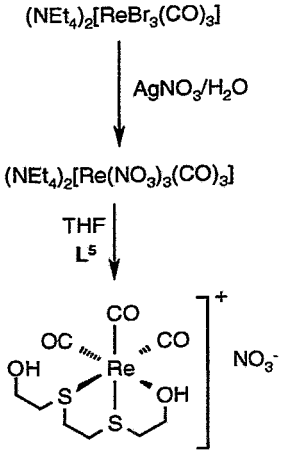

Re 8

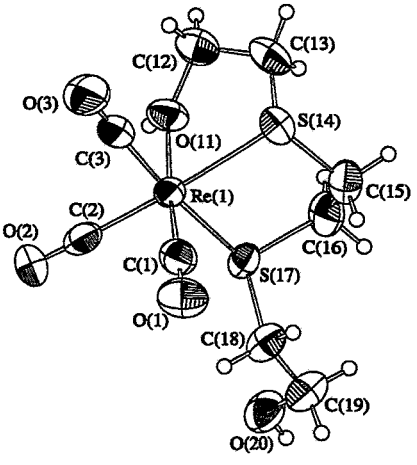

Fig. 2. Molecular structure of complex **Re8**

In water and with equimolar amounts of NaOH the ligand exchange reaction of the carboxylic group bearing ligands H_3C–S-CH_2CH_2-S-CH_2CH_2-COOH and HOOC-CH_2–S-CH_2CH_2-S-CH_2-COOH with $(NEt_4)_2[ReBr_3(CO)_3]$ led to complexes in which the bromide is replaced by the carboxylic group. The X-ray structure analysis of the complex **Re6** shows the second carboxylic group non-coordinated offering an ideal site for functionalization or coupling a biomolecule.

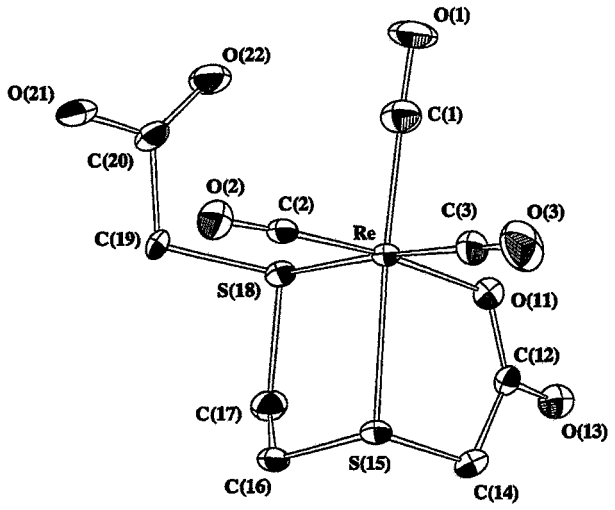

Fig. 3. Molecular structure of complex **Re6**

Technetium-99m chemistry

The no-carrier-added preparation of the analogue ^{99m}Tc(I) carbonyl thioether complexes could be performed using the precursor *fac*-[^{99m}Tc(H$_2$O)$_3$(CO)$_3$]$^+$ with yields up to 90 % (Scheme 3). In order to establish the structure of the ^{99m}Tc complexes prepared at tracer level, comparison by HPLC with the respective rhenium complexes prepared in macroscopic amounts was pursued applying parallel radiometric and photometric detection. Thus, after co-injection of complexes **Tc1** and **Re1**, practically identical retention times were observed, while the recovery through the column was quantitative. Similarly, co-injections of the complex couples **Tc2/Re2 – Tc6/Re6** led to identical R_t values for the respective compounds, revealing their structural analogy.

Scheme 3

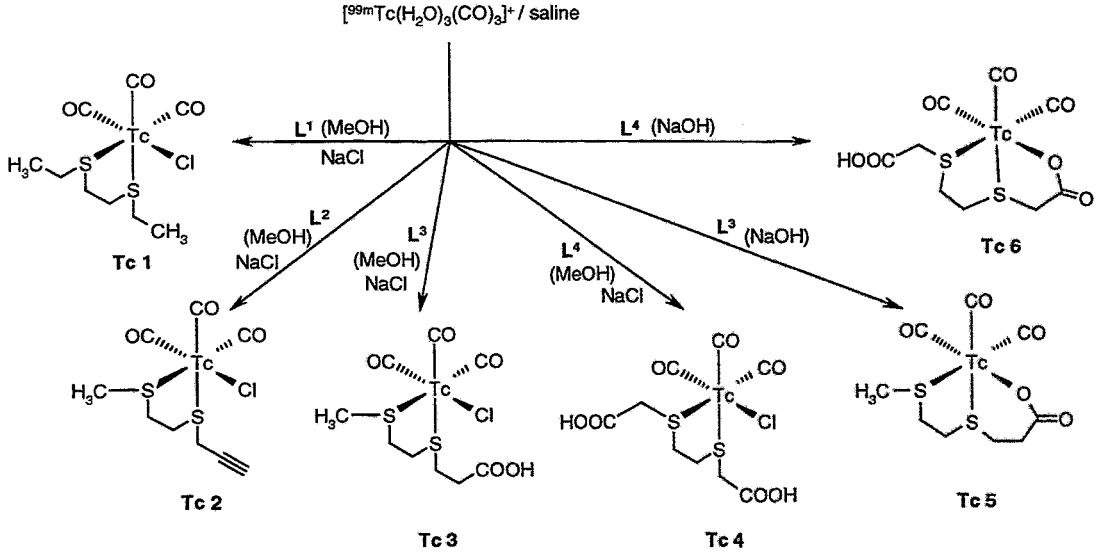

The behaviour of the chlorine containing ^{99m}Tc complex **Tc1** in aqueous solution at physiological pH value was investigated. In saline the chromatographically separated compound was stable for at least 120 min. However, in chloride free aqueous solution a water-coordinated cationic species **Tc1a** occured (Scheme 4 and Fig. 4).

Scheme 4

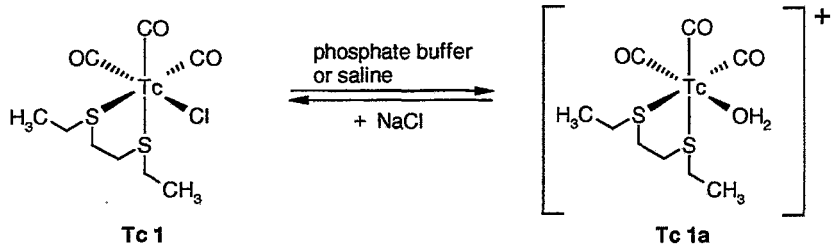

Tc 1 **Tc 1a**

The cationic charge of the conversion product **Tc1a** was confirmed by capillary and paper electrophoresis (Fig. 5).

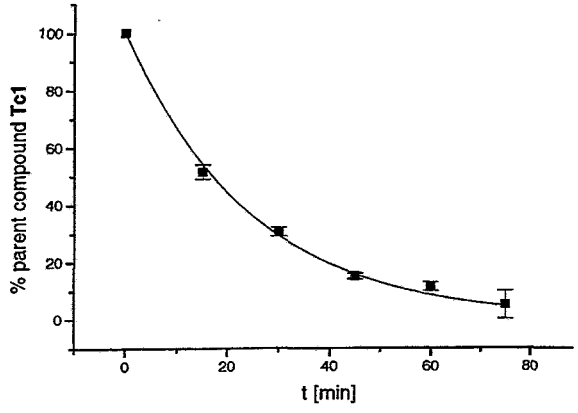

Fig 4. Time course of conversion of the complex **Tc1** into the complex **Tc1a** in a solution of 45 % H_2O/45 %MeOH/10 % propylene glycol

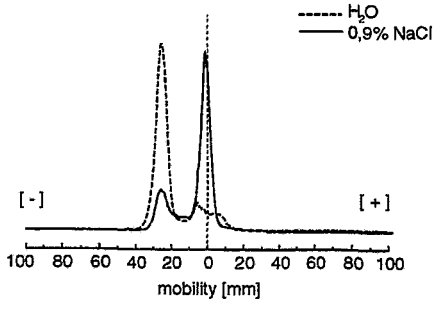

Fig. 5. Mobility of **Tc1a** in the electrical field (paper electrophoresis)

By the introduction of a carboxylic group into the thioether ligand as a third donor group the conversion is suppressed and thus the neutrality of the complex preserved. So, **Tc5** and **Tc6** with a coordinated carboxylic group were stable in all investigated solutions at least for 120 min. Capillary electrophoretical studies of the complex couple **Tc3/Tc5** support the assumption that the chloride ligand in the abovely described complexes of the general formula [^{99m}TcCl(CO)$_3$L] is responsible for their reactivity in aqueous solution. **Tc3** was found to be an anionic species in the pH range of 9.3 - 7.0 and a neutral one at pH 2.5 indicating the protonation of the free carboxylic group. **Tc5** is a neutral species over the whole pH range showing the same migration time as the neutral marker acetone.

Glutathione challenge experiments

Glutathione (GSH), the most abundant thiol compound in tissues, is present in almost all animal cells in relatively high concentrations (0.5 mM to 12 mM). Therefore it has to be considered as a potential agent for transchelating reactions *in vivo*. In fact, GSH is responsible for the *in vivo* reactivity of so-called "3+1" mixed-ligand ^{99m}Tc(V) complexes which consist of a monodentate thiol ligand and a tridentate dithiol. In view of these experience it would be useful to explore also the behaviour of ^{99m}Tc(I) thioether carbonyl complexes against GSH ligand exchange reactions although the difference in the oxidation state (+1 versus +5) does not predispose these complexes for such a ligand exchange.

Saline containing preparations of the ^{99m}Tc compounds were diluted with a 10 mM GSH solution immediately after HPLC purification. In all cases no additional peaks, indicating Tc-GSH mixed ligand species, were observed in HPLC studies. In contrast, addition of a 10 mM GSH solution to chlorine-free preparations of **Tc1** and **Tc2** led to the cationic species characterized above.

These results clearly indicate that glutathione has no negative effect on the stability of ^{99m}Tc thioether carbonyl complexes in solutions. Obviously, no transchelation reaction by GSH occurs *in vivo*. This behaviour is considered to be an advantage of the ^{99m}Tc thioether carbonyl complexes over mixed-ligand ^{99m}Tc oxocomplexes in the oxidation state +5 [7].

Biodistribution studies in rats

The biodistribution of the complexes **Tc1**, **Tc2**, **Tc5** and **Tc6** in the rat were studied. All four compounds show similar radioactivity in blood at 5 min. p.i., which thereafter decreases within 120 min to a similar extent, except for anionic **Tc6** with its fast clearance (Table 1).

Complexes **Tc1** and **Tc2** showed significant initial brain uptake (1,03± 0.25 and 0.78± 0.08 % ID/organ at 5 min. p.i.). This is consistent with the absence of charge of the complexes and their low molecular weight but astonishing in so far as the octanol/water partition coefficients are as low as log P = 0.9 for **Tc1** and log P = 0.7 for **Tc2**. The complex **Tc5**, which is also neutral but more hydrophilic (log P = 0.4), and the anionic complex **Tc6** (log P= -1.8) exhibit only low brain uptake.

Table 1. Biodistribution data of complexes **Tc1**, **Tc2**, **Tc5** and **Tc6** in male Wistar rats

Complex	Time p.i. [min]	Blood [% ID/g]	Brain	Heart	Lungs [% ID]	Kidneys	Liver
Tc1	5	1.01± 0.30	1.03± 0.25	0.65± 0.09	9.19± 1.82	5.58± 0.57	23.44± 3.82
	120	0.71± 0.14	0.55± 0.08	0.45± 0.03	12.12± 1.41	5.06± 0.55	29.54± 3.24
Tc2	5	0.92± 0.03	0.78± 0.08	0.53± 0.05	21.57± 3.01	4.83± 0.30	24.35± 2.13
	120	0.63± 0.06	0.55± 0.07	0.40± 0.03	24.97± 1.69	4.66± 0.54	27.18± 2.58
Tc5	5	1.09± 0.25	0.07± 0.01	0.56± 0.10	1.46± 0.26	6.19± 0.53	25.01± 2.32
	120	0.62± 0.06	0.05± 0.01	0.30± 0.04	0.97± 0.07	4.56± 0.64	32.37± 1.04
Tc6	5	0.91± 0.07	0.09± 0.01	0.15± 0.02	0.70± 0.17	8.50± 1.09	15.58± 1.30
	120	0.25± 0.02	<0.05	<0.05	0.14± 0.01	1.39± 0.06	4.72 ± 0.35

References

[1] Alberto R., Schibli R., Egli A., Schubiger P. A., Herrmann W. A., Artus G., Abram U. and Kaden T. A. (1995) Metal carbonyl syntheses XXII. Low pressure carbonylation of $[MOCl_4]^-$ and $[MO_4]^-$: The Tc(I) and Re(I) compexes $[NEt_4]_2[MCl_3(CO)_3]$. *J. Organomet. Chem.* **493**, 119-127.

[2] Alberto R. (1996) High- and low-valency organometallic compounds of technetium and rhenium. *Topics in Current Chemistry*, Springer-Verl., Berlin, Heidelberg vol. **176**, 149-187.

[3] Egli A.; Hegetschweiler K.; Alberto R.; Abram U.; Schibli R.; Hedinger R.; Gramlich V., Kissner R. and Schubiger P. A. (1997) Hydrolysis of the organometallic aqua ion fac- triaquatricarbonylrhenium(I). Mechanism, pK(a), and formation constants of the polynuclear hydrolysis products. *Organometallics* **16**, 1833-1840.

[4] Alberto R., Schibli R., Abram U., Egli A., Knapp F. F. and Schubiger P. A. (1997) Potential of the "$[M(CO)_3]^{+n}$" (M = Re, Tc) moiety for the labeling of biomolecules. *Radiochim. Acta* **7**, 999-103.

[5] Alberto R., Schibli R., Angst D., Schubiger P. A., Abram U., Abram S. and Kaden T. A. (1997) Application of technetium and rhenium carbonyl chemistry to nuclear medicine. *Trans. Met Chem.* **22**, 597-601.

[6] Schibli R., Alberto R., Abram U., Abram S., Egli A., Schubiger P. A. and Kaden T. A. (1998) Structural and Tc-99 NMR investigations of complexes with fac-$[Tc(CO)_3]^+$ moieties and macrocyclic thioethers of various ring sizes: Synthesis and X-ray structure of the complexes fac-[Tc(9-ane-S-3)$(CO)_3$]Br, fac-$[Tc_2(tosylate)_2(18\text{-ane-S-6})(CO)_6]$, and fac-$[Tc_2(20\text{-ane-S-6-OH})(CO)_6]$-$[tosylate]_2$. *Inorg. Chem.* **37**, 3509-3516.

[7] Syhre R., Seifert S., Spies H., Gupta A. and Johannsen B. (1998) Stability versus reactivity of "3+1" mixed-ligand technetium-99m complexes in vitro and in vivo. *Eur. J. Nucl. Med.* **25**, 793-796.

26. Studies on Tc Complexes Derived from Etomidate

B. Noll, M. Netter[1], St. Noll, H.-J. Pietzsch, R. Syhre, H. Spies, I. Zolle[1]
[1]Universität Wien

Etomidate (**1**), the ethyl ester of (+)-1-(1-phenylethyl)-imidazole-5-carboxylic acid (**2**), was known as inhibitor of 11β-hydroxylase activity in the adrenal cortex [1].

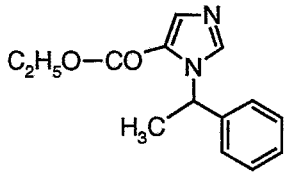

Fig. 1. (+)-1-(1-Phenylethyl)-imidazol-5-carboxylic acid ethyl ester (etomidate)

Bergström *et al.* [2] demonstrated in vitro and in animals that the ^{11}C-labelled methyl ester of **2** is an excellent tool for the identification of 11β-hydroxylase in the adrenal cortex and in adrenal cortical tumours.
Here we describe attempts to combine the (+)-1-(1-phenylethyl)-imidazole-5-carboxylic acid moiety with various Tc/Re chelators in order to see whether the appropriate ^{99m}Tc complexes are suitable for inhibiting 11β-hydroxylase activity despite considerable changes in the etomidate molecule and may therefore have the potential for imaging the adrenals.
Since the charge of the metal complexes with etomidate derivatives plays an essential role in the distribution in the organism, various complex types with rhenium and technetium at the oxidation states +5 and +1 leading to neutral and charged complexes were investigated. To make it possible for **2** to bind to the metal, etomidate had to be derivatized. For this purpose a spacer was introduced with either a mercapto group (3+1 approach) [3], a dithioether donor group that can act as a bidentate ligand, or a tetradentate ligand. These groups were coupled by a peptide bond. The following methods of complex formation of the etomidate derivatives with ^{99m}Tc were used:

a) ^{99m}Tc complexes according to the "3+1" approach with etomidate functionalized by a mercapto group acting as a monodentate ligand. With HS-CH_2-CH_2-N(CH_3)-CH_2-CH_2-SH as a tridentate ligand and ^{99m}Tc gluconate as a precursor, a neutral oxotechnetium(V) complex **3** was formed (Fig. 2).

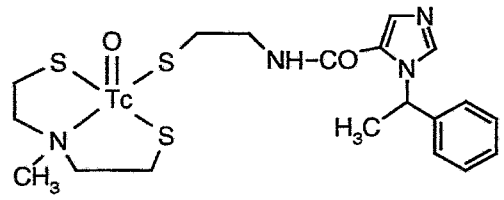

Fig. 2. ^{99m}Tc complex **3** according to the "3+1" principle at oxidation state +5.

b) An anionic ^{99m}Tc complex **4** at oxidation state +5 was formed with the tetradentate MALYG ligand [4] and ^{99m}Tc gluconate as a precursor. The pendant amino group of MALYG (N-mercaptoacetyl-lysyl-glycine) was coupled to etomidate by a peptide bond.

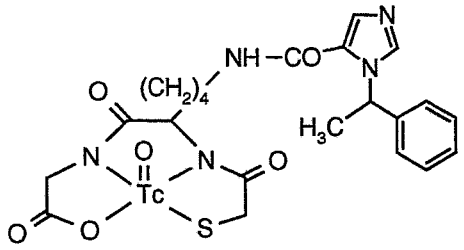

Fig. 3. ^{99m}Tc complex **4** with the MALYG-functionalized etomidate
(MALYG = mercaptoacetyl-lysyl-glycin)

c) A ^{99m}Tc complex **5** with a "$Tc(CO)_3$" moiety at oxidation state +1 was formed with **2** functionalized by a bifunctional thioether ligand and $[TcCl_3(CO)_3]^{2-}$ as a precursor.

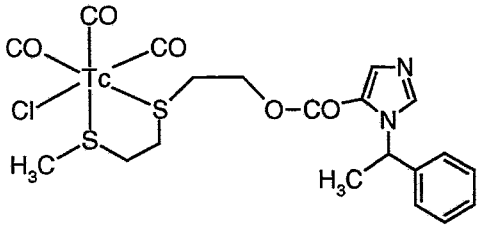

Fig. 4. ^{99m}Tc thioether-functionalized etomidate carbonyl complex **5**

The ^{99m}Tc complexes are purified by RP-HPLC and their biological behaviour is studied in rats. As shown in Table 1 only a rather low accumulation of activity in the adrenal cortex was obtained. Nevertheless a difference was observed between the ^{99m}Tc complex with the MALYG-functionalized etomidate (**4**), the ^{99m}Tc(I) thioether-functionalized etomidate carbonyl (**5**) and the ^{99m}Tc complex according to the "3+1" principle (**3**). The Tc(I) complex and the ^{99m}Tc complex according to the "3+1" principle show about a 10 times higher accumulation than the ^{99m}Tc complex with the MALYG-functionalized etomidate. Most likely, the negative charge of this complex is responsible for this behaviour. The Tc(I) complex shows a remarkably low uptake in the blood.

In summary, investigations with further ^{99m}Tc complexes are required to decide whether they have some potential for being significantly accumulated in the adrenals or whether the change in the etomidate molecule by the chelate is accompanied by a complete loss of biological activity.

Table 1. Biodistribution of ^{99m}Tc etomidate complexes in 5 - 6 weeks old male Wistar rats (means ± SD, n = 6)

Complex	Time p.i. [min]	Adrenals	Kidneys	Brain	Heart	Lungs	Liver
				[% ID]			
4	5	0.015 ± 0.003	17.0 ± 0.6	0.04 ± 0.01	0.18 ± 0.09	0.60 ± 0.18	12.1 ± 2.4
	60	0.004 ± 0.001	7.9 ± 0.5	0.01 ± 0.01	0.04 ± 0.01	0.10 ± 0.03	1.2 ± 0.6
5	5	0.143 ± 0.049	7.4 ± 0.9	0.10 ± 0.02	0.70 ± 0.07	1.56 ± 0.34	33.3 ± 3.1
	60	0.062 ± 0.029	6.3 ± 0.6	0.07 ± 0.01	0.46 ± 0.05	1.17 ± 0.20	44.2 ± 3.2
3	5	0.182 ± 0.008	3.6 ± 0.2	0.05 ± 0.00	0.34 ± 0.00	0.93 ± 0.18	39.1 ± 1.2
	60	0.034 ± 0.003	2.5 ± 0.4	0.02 ± 0.00	0.09 ± 0.03	0.41 ± 0.04	36.9 ± 0.3

		Blood	Adrenals	Kidneys
			[% ID/g]	
4	5	0.54 ± 0.20	0.34 ± 0.08	12.9 ± 1.9
	60	0.12 ± 0.06	0.09 ± 0.01	6.1 ± 0.3
5	5	1.29 ± 0.41	3.37 ± 0,81	4.2 ± 0.9
	60	0.94 ± 0.36	1.52 ± 0.42	3.5 ± 0.9
3	5	0.65 ± 0.08	2.57 ± 0.13	2.9 ± 0.4
	60	0.28 ± 0.04	0.49 ± 0.04	1.5 ± 0.1

References

[1] Vanden Bossche H., Willemsens G., Cools W. and Bellens D. (1984) Effects of etomidate on steroid biosynthesis in subcellular fractions of bovine adrenals. *Biochem. Pharmacol.* **33**, 3861-3868.

[2] Bergström M., Bonasera T. A., Lu L., Bergström M., Sundin A., Juhlin C.and Langström B. (1997) *In vitro and in vivo primate evaluation of carbon-11-etomidate and carbon-11-metomidate as potential tracers for PET imaging of the adrenal cortex and its tumors.* *J. Nucl. Med.* **39**, 982-989.

[3] Pietzsch H.-J., Spies H. and Hoffmann S. (1989) Lipophilic Tc complexes. VI.Neutral Tc(V) complexes with tridentate dithiole/monothiole ligand coordination. *Inorg. Chim. Acta* **165**, 163-166.

[4] Noll St., Noll B., Spies H., Zolle I. and Johannsen B. (1997) Mercaptoacetyllysylglycine (MALYG), a new ligand for coupling technetium and rhenium to biomolecules. *Annual Report 1997,* Institute of Bioinorganic and Radiopharmaceutical Chemistry, FZR-200, pp. 82-84.

[5] Pietzsch H.-J., Reisgys M., Alberto R., Hoepping A., Scheunemann M., Seifert S., Wüst F., Spies H., Schubiger P. A. and Johannsen B. (1999) Thioether ligands as anchor groups for coupling the "$Tc(CO)_3$" and "$Re(CO)_3$" moieties with biologically active molecules. In: *Technetium and Rhenium in Chemistry and Nuclear Medicine* **5** (M. Nicolini, U. Mazzi Eds.) SGEditoriali, Padova, pp.313-316.

27. Basicity of Amine Group Containing "3+1" Re Complexes Studied by HPLC

R. Berger, M. Friebe, M. Glaser, H.-J. Pietzsch, T. Maina[1], E. Chiotellis[1], H. Spies
[1]Institute of Radioisotopes - Radiodiagnostic Products, National Centre for Scientific Research "Demokritos", Athens, Greece

The basicity (expressed by the pK_a values) of protonable amine group containing Re complexes depends on the position of the amine function and on the nature of substituents which the nitrogen atom bears. Here we compare the pH-dependent acid-base behaviour of four types of "3+1" Re complexes (Fig. 1). Types **1** and **2** include complexes having pendent amine groups attached either to the monodentate or the tridentate ligand, whereas the amine group as part of the tridentate ligand SNN (type **3**) or SNS (type **4**) is assumed to be involved in coordination to the metal.

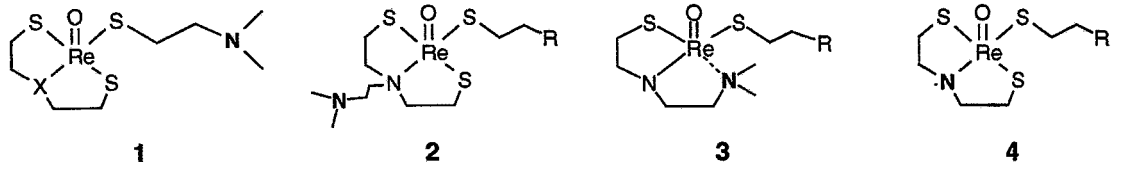

Fig. 1. Types 1 - 4 of amine-group-containing Re complexes
[X = N, O, S; R = alkyl and/or aryl residue]

The pK_a values of these compounds derive from turning points in lipophilicity/pH profiles determined by HPLC. The measured values are corrected ($pK_{a(c)}$) with the aid of a calibration curve based on some amines with known pK_a values as standards [1].

Neutral "3+1" complexes having a pendent amine group behave as amines, which is reflected in the pH dependence of the partition coefficient [2, 3]. Some $pK_{a(c)}$ values of structure-related Re/Tc(=M) "3+1" complexes (type **1**) with diethylamine, piperidine and morpholine in the monodentate chelate part are compiled in Table 1. For these complexes, in which the amine group is attached to the monodentate thiolate ligand, turning points between the protonated and unprotonated forms were found at about 7 - 10. Compared with the free amines, the basicity of the amine group of the complexes is shifted to lower pK_a values at about 1 to 2 units. The difference in basicity between diethylamine/piperidine and morpholine is reflected in the corresponding complexes. The influence of the neutral donor group X on $pK_{a(c)}$ is relatively small and is in the sequence S < O < N.

Table 1. Some $pK_{a(c)}$ values [1]) of structure-related Re/Tc(=M) "3+1" complexes with diethylamine, piperidine and morpholine structural moieties

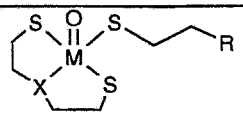

R	Amine [2]) (RH)	X				
		N-Met	N-Et	N-But	O	S
N-(Ethyl)$_2$	10.49	9.74	9.54	9.84	9.69	9.58
Piperidyl	11.12	9.48	9.42	9.64	9.24	9.12
Morpholinyl	8.33	7.16	7.21	7.42	7.24	7.22

[1]) mean values of refering Tc and Re complexes, [2]) pK_a values from [4]

However, basicity decreases further in complexes of the type **2**, in which the amine group is located at the N-atom coordinated with the tridentate ligand [5]. An example is given in Table 2. This change is due to the electron-withdrawing effect of the coordinated nitrogen atom of the tridentate ligand.
In complexes of types **3** and **4** the amine group is formally part of the coordination sphere.
A group of "3+1" mixed-ligand Re complexes in which the tridentate ligand has an SN^1N^2 donor set (N^2 = diethylamine or pyrrolidinyl) (type **3** complexes) was recently described by Chiotellis *et al.* [6]. Three representatives were measured and are of the same order as observed for complexes **2**, which have non-coordinated amine groups. As shown below for compound **4**, the coordinated amine group refuses to be protonated under the conditions used. It is therefore difficult to reconcile the $pK_{a(c)}$ values found for **3** with the formulation of a coordination of the N^2 amine group. However, when we assume the amine group to be free, what then is coordinated at the remaining unpossessed coordination site? This question has yet to be answered.
Compounds of type **3** have to be studied further because of their unexpected behaviour.

Table 2. Comparison of the $pK_{a(c)}$ values of type **1**, **2**, **3** complexes (diethylamine derivatives)

Type	Structure	$pK_{a(c)}$
1	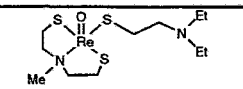	9.78
2	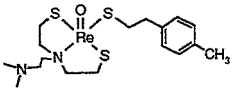	8.34
3	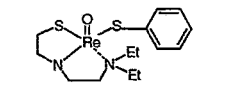	8.32
3	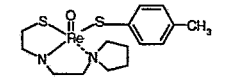	7.43
3	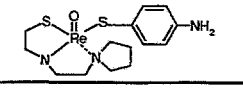	7.38

The neutral complex $[ReO(NH(CH_2CH_2S)_2)(SC_6H_5)]$ 4 was measured for comparison. The complex was formed as a result of a reaction between $[Re(O)(SPh)_4]^-$ and $N(CH_2CH_2SH)_3$ [7]. Unlike the compounds of types **1**, **2**, **3** discussed above, the complex is neutral at low pH and becomes negatively charged in an alkaline medium, thus showing a dissociation behaviour like an acid. The proton of the coordinated tridentate ligand obviously becomes acidic due to the N-Re coordination. The measured pK_{HPLC} value was corrected to $pK_{a(c)}$ by means of a calibration curve, using some organic acids as standards [8] (Fig. 2).

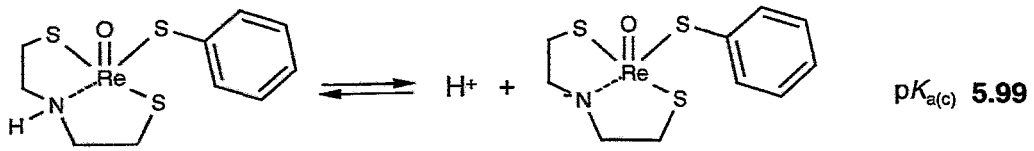

Type **4**

Fig. 2. Complex of type 4 (structure, dissociation, $pK_{a(c)}$ value)

To conclude, the nature and position of the amine group in Re/Tc complexes are tools for directing the basicity so as to either bring about a small decrease in basicity compared with that of the basic amines or to produce species of drastically reduced basicity. As the basicity of a tracer is an important property that governs its *in vivo* transport, a knowledge of structure-basicity relationships is essential in radiotracer design.

References

[1] Berger R., Scheunemann M., Pietzsch H.-J., Noll B., Noll St., Hoepping A., Glaser M., Fietz T., Spies H. and Johannsen B. (1995) pK_a value determinations by HPLC of some Tc and Re complexes containing an ionizable group. *Annual Report 1995*, Institute of Bioinorganic and Radiopharmaceutical Chemistry, FZR-122, pp. 73-79.

[2] Spies H., Syhre R. and Pietzsch H.-J. (1990) Radiopharmacological studies on technetium complexes with tridentate/monodentate thiole ligands. *Plzen. lek. Sborn.* **62**, 85-86.

[3] Friebe M., Spies H., Berger R., Syhre R., Papadopoulos M., Chiotellis E., Suda K., Wunderli-Allenspach H. and Johannsen B. (1999) Amine group bearing '3+1' oxotechnetium(V) and oxorhenium(V) complexes: Synthesis, characterization of lipophilicity and permeation through the blood-brain barrier. In: *Technetium, Rhenium and Other Metals in Chemistry and Nuclear Medicine* **5** (M. Nicolini, U. Mazzi Eds.), SGEditoriali, Padova, pp. 627-631.

[4] Lide D.R. ed. (1992-1993) *CRC Handbook of Chemistry and Physics*,. CRC Press, Tokyo, pp. 8-37.

[5] Papadopoulos M., Pirmettis I., Raptopoulou C., Chiotellis E., Friebe M., Berger R., Spies H., and Johannsen B. (1998) Synthesis, structure, lipophilicity and protonation behaviour of mixed ligand rhenium chelates functionalized by amine groups. *Appl. Radiat. Isot.* **49**, 961-965.

[6] Papadopoulos M., Tsoukalas C., Pirmettis I., Nock B., Maina T., Abedin Z., Raptopoulou C. P., Terzis A. and Chiotellis E. (1999) Synthesis and characterization of five-coordinate rhenium(V) and technetium(V) mixed ligand bifunctional complexes carrying the SNS/S or the SNN/S donor atom set. Crystal structure of ReO{[$(C_2H_5)_{(2)}$$NCH_2CH_2N(CH_2CH_2S)_{(2)}$]($P$-$H_2N$-PhS)} and ReO{[$(CH_2)_{(4)}$$NCH_2CH_2NCH_2CH_2S$]($P$-$H_2N$-PhS)}. *Inorg. Chim. Acta* **285**, 97-106.

[7] Glaser M., Spies H., Berger R., Hahn F. E., Lügger T. and Johannsen B. (1997) Unexpected formation of the new oxorhenium(V) complex [ReO($NH(CH_2CH_2S)(SC_6H_5)$)] obtained by N-C cleavage of the tripodal ligand $N(CH_2CH_2SH)_3$. *Inorg. Chim. Acta* **257**, 853-863.

[8] Berger R. and Spies H. (1998) Some additions to the determination of log P and pK_a values by using reversed phase HPLC. *Report January 1998 - June 1999*, Institute of Bioinorganic and Radiopharmaceutical Chemistry, FZR-270, pp. 194-197.

28. Interactions of Medicinally and Biologically Relevant Anions with Photo- and pH-Responsive Dendrimers

H. Stephan, H. Spies, B. Johannsen, C. Kauffmann[1], F. Vögtle[1]
[1]Kekulé-Institut für Organische Chemie und Biochemie, Universität Bonn

Introduction

Dendrimer chemistry is a rapidly expanding field for both fundamental studies and applications [1 - 5]. Their unique structural features and properties make them ideally suited for use in diagnostic imaging and therapy [5 - 13], transfection [14 - 22], and drug delivery [23 - 34]. We are especially interested in the efficient binding and controlled release of anionic substrates with dendrimers tailored [35].

In this paper we report the binding behaviour of dendrimers having the photo- and pH-switchable units azobenzene and methyl orange at the periphery towards pertechnetate, and the nucleotides AMP, ADP and ATP. Liquid-liquid partition of $^{99}TcO_4^-$ and ^{14}C-labelled nucleotides in a $CHCl_3$/aqueous buffer system was chosen to characterize the binding properties of dendrimers.

Experimental

All chemicals were reagent grade and used as obtained. Dendrimers **1** and **2** (generation 3) were obtained by reaction of poly(propylene imine)-dendrimer-$(NH_2)_{16}$ with 4-(phenylazo)benzoic acid chloride, and 4-(p-[dimethylamino]phenylazo)benzenesulfonic acid chloride, respectively.

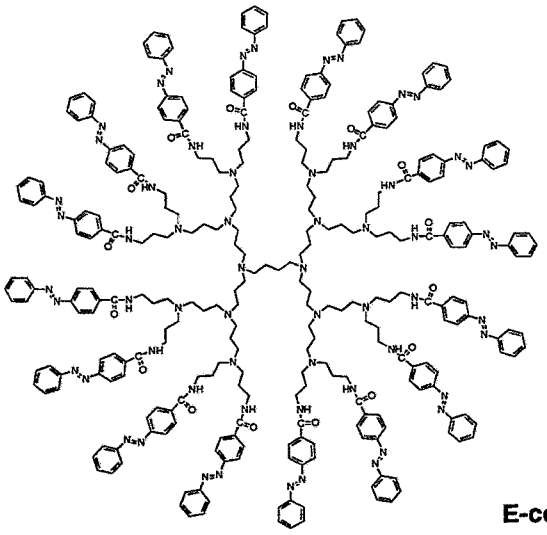

E-configuration

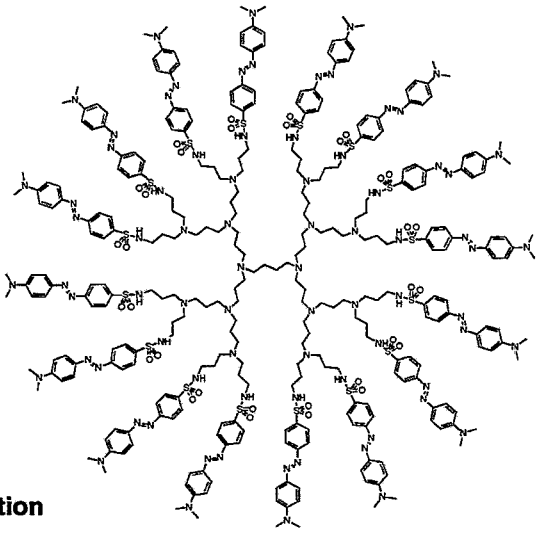

1 **2**

The extraction studies were performed at 25 ± 1°C in 2 ml micro centrifuge tubes by mechanical shaking. The phase ratio $V_{(org)}$:$V_{(w)}$ was 1:1 (0.5 ml each); the shaking period was 30 min. The extraction equilibrium was achieved during this period. All samples were centrifuged after extraction. The anion concentration in both phases was determined radiometrically using the β-radiation measurements of $^{99}TcO_4^-$ (Amersham), and ^{14}C-labelled nucleotides (NEN Life Science Products) in a liquid scintillation counter (LS 6000 LL, Beckman). The aqueous solution was adjusted using 0.05 M NaOAc/HCl- (pH 2,0...5.5), 4-morpholinoethanesulphonic acid (MES)/NaOH- (5,4...6.5) and 4-(2-hydroxyethyl)-piperazine-1-ethanesulphonic acid (HEPES)/NaOH-buffer (7.0...8.0).

Results and Discussion

The investigations performed show that the dendrimers **1** and **2** are capable of extracting especially the oxyanions pertechnetate and ATP even at very low concentration of dendrimer ($c_{1,2} = 1 \cdot 10^{-4}$ M in $CHCl_3$). As expected the efficacy is enhanced with decreasing pH caused by increasing protonation of dendrimers. Further experiments revealed a clear dendritic effect and consequently pertechnetate may quantitatively transferred into the organic phase using azobenzene and methyl orange functionalized dendrimers of generation 5 at physiological pH [36]. Especially dendrimer **2** having methyl orange units at the periphery show an unique phase transfer behaviour with respect to pH changes. For extraction of pertechnetate we found that the organic phase is entirely discoloured accompanying by formation of a reddish brown flocky precipitation at the aqueous phase in the pH range of 2.0 to 4.5 (cf. Fig. 2). This finding points to a strong interaction of the positively charged dendrimer periphery with pertechnetate anions. Further increase of pH leads to the formation of a lipophilic complex of dendrimer **2** with pertechnetate which is completely soluble in $CHCl_3$. Obviously the pertechnetate anion migrates into the inside of the dendrimer. So, TcO_4^- is bound by tertiary amine groups of the core, and the anion is shielded by the hydrophobic periphery. A controlled release of pertechnetate from the dendrimer is be achieved by graduated deprotonation of these amino groups. A very interesting property of the dendrimers investigated is the possibility to alter the structure by photoisomerization. It could be shown that the E form of azobenzene-functionalized dendrimers can be reversibly switched to their Z form by light excitation [37]. As expected encapsulated species like the dianion eosin can be stronger shielded from the environment by the Z form. Investigations about the controlled inclusion and release of pertechnetate with methyl orange dendrimers by photoswitching are under way.

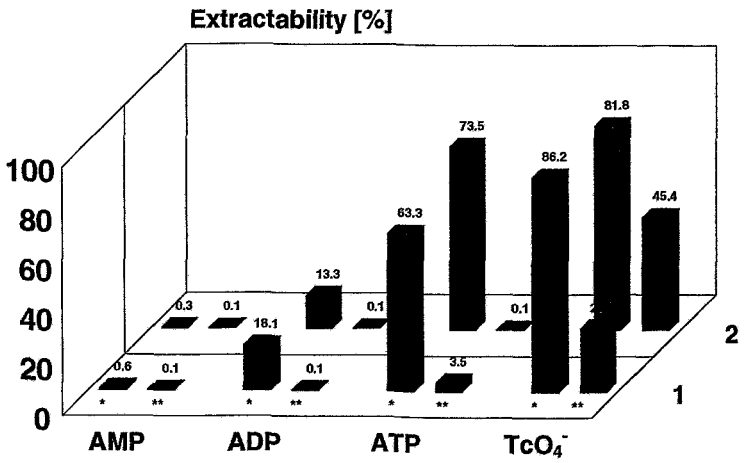

Fig. 1. Extractability of nucleotides and pertechnetate with dendrimers **1** and **2**
[nucleotide, $(KTcO_4)$] = $1 \cdot 10^{-4}$ M; [dendrimer] = $1 \cdot 10^{-4}$ M in $CHCl_3$
* pH = 5.4 (MES/NaOH buffer); ** pH = 7.4 (HEPES/NaOH buffer)

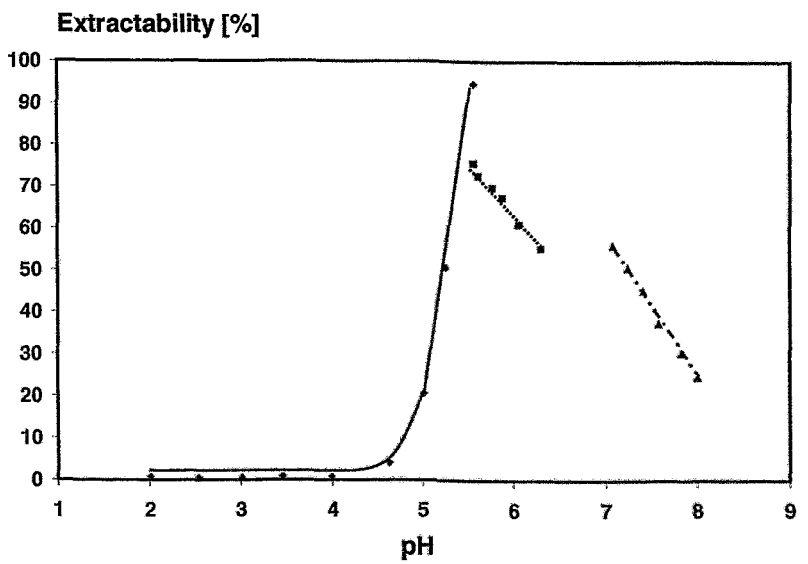

Fig. 2. Extractability of pertechnetate with dendrimer **2** as function of pH
[$KTcO_4$] = $1 \cdot 10^{-4}$ M; [2] = $1 \cdot 10^{-4}$ M in $CHCl_3$; pH = 2.0...5.5 (NaOAc/HCl buffer, ——)
pH = 5.4...6.5 (MES/NaOH buffer, ▪▪▪▪▪▪); pH = 7.0...8.0 (HEPES/NaOH buffer, — ▪ —)

References

[1] Fischer M. and Vögtle F. (1999) Dendrimere: vom Design zur Anwendung - ein Fortschrittsbericht. *Angew. Chem.* **111**, 934-955.

[2] Newkome G. R., Moorefield C. N. and Vögtle F. (1996) *Dendritic Molecules: Concepts, Syntheses, Perspectives*, VCH, Weinheim.

[3] Tomalia D. A., Naylor A. M. and Goddard III W. A. (1990) Starburst-Dendrimere: Kontrolle von Größe, Gestalt, Oberflächenchemie, Topologie und Flexibilität beim Übergang von Atomen zu makroskopischer Materie. *Angew. Chem.* **102**, 119-238.

[4] Kim Y. and Zimmermann S. C. (1998) Applications of dendrimers in bio-organic chemistry. *Curr. Opin. Chem. Biol.* **2**, 733-42.

[5] Bosman A. W., Janssen H. M. and Meijer, E. W. (1999) About dendrimers: Structure, physical properties, and applications. *Chem. Rev.* **99**, 1665-1688.

[6] Turunen M. P., Hiltunen M. O., Ruponen M., Virkamäki L., Szoka Jr. F. C., Urtti A. and Ylä-Herttuala S. (1999) Efficient adventitial gene delivery to rabbit carotid artery with cationic polymer-plasmid complexes. *Gene Ther.* **6**, 6-11.

[7] Orentas R. J., Rospkopf S. J., Casper J. T., Getts R. C. and Nilsen T. W. (1999) Detection of Epstein-Barr virus EBER sequence in post-transplant lymphoma patients with DNA dendrimers. *J. Virol. Methods* **77**, 153-63.

[8] Jang Y. H., Blanco M., Dasgupta S., Keire D. A., Shively J. E. and Goddard III W. A. (1999) Mechanism and energetics for complexation of Y-90 with 1,4,7, 10-tetraazacyclododecane-1,4,7,10-tetraacetic acid (DOTA), a model for cancer radioimmunotherapy. *J. Am. Chem. Soc.* **121**, 6142-6151.

[9] Prevote D., Donnadieu B., Moreno-Manas M., Caminade A. M. and Majoral J. P. (1999) Grafting of tetraazamacrocycles on the surface of phosphorus-containing dendrimers. *Eur. J. Org. Chem.* 1701-1708.

[10] Newkome G. R., Moorefield C. N., Keith J. M., Baker G. R. and Escamilla G. H. (1996) Chemische Umsetzungen im Inneren einer Vorstufe von unimolekularen Micellen: Bor-Supercluster durch ortsspezifische Addition von $B_{10}H_{14}$ an Kaskadenmoleküle. *Angew. Chem.* **106**, 701-03.

[11] Capala J., Barth R. F., Bendayan M., Lauzon M., Adams D. M., Soloway A. H., Fenstermacher R. A. and Carlsson J. (1996) Boronated epidermal growth factor as a potential targeting agent for boron neutron capture therapy of brain tumors. *Bioconjug. Chem.* **7**, 7.

[12] Service R. F. (1995) Dendrimers: Dream Molecules Approach Real Applications. *Science* **267**, 458-59.

[13] Wu C., Brechbiel M. W., Kozak R. W. and Gansow O. A. (1994) Metal-chelate-dendrimer-antibody constructs for use in radioimmunotherapy and imaging. *Bioorg. Med. Chem. Lett.* **4**, 449-454.

[14] Barth R. F., Adams D. M., Soloway A. H., Alam F. and Darby M. V. (1994) Boronated starburst dendrimer-monoclonal antiboby immunoconjugates: Evaluation as a potential delivery system for neutron capture therapy. *Bioconjug. Chem.* **5**, 58-66.

[15] Bielinska A. U., Chen C., Johnson J. and Baker Jr. J. R. (1999) DNA complexing with polyamidoamine dendrimers: implications for transfection. *Bioconjug. Chem.* **5**, 843-850.

[16] Kuhn P. S., Barbosa M. C. and Levin Y. (1999) Complexation of DNA with cationic surfactant. *Physica A* **269**, 278-284.

[17] Helin V., Gottikh M., Mishal Z., Subra F., Malvy C. and Lavignon M. (1999) Cell cycledependent distribution and specific inhibitory effect of vectorized antisense oligonucleotide in cell culture. *Biochem. Pharmacol.* **58**, 95-107.

[18] Bielinska A. U., Kukowska-Latallo J. F. and Baker Jr. J. R. (1997) The interaction of plasmid DNA with polyamidoamine dendrimers: mechanism of complex formation and analysis of alterations induced in nuclease sensitivity and transcriptional activity of the complexed DNA, *Biochim. Biophys. Acta* **1353**, 180-190.

[19] Hughes J. A., Aronsohn A. I., Avrutskaya A. V. and Juliano R. L. (1996) Evaluation of adjuvants that enhance the effectiveness of antisense oligodexynucleotides. *Pharm. Res.* **13**, 404-10.

[20] Bielinska A. U., Kukowska-Latallo J. F., Johnson J., Tomalia D. A. and Baker Jr. J. R. (1996) Regulation of in vitro gene expression using antisense oligonucleotides or antisense expression plasmids transfected using starburst PAMAM dendrimers. *Nucleic Acids Res.* **24**, 176-82.

[21] Tang M. X., Redemann C. T. and Szoka Jr. F. C. (1996) In vitro gene delivery by degraded polyamidoamine dendrimers. *Bioconjug. Chem.* **7**, 703-714.

[22] Kukowska-Latallo J. F., Bielinska A. U., Johnson J., Spindler R., Tomalia D. A. and Baker Jr. J. R. (1996) Efficient transfer of genetic material into mammalian cells using starburst polyamidoamine dendrimers. *Proc. Natl. Acad. Sci.* USA **93**, 4897-4902.
[23] Haensler J. and Szoka Jr. F. C. (1993) Polyamidoamine cascade polymers mediate efficient transfection of cells in culture. *Bioconjug. Chem.* **4**, 372-379.
[24] Jansen J. F. G. A., Meijer E. W. and De Brabander-van den Berg E. M. M. (1995) The dendritic box: Shape-selective liberation of encapsulated guests. *J. Am. Chem. Soc.* **117**, 4417-18.
[25] Poxon S. W., Liang P. M. and Hughes J. A. (1996) Dendrimer delivery of oligonucleotide. *Drug Delivery* **3**, 255-261.
[26] Sakthivel T., Toth I., and Florence A. T. (1998) Synthesis and physiochemical properties of lipophilic polyamide dendrimers. *Pharm. Res.* **15**, 776-782.
[27] Grayson S. M., Jayaraman M. and Fréchet J. M. J. (1999) Convergent synthesis and 'surface' functionalization of a dendritic analog of poly(ethylene glycol). *Chem. Commun.* 1329-1330.
[28] Liu M. J. and Fréchet J. M. J. (1999) Designing dendrimers for drug delivery. *Pharm. Sci. Technol. Today* **10**, 393-401.
[29] Liu M. J., Kono K. and Fréchet J. M. J. (1999) Water-soluble dendrimer-poly(ethylene glycol) starlike conjugates as potential drug carriers. *J. Polym. Sci. Part a – Polym. Chem.* **37**, 3492-3503.
[30] Kim Y., Zeng F. W. and Zimmerman S. C. (1999) Peptide dendrimers from natural amino acids. *Chem. Eur. J.* **5**, 2133-2138.
[31] Twyman L. J., Beezer A. E., Esfand R., Hardy M. J. and Mitchell, J. C. (1999) The synthesis of water soluble dendrimers, and their application as possible drug delivery systems. *Tetrahedron Lett.* **40**, 1743-1746.
[32] Zhuo R. X., Du B. and Lu Z. R. (1999) In vitro release of 5-fluorouracil with cyclic core dendritic polymer. *J. Control. Release* **57**, 249-257.
[33] Sakthivel T., Toth I. and Florence A. T. (1998) Synthesis and physiochemical properties of lipophilic polyamide dendrimers. *Pharm. Res.* **15**, 776-782.
[34] Jagur-Grodzinski J. (1999) Biomedical application of functional polymers. *React. Funct. Polym.* **2**, 99-138.
[35] Stephan H., Spies H., Johannsen B., Klein L. and Vögtle F. (1999) Lipophilic urea-functionalized dendrimers as efficient carriers for oxyanions. *Chem. Commun.* 1875-1876.
[36] Stephan H., Spies H., Johannsen B., Gestermann S., Gorka M., Hesse R., Kauffmann C., Klein L. and Vögtle F. (1999) Interactions of medicinally and biologically relevant anions with functionalized dendrimers. *Proc. 1st Int. Dendrimer Symp. (Frankfurt/Main)* 85-86.
[37] Archut A., Azzellini G. C., Balzani V., De Cola L. and Vögtle F. (1998) Toward photoswitchable dendritic hosts. Interaction between azobenzene-functionalized dendrimers and eosin. *J. Am. Chem. Soc.* **120**, 12187-12191.

29. Binding of Pertechnetate by Novel Scorpion-Like Macrocyclic Phosphonium Hosts

H. Stephan, H. Spies, B. Johannsen, J. Gläser[1], E. Vogel[1], F. Vögtle[1]
[1]Kekulé-Institut für Organische Chemie und Biochemie, Universität Bonn

Introduction

Due to their unique complexing properties macrocyclic compounds like crown ethers, cryptands and calixarenes win increasing importance for effective and selective binding of technetium(VII) species [1 - 6]. Thus, pertechnetic acid may be directly bound in acidic milieu by macrocycles. On the neutral and alkaline-side ion pairing of metal cations complexed with pertechnetate anion dominates. Recently, the cooperative sodium cation - pertechnetate anion binding was realised using a tripodal tris(amido benzo-15-crown-5) ligand [6]. Knowing the exciting anion binding properties of macrocyclic tetralactams [7] we are especially interested to design a pertechnetate host on the basis of such structure. The present short paper outlines our concept and we report the first results on binding of pertechnetate with scorpion-like phosphonium salts using solvent extraction studies. As can be seen from Fig. 1 the tetrahedral anion pertechnetate may be stabilised in the tetralactam cavity via hydrogen bonds. The charge should be compensated by the phosphonium spine. The phosphonium moiety was chosen owing to their suitable synthetic handling. Furthermore phosphonium salts are known as extractants for pertechnetate [8-10].

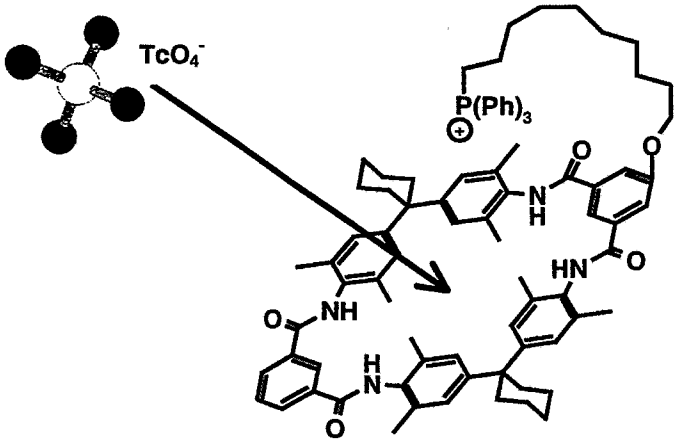

Fig. 1. Conceptual design of a scorpion-like macrocyclic phosphonium host for pertechnetate

Experimental

All chemicals were reagent grade and used as obtained. Macrocycles **1a** and **2a** were synthesized as described earlier [11, 12]. Compound **1b** and **2b** were obtained by reaction of hydroxy-functionalized **1a** and **2a**, resp., with diiododecan and subsequent treatment with triphenylphosphine. The iodide salts isolated were converted into the chlorides using anion exchange with serdolit AS-1 (Serva).

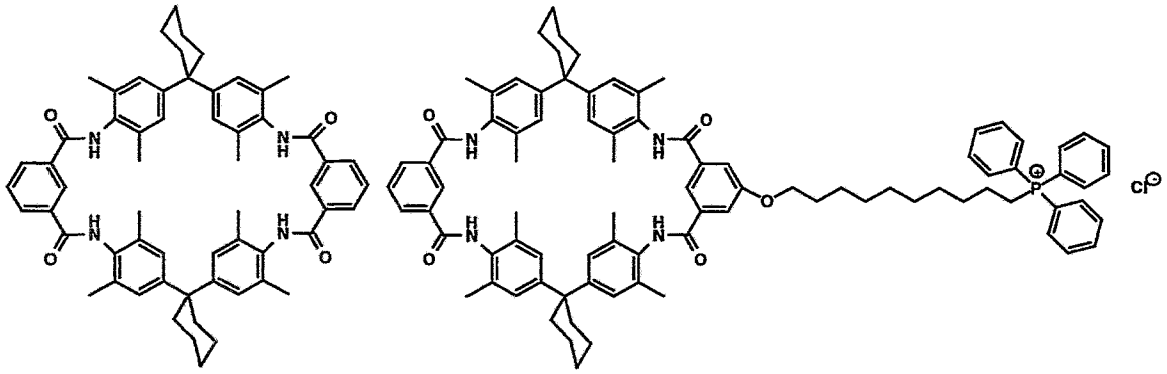

1a **1b**

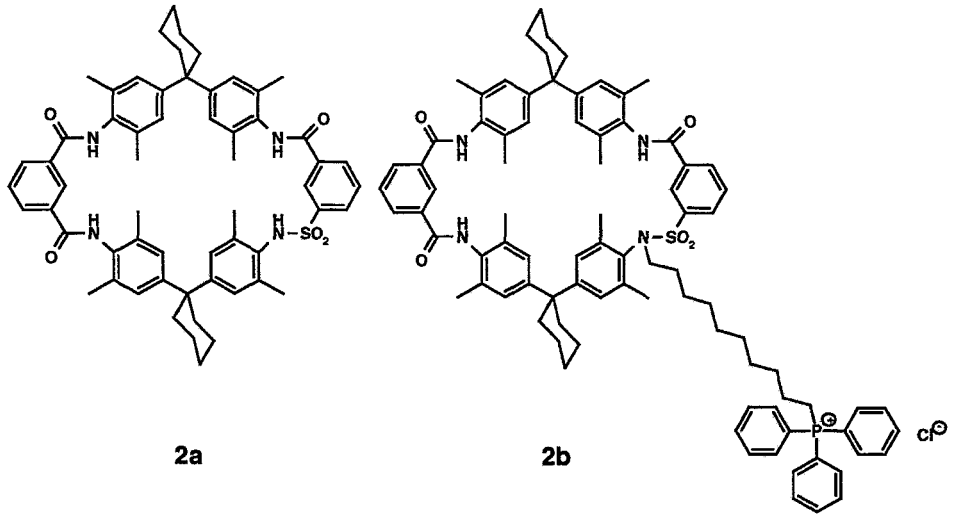

2a **2b**

The extraction studies were performed at 25 ± 1°C in 2 ml micro centrifuge tubes by mechanical shaking. The phase ratio $V_{(org)}$:$V_{(w)}$ was 1:1 (0.5 ml each); the shaking period was 30 min. The extraction equilibrium was achieved during this period. All samples were centrifuged after extraction. The anion concentration in both phases was determined radiometrically using the β-radiation measurement of $^{99}TcO_4^-$ (Amersham) in a liquid scintillation counter (LS 6000 LL, Beckman). The aqueous solution was adjusted using 0.05 M 4-(2-hydroxyethyl)-piperazine-1-ethanesulphonic acid (HEPES)/NaOH-buffer (7.0...8.0).

Results and Discussion

Preliminary investigations showed that the tetralactams **1a** and **2a** are not able to transfer the anions chloride, bromide, iodide, acetate and pertechnetate from aqueous solution (pH = 7.4) into chloroform (c_{Ligand} = $1 \cdot 10^{-3}$ M in $CHCl_3$). At higher ligand concentration weak interaction of **1a** and **2a** with pertechnetate was observed. Thus, **2a** (c_{ligand} = $5 \cdot 10^{-3}$ M in $CHCl_3$) extracts approximately 1 % TcO_4^-. A drastically increase of efficiency is obtained using the phosphonium-functionalized macrocycles **1b** and **2b**. Pertechnetate is quantitatively extracted at higher ligand concentrations. The results, shown in Fig. 2, reveal a linear relationship between the technetium concentration and the ligand concentration. The data obtained with slopes of unity were consistent with preferential 1:1 complex formation of pertechnetate with these ligands. It is worth mentioning that compound **2a** gives the highest extraction constant (Log K_{ex} = 6.22) for anion exchanger published up to now [13]. But molecular modeling calculation using ZINDO/1 (Hyperchem 5.1) [14] show that some structural optimization of the host is necessary. The macrocyclic ring size is too large and consequently only one hydrogen bond between the pertechnetate anion and amide proton may be formed. Altogether, further improvement of binding strength for the pertechnetate anion is expected if the macrocyclic ring size decreases. Additional the pertechnetate anion should be fixed at the macrocycle using a positively charged clamp.

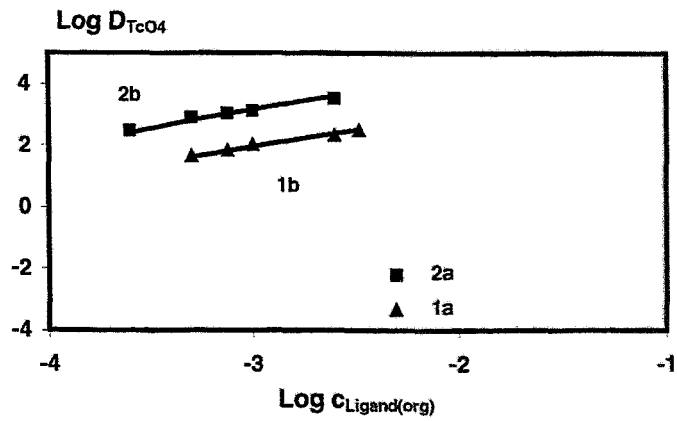

Fig. 2. Extraction of pertechnetate with ligands **1a**, **1b**, **2a** and **2b**

[$KTcO_4$] = $1 \cdot 10^{-4}$ M; pH = 7.4 (HEPES/NaOH buffer); [ligand] = $2.5 \cdot 10^{-4}$..$5 \cdot 10^{-3}$ M in $CHCl_3$ (points represent the experimental data; lines correspond to 1:1 complex formation)

References

[1] Jalhoom M. G. (1986) Extraction of pertechnetate ions by use of crown ethers from sulphuric acid solutions. *Radiochim. Acta* **39**, 195-97.

[2] Jalhoom M. G. (1986) Extraction of technetium by crown ethers and cryptants. *J. Radioanal. Nucl. Chem.* **104**, 131-40.

[3] Bonnesen P. V., Moyer B. A.., Presley D. J., Armstrong V. S., Haverlock T. J., Counce R. M. and Sachleben R. A. (1996) Alkaline-side extraction of technetium from tank waste using crown ethers and other extractants. *Oak Ridge National Laboratory (ORNL)-Report TM 13241.*

[4] Leonard R. A., Conner C., Liberatore M. W., Bonnesen P. V., Presley D. J., Moyer B. A. and Lumetta G. J. (1999) Developing and testing an alkaline-side solvent extraction process for technetium separation from tank waste. *Sep. Sci. Technol.* **34**, 1043-1068.

[5] Grunder M., Dozol J. F., Asfari Z. and Vicens J. (1999) Simultaneous removal of technetium and cesium by functionalized calixarenes from acidic liquid waste. *J. Radioanal. Nucl. Chem.* **241**, 59-67.

[6] Beer P. D., Hopkins P. K., McKinney J. D. ((1999) Cooperative halide, perrhenate anion-sodium cation binding and pertechnetate extraction and transport by novel tripodal tris(amido benzo-15-crown-5) ligand. *Chem. Commun.* 1253-1254.

[7] Hübner G. M., Gläser J., Seel C. and Vögtle F. (1999) Hocheffiziente Synthese von Rotaxanen mit einem anionischen Templat. *Angew. Chem.* **111**, 395-398.

[8] Bock R. and Jainz J. (1963) Verteilung der Tetraphenylphosphoniumverbindungen anorganischer Anionen zwischen wäßrigen Lösungen und Chloroform. *Z. Analyt. Chem.* **198**, 315-321.

[9] Tse P.-K. and Horwitz E. P. (1990) Alkyl and arylphosphonium nitrate salts as extractants for pertechnetate. *Solvent Extr. Ion Exch.* **8**, 353-360.

[10] Kopunec R., Abudeab F. N. and Skraskova S. (1998) Extraction of pertechnetate with tetraphenyl-phosphonium in the presence of various acids, salts and hydroxides. *J. Radioanal. Nucl. Chem.* **230**, 51-60.

[11] Ottens-Hildebrandt S., Schmidt T., Harren J. and Vögtle F. (1995) Sulphonamide-based catenanes – regioselective template synthesis. *Liebigs Ann.* 1855-1860.

[12] Jäger R. and Vögtle F. (1997) A new synthetic strategy towards molecules with mechanical bonds: nonoionic template synthesis of amide-linked catenanes and rotaxanes. *Angew. Chem. Int. Ed. Engl.* **36**, 930-944.

[13] Stephan H., Berger R., Spies H., Johannsen B. and Schmidtchen F. P. (1999) Efficient phase transfer of pertechnetate with bicyclic guanidinium compounds. *J. Radioanal. Nucl. Chem.* **242**, 399-403.

[14] HyperChem 5.1 (Hypercube; serial no. 500-10009099).

II. PUBLICATIONS, LECTURES, PATENTS AND AWARDS

PUBLICATIONS

Fietz T., Leibnitz P., Spies H., Johannsen B.
Synthesis and reactions of new oxorhenium(V) complexes with Re–halogen bonds. X–ray crystal structure of (3–(benzyl)azapentane-1.5-dithiolato)iodo oxorhenium(V).
Polyhedron **1999**, 18, 1793-1797.

Papadopoulos M., Pirmettis I., Tsoukalas C., Nock B., Maina T., Raptopoulou C. P., Pietzsch, H.-J., Friebe M., Spies H., Johannsen B., Chiotellis E.
Study on the formation of mixed ligand oxorhenium and oxotechnetium complexes (SNS/S combination).
Inorg. Chim. Acta **1999**, 295, 1-8.

Preusche St., Füchtner F., Steinbach J., Zessin J., Krug H., Neumann W.
Long-distance transport of radionuclides between PET cyclotron and PET radiochemistry.
Appl. Radiat. Isot. **1999**, 51, 625-630.

Römer J., Steinbach J.
Herstellung und Charakterisierung der Sulfamate von Estra-3,17ξ-diolen. Schnelle Umsetzung von 16α-Fluorestradiol zum 16α-Fluorestradiol-3,17β-disulfamat.
J. Prakt. Chem. **1999**, 341, 574-583.

Skaddan M. B., Wüst F., Welch M. J., Katzenellenbogen J. A.
Synthesis and biological evaluation of 7alpha Re/Tc "3+1" and cyclopentadienyl tricarbonyl metal (CpTM) estrogen mimics based on the conjugated design.
J. Labelled Cpd. Radiopharm. **1999**, 42, S153-S155.

Spies H., Fietz T., Zablotskaya A., Belyakov S., Lukevics E.
Silyl modification of biologically active compounds. 6. Organosilicon complexes of rhenium(V) with mixed ligands.
Chem. Heterocycl. Compd. **1999**, 35, 112-120.

Srinivas P., Subramanian A. R., Brust P., Raghavan S. A. V., Rangisetty J. B., Gupta C. N. V. H. B., Sridhar N., Veeranjaneyulu A., Parimoo P.
Synthesis and preliminary pharmacological investigations of 1-(1,2-dihydro-2-acenaphthylenyl)-piperazine derivatives as potential atypical antipsychotic agents in mice.
IL FARMACO **1999**, 54, 567-572.

Stephan H., Spies H., Johannsen B., Klein L., Vögtle F.
Lipophilic urea-functionalized dendrimers as efficient carriers for oxyanions.
Chem. Commun. **1999**, 1875-1876.

Stephan H., Berger R., Spies H., Johannsen B., Schmidtchen F.-P.
Efficient phase transfer of pertechnetate with bicyclic guanidinium compounds.
J. Radioanal. Nucl. Chem. **1999**, 242, 399-403.

Wüst F., Skaddan M. B., Leibnitz P., Spies H., Katzenellenbogen J. A., Johannsen B.
Synthesis of novel progestin-rhenium conjugates as potential ligands for the progesterone receptor.
Bioorg. Med. Chem. **1999**, 7, 1-9.

Zessin J., Steinbach J., Johannsen B.
Synthesis of triphenylarsonium [^{11}C]methylide, a new ^{11}C-precursor. Application in the preparation of [2-^{11}C]indole.
J. Labelled Compd. Radiopharm. **1999**, 42, 725-736.

Zessin J., Gucker P., Ametamey S. M., Steinbach J., Brust P., Vollenweider F. X., Johannsen B., Schubiger P. A.
Efficient synthesis of enantimerically pure thioester precursors of [^{11}C]McN-5652 from racemic McN-5652. J. Labelled Compd. Radiopharm. **1999**, 42, 1301-1312.

PROCEEDINGS

Jankowsky R., Kirsch S., Spies H., Johannsen B.
EXAFS spectroscopy of technetium and rhenium complexes relevant to nuclear medicine. Speciation, techniques and facilities for radioactive materials at synchrotron light sources. Nuclear Energy Agency 1999, Workshop Proceedings Grenoble, France, 04.-06.10.1999.

Stephan H., Spies H., Berger R., Johannsen B., Schmidtchen F. P.
Complexation and phase transfer of perrhenate and pertechnetate with guanidium hosts.
XXIV. International Symposium on Macrocyclic Chemistry, Barcelona, Spain, 18.-23.07.1999.

Stephan H., Spies H., Johannsen B., Gestermann S., Gorka M., Hesse R., Kauffman C., Klein L., Vögtle F.
Interactions of medicinal and biological relevant anions with functionalized dendrimers.
1st International Dendrimer Symposium, Frankfurt/Main, 03.-05.10.1999.

ABSTRACT

Mäding P., Scheunemann M., Steinbach J., Bergmann R., Iterbeke K., Tourwe D., Johannsen B.
Development of potential tumour imaging agents by 4-[^{18}F]fluorobenzolation of neurotensin analogues.
J. Labelled Compd. Radiopharm. **1999**, 42, 987.

LECTURES AND POSTERS

Bergmann R., Scheunemann M., Rodig H., Brust P., Mäding P., Steinbach J., Iterbeke K., Tourwe D., Johannsen B.
^{18}F-markierte Neurotensinderivate für die Positronen-Emissions-Tomographie.
Jahrestagung der WGL, München, 13.10.1999.

Beuthien-Baumann B.
Einsatz der PET bei der Erforschung und Diagnostik ausgewählter Hirnerkrankungen. PET-Symposium FZ Rossendorf, 14.07.1999.

Beuthien-Baumann B., Handrick W., Schmidt T., Burchert W., Schackert G., Franke W.-G.
Charakterisierung der gestörten Hirnfunktion beim apallischen Syndrom: Durchblutung und Glukosestoffwechsel, gemessen mit emissionstomographischen Verfahren.
Jahrestagung der WGL, München, 13.10.1999.

Beuthien-Baumann B.
Übersichtsvortrag: PET in der Inneren Medizin.
Jahrestagung der Sächsischen Gesellschaft für Innere Medizin, Chemnitz, 12.11.1999.

Beuthien-Baumann B.
Übersichtsvortrag: PET-Anwendung in der Onkologie.
Krankenhaus Pirna, Klinik für Innere Medizin, 25.11.1999.

Beuthien-Baumann B.
Positronen-Emissions-Tomographie: Ein Überblick.
Übersichtsvortrag im Rahmen der Fortbildungsreihe der Klinik und Poliklinik für Kinderheilkunde, Universitätsklinikum Carl-Gustav-Carus Dresden, 08.12.1999.

Brust P., Bauer R., Vorwieger G., Walter B., Bergmann R., Füchtner F., Steinbach J., Zwiener U., Johannsen B.
Untersuchung der Dopaminsynthese bei neonataler Asphyxie mittels Positronen-Emissions-Tomographie.
Jahrestagung der WGL, München, 13.10.1999.

Johannsen B.
Technetium-99m, das Arbeitspferd der nuklearmedizinischen Diagnostik.
Jahrestagung 1999 der Deutschen Pharmazeutischen Gesellschaft (DPhG), Frankfurt am Main, 06.10.1999.

Johannsen B.
Fortschritte auf dem Weg zu ZNS-rezeptoraffinen ^{99m}Tc-Komplexen.
Seminar am Deutschen Krebsforschungszentrum Heidelberg, 21.10.1999.

Johannsen B.
Research at the Institute of Bioinorganic and Radiopharmaceutical Chemistry. In: Presentation of the Rossendorf Institutes. Bulgarian Academy of Sciences, Sofia, Bulgaria, 01.11.1999.

Johannsen B.
Metalle in Biosystemen.
Zentrumsseminar, FZ Rossendorf, 11.11.1999.

Kretzschmar M., Brust P., Pietzsch H.-J., Scheunemann M., Seifert S., Gupta A., Zessin J., Syhre R., Johannsen B.
Spezifische und selektive Bindung von ^{99m}Tc-Verbindungen an den Serotonin-($5HT_{2A}$)-Rezeptor des Gehirns.
Jahrestagung der WGL, München, 13.10.1999.

Preusche St., Steinbach J., Füchtner F., Linemann H., Will E. (1999)
Positronen-Emissions-Tomographie: ein kurzer methodischer Überblick
Vortrag vor Physikstudenten der TU Chemnitz, Rossendorf, 05.07.1999

Preusche St., Füchtner F.,Steinbach J., Roß H.
Betrieb und Wartung des Rossendorfer PET-Zyklotrons "CYCLONE 18/9"
Zyklotron-Workshop 1999 der Betreiber kleiner deutscher Zyklotrons, Rossendorf, 09.-10.09.1999

Preusche St., Steinbach J., Linemann H., Will E.
Positron emission tomography - a short course on methodology.
SOKRATES course, FZ Rossendorf, 13.10.1999.

Steinbach J.
Radiopharmazeutische Arbeiten zur Entwicklung von Tumordiagnostika
Symposium FZ Rossendorf, 14.07.1999.

Steinbach J., Johannsen B.
Positron emission tomography merges chemistry with biological imaging.
SOKRATES course, FZ Rossendorf, 13.10.1999.

Stephan H., Spies H., Berger R., Johannsen B., Schmidtchen F. P.
Complexation and phase transfer of perrhenate and pertechnetate with guanidium hosts.
XXIV. International Symposium on Macrocyclic Chemistry, Barcelona, Spain, 18.-23.07.1999.

Stephan H., Spies H.
Supramolekulare Rezeptoren zur Bindung von Pertechnetat und Perrhenat.
Institutskolloquium, Universität Potsdam, Institut für Anorganische Chemie, 29.09.1999.

Stephan H., Spies H., Johannsen B., Gestermann S., Gorka M., Hesse R., Kauffman C., Klein L., Vögtle F.
Interactions of medicinal and biological relevant anions with functionalized dendrimers.
1st International Dendrimer Symposium, Frankfurt/Main, 03.-05.10.1999.

Stephan H., Spies H., Johannsen B., Seidel J., Wolf G., Vögtle F.
Entwicklung und Charakterisierung funktionaler supramolekularer Systeme.
2. Workshop Kontaktforum Chemieforschung, VCI Nordost, Dresden, 26.-27.10.1999.

PATENTS

Füchtner F., Steinbach J., DE 195 15 212 A 1
Verfahren zur Herstellung von 2-[^{18}F]Fluor-2-desoxy-D-glucose und 2-[^{18}F]Fluor-2-desoxy-D-galactose.

Jankowsky R., Friebe M., DE 197 50 832 A 1
Verfahren zur Auftrennung von Substanzgemischen.

Noll B., Noll St., Knieß T., ha1158, AZ 199 51 715.0
^{18}F-Radiotracer und deren Verwendung zum Monitoring der Expression der Cytosin-Deaminase nach Gentransfer sowie Verfahren zur Herstellung der ^{18}F-Radiotracer.

AWARD

Dr. Frank Wüst
FZR-Doktorandenpreis 1999
Rhenium- and Technetium-containing steroids as ligands for the estrogen receptor, progesterone receptor and androgen receptor.

PhD THESIS

Jannette Wober
Untersuchungen von Oxorhenium(V)- und Oxotechnetium(V)-Koordinationsverbindungen als potentielle Liganden neuronaler Serotoninrezeptoren.
Dresden University of Technology, 30.11.1999.

DIPLOMA THESIS

Martina Netter
Untersuchungen zur ^{99m}Tc-Markierung von Etomidat, einem potentiellen Tracer für die funktionelle Nebennierenszintigraphie.
Institut für Pharmazeutische Chemie, Universität Wien, November 1999.
Betreuer im FZR: Dr. B. Noll.

III. SCIENTIFIC COOPERATION

COOPERATIVE RELATIONS AND JOINT PROJECTS

In multidisciplinary research such as carried out by this Institute, collaboration, the sharing of advanced equipment and, above all, exchanges of ideas and information play an important role. Effective collaboration has been established with colleagues at universities, in research centres and hospitals.

Dresden University of Technology has been a major partner in our cooperative relations. Cooperation with various groups in the Department of Chemistry and the Faculty of Medicine was again significantly extended last year. Common objects of radiopharmacological and medical research link the Institute with the Dresden University Hospital, above all with its Department of Nuclear Medicine (Prof. Franke). A joint team of staff members from both the Institute and the Clinic of Nuclear Medicine are currently working at the Rossendorf PET Centre.
The Institute cooperates with the Department of Surgical Research (Prof. Schackert) on a project concerning gene therapy monitoring. The Institute of Analytical Chemistry (Prof. Salzer) plays not only an important part in tracer research by performing analytical characterization (Dr. Scheller) but also cooperates in tumour research.

Very effective cooperation exists with the *Federal Material Research Institute in Berlin* (Mr. Leibnitz, Dr. Reck), whose staff members carried out X-ray crystal structure analysis of new technetium and rhenium complexes. The Institute of Organic Chemistry (Dr. Seichter) of the *Freiberg University of Mining & Technology* also contributes to analysing coordination compounds.

Our Institute is linked with the Institute of Pathology (Prof. Zwiener, Dr. Bauer) of *Jena's Friedrich-Schiller University* by long-standing fruitful cooperation on the pathophysiological aspects of brain functions.

In the field of PET tracers (steroid chemistry) the Institute works together with the *Hans-Knöll- Institute for Natural Products Research,* Jena (Prof. Hinnen, Dr. Kasch).

The fruitful collaboration with the *Paul Scherrer Institute* (Prof. Schubiger) of Villigen, Switzerland, which involves bioinorganic, radiochemical and biological topics, is much appreciated. PSI is also one of the main partners in the current BIOMED2 project on tumour-affine neuropeptides.

Our long-standing cooperation with the *"Demokritos" National Research Centre for Physical Sciences* in Athens (Dr. Chiotellis) has been continued. Various joint projects on technetium and rhenium chemistry were dealt with.

A field of cooperation with the Department of Pharmacy (Prof. Folkers, Prof. Wunderli-Allenspach) of the *Swiss Federal Institute of Technology Zurich (ETH Zürich)* was the chemical and biological characterization of technetium and rhenium complexes.

Based on PhD student and post doc visits, joint research into labelled steroids was carried out with the Department of Chemistry (Prof. Katzenellenbogen) of the *University of Illinois,* Urbana, USA, and the Division of Radiological Sciences (Prof. Welch) of the *Washington University School of Medicine,* St. Louis, USA.

Cooperation on a special subject concerning bioinorganic chemistry is in progress with *ASTA Medica Frankfurt* (Prof. Kutscher, Dr. Bernd).

In the field of supramolecular chemistry, successful cooperation was established with the Institute of Organic Chemistry and Biochemistry (Prof. Schmidtchen) of *Technische Universität München* and with the Kekulé Institute of Organic Chemistry and Biochemistry (Prof. Vögtle) of the *University of Bonn.*

The identification of common objects in PET radiopharmacy has led to collaborative research with the Department of Nuclear Medicine (Prof. Georgi) of the *University of Leipzig.*
Effective cooperation also exists with the *Riga Institute of Organic Chemistry* (Dr. Zablotskaya), Latvia.

Cooperation in PET tracer chemistry has been established with the *Turku Medical PET Centre* (Dr. Solin).

The Institute works with the *Bar-Ilan University* in Ramat-Gan, Israel (Prof. Nudelman), with the *West Virginia University Morgantown,* USA (Prof. H. Kuwabara), the *PET Centre Aarhus,* Denmark (Prof. A. Gjedde), *the Birla Institute of Technology and Science, Pilani,* India (Dr. P. Srinivas) on the biochemical aspects of radiotracer research.

LABORATORY VISITS

J.-U. Künstler
ESRF Grenoble, France
August 29 – September 11, 1999

S. Seifert
ESRF Grenoble, France
September 5 - 12, 1999

M. Scheunemann
Klinikum rechts der Isar München
September 13 – 15, 1999

A. Jordanova
Klinikum rechts der Isar München
September 13 – 15, 1999

J. Zessin
National PET-Centre Turku, Finland
September 20 - 26, 1999

J. Steinbach
National PET-Centre Turku, Finland
September 20 - 26, 1999

J. Zessin
National PET-Centre Turku/Finland
November 15 - 27, 1999

S. Seifert
ESRF Grenoble, France
November 19 - 26, 1999

J.-U. Künstler
ESRF Grenoble, France
November 19 - 28, 1999

M. Grote
ETH Zurich, Switzerland
December 13 - 15, 1999.

GUESTS

Dr. A. Zablotskaya
Latvian Institute of Organic Synthesis, Riga, Latvia
August 23 - October 6, 1999.

Dr. Z. Abedin
Institut for Research Establishment Savar, Bangladesh
September 7, 1999 - January 6, 2000.

Dr. P. Cumming
University of Aarhus, Denmark
October 10 - November 11, 1999.

K. Chavatte
Vrije Universität Brussels, Belgium
December 27 – 30, 1999.

MEETINGS ORGANIZED

Symposium "Aktuelle Aspekte der Positronen-Emissions-Tomographie"
FZ Rossendorf, July 14, 1999.

Workshop with Working Group "Isotope Chemists" of the pharmaceutical industry
"How relevant is PET in drug development?"
FZ Rossendorf, October 29, 1999.

Workshop on Radiotracers in Drug Research and Diagnostic Nuclear Medicine
FZ Rossendorf, December 2, 1999.

Rhenium-188 Meeting
FZ Rossendorf and Dresden University Hospital, December 8 - 9, 1999.

TEACHING ACTIVITIES

Winter term 1999/2000

B. Johannsen
One-term course on Radiopharmaceutical Chemistry.

H. Spies
Laboratory course on Radiopharmaceutical Chemistry.

OTHER ACTIVITIES

1. B. Johannsen
   Chairman of the DGN Working Group on Radiochemistry and Radiopharmacy.

2. B. Johannsen
   Co-editor of the journal "Nuclear Medicine and Biology".

3. B. Johannsen
   Co-chairman of the meeting: Naturwissenschaftlich-technische Beiträge zur modernen Entwicklung der Medizin.
   Meeting of the research association Wissenschaftsgemeinschaft Gottfried Wilhelm Leibniz (WGL)
   München, October 13, 1999.

4. F. Füchtner
   Expert mission for the International Atomic Energy Agency (IAEA) at the Hadassah University Hospital, Jerusalem, Israel.
   September 30 – Oktober 11, 1999.

5. St. Preusche
   Chairman of the CYCLONE 18/9 & 10/5 User Community.

6. St. Preusche
   Technical co-operation expert mission for the International Atomic Energy Agency for the acceptance tests of the CYCLONE 18/9 cyclotron in Prague/Czech Republic.
   November 1 - 8, 1999.

IV. SEMINARS

TALKS OF VISITORS

Dr. M. Brandsch, Biozentrum Halle
Substrat- und Konformationsspezifität des Peptidtransporters an Darm und Niere.
03.09.1999.

Prof. Golovinski, Institut für Molekularbiologie Sofia, Bulgarien
Inhibitoren der Glucuronosyltransferase.
03.09.1999.

Dr. Th. Behr, Georg-August-Universität Göttingen
Cholecystokinin-B/Gastrin-Rezeptorliganden zur Diagnostik und Therapie CCK-B-Rezeptor-exprimierender Tumoren.
08.09.1999.

Dr. Blasig, Institut für Molekulare Pharmakologie Berlin
Oxydativer Stress in Myokard und Endothel.
10.09.1999.

Prof. Dr. H.-P. Schreiber, ETH Zürich, Schweiz
Biologie und Ethik.
28.10.1999 (FZR, Zentrumsseminar).

Dr. G. Richter, Astrophysikalisches Institut Potsdam
Astronomie auf "Abwegen". Fachübergreifende Aspekte der Bildverarbeitung.
03.12.1999.

Dr. F. Wüst, Washington University, School of Medicine, St. Louis, USA
- Produktion von Nichtstandardisotopen unter besonderer Berücksichtigung von Technetium-94m.
- Synthese von [C-11]Fettsäuren.
10.12.1999.

INTERNAL SEMINARS 1999

P. Brust
Serotonintransporterliganden für PET und SPECT.
07.07.1999.

S. Seifert
Reaktivität und Stabilität von ^{99m}Tc-Gemischtligandkomplexen.
01.09.1999.

A. Gupta
Stabilität und Metabolisierung von "3+1"-^{99m}Tc-Gemischtligandkomplexen.
08.09.1999.

I. Heimbold
Synthese und Charakterisierung von Liganden der Ketanserin-Reihe.
29.09.1999.

A. Friedrich
Transportstudien an RBE4-Zellen.
27.10.1999.

R. Bergmann
Tracer in Tumormodellen.
01.12.1999.

V. ACKNOWLEDGEMENTS

ACKNOWLEDGEMENTS FOR FINANCIAL SUPPORT

The Institute is part of the Research Center Rossendorf Inc., which is financed by the Federal Republic of Germany and the Free State of Saxony on a fifty-fifty basis.

Two projects were supported by Commission of the European Communities:

- Peptide radiopharmaceuticals in oncology
  BIOMED II
  in collaboration with Belgium, Greece and Switzerland
  (PL 963198-SC), 04/1998 – 03/2001.

- Radiotracers for in vivo assessment of biological function
  COST B12
  in collaboration with Sweden, Italy and Switzerland
  02/1999 – 02/2004.

Three research projects concerning technetium tracer design, biochemistry and PET radiochemistry were supported by the Deutsche Forschungsgemeinschaft (DFG):

- PET with steroids
  Ste 601/3-3 (J. Steinbach), 01/1998 – 12/1999.

- Tc labelled fatty acids for myocardium diagnosis
  Sp 401/6-1 (H. Spies), 06/1999 – 05/2001.

- Redox transport system for ^{99m}Tc radiopharmaceuticals
  Sp 401/5-1 (H. Spies), 06/1999 – 06/2001.

The Sächsisches Staatsministerium für Wissenschaft und Kunst provided support for the follwing projects:

- Technetium(VII) complexes with supramolecular receptors
  SMWK-No. 4-7533-70-844-98/4, 07/1998 – 12/2000.

- ^{18}F labelled substrates of virus thymidine kinase for monitoring of gene therapy of cancer
  SMWK-No. 4-7531.50-03-844-98/2, 07/1998 – 12/2000.

- Molecular modelling of solid tumours by molecule spectroscopy in combination with PET
  SMWK-No. 4-7531.50-03-0370-98/3, 07/1998 – 12/2000.

The International Atomic Energy Agency supported a co-ordinated research program: "Development of agents for imaging central neural system receptors based on Tc-99m".
Agreement No. 8959 – 12/1995 – .

One project was supported by cooperation with the pharmaceutical industry:

- Cooperation in nuclear diagnostic
  Schering AG Berlin
  07/1996 – 06/2000.

Bilateral cooperation (WTZ) with Latvia:

- Silyl group-functionalized Tc complexes
  LET-008-97, 07/1997 – 12/2001.

VI. PERSONNEL

per 30 November 1999

Director

Prof. Dr. B. Johannsen

Administrative Staff

L. Kowe
G. Neubert
M. Kersten

Scientific Staff

Dr. Bergmann, R.
Dr. Brust, P.
Dr. Füchtner, F.
Dr. Heimbold, I.*
Hinz, R .*
Kretzschmar, M.
Mäding, P.
Dr. Noll, B.
Dr. Noll, St.
Dr. Pietzsch, H.-J.
Preusche, S.
Dr. Römer, J.*
Dr. Scheunemann, M.*
Dr. Seifert, S.
Smolinka, K.*
Dr. Spies, H.
Dr. Steinbach, J.
Dr. Stephan, H.
Dr. Syhre, R.
Dr. Will, E.

Technical Staff

Dohn, N.
Fischer, K.
Gläser, H.
Görner, H.
Große, B.
Herrlich, R.
Hüller, R.
Kasper, H.
Kolbe, U.
Krauß, E.*
Kreisl, B.
Kunadt, E
Landrock, K.
Lehnert, S.
Lenkeit, U.
Lösel, E
Lücke, R.
Nicolai, R.
Roß, H.
Smuda, C.*
Sterzing, R.
Suhr, A.*

Post Docs

Dr. Knieß, T.*
Dr. Zessin, J.

* term contract

PhD Students

Drews, A.
Friedrich, A.
Grote, M.
Gupta, A.
Jordanova, A.
Jung, Ch.
Künstler, J.-U.
Rodig, H.

Former Personnel

(who left during the period covered by the report)

Post Docs: Dr. Krishnan